DIRECT REDOX REGULATION OF F-ACTIN ASSEMBLY AND DISASSEMBLY BY MICAL

APPROVED BY SUPERVISORY COMMITTEE

Jonathan R. Terman, Ph.D. (Mentor)

Robin P. Hiesinger, Ph.D. (Chair)

Michael K. Rosen, Ph.D.

Helen Yin, Ph.D.

DEDICATION

I dedicate this dissertation to my parents, Ting-Yu Hong and Shue-Meei Juang,

for their endless support and love.

ACKNOWLDEGEMENTS

This work would not have been possible without the immense support and assistance of the kind people around me.

I owe my deepest gratitude to my mentor, Dr. Jonathan Terman, for his immeasurable support, caring and encouragement. Over the past seven years, he was always there with me for every hurdle I encountered, encouraging me when the experiments didn't work, allowing me to go to The Netherlands to learn techniques that were needed for my graduate research, guiding me to navigate this exciting path towards my Ph.D. and helping with my English writing in scientific communication. I cannot find words to express my gratitude to him for shaping me to become who I want to be and for sharing this exciting journey in science with me.

I am indebted to each member of my dissertation committee: Drs. Robin Hiesinger, Michael Rosen and Helen Yin for their extensive support and invaluable advice throughout my graduate studies. I would also like to thank Dr. Rosen in particular for providing both his generous input and experimental resources to my graduate work. Also, I would like to specifically thank several of his lab members: Chi Pak for contributing his extensive time and help to make a success of the TIRF experiments we performed together and for his insightful comments on my graduate work; and Zhucheng Chen and Hui-Chun Cheng for their discussions and technical support.

I am heartily thankful to Dr. Chen-Yong Lin, Dr. Hwan-You Chang and Dr. Chuan-Chin Chiao for inspiring my pursuit of science in the United States during the days of my undergraduate studies in Taiwan.

I would like to thank Dr. Willem van Berkel and Adrie Westphal for sharing their expertise on flavoprotein enzymology during my time at Wageningen University, The Netherlands

I would like to show my gratitude to the past and the current members of the Terman lab for providing me a friendly and rich-learning environment. In particular, I would like to thank Taehong Yang for sharing with me his valuable experience and advice on coursework, taking the qualify exam, performing experiments and on a graduate school life. I would like to thank Jimok Yoon for her support and for being a great classmate and labmate with me. I would like to thank Zhiyu Huang and Umar Yazdani for their help and kindness when I started my graduate work in the lab. I would like to thank Laura Alto and Chris Spaeth for their help and advice on postdoctoral research directions.

I would like to thank every member of Taiwanese student association in Dallas for their help in my daily life. In particular, I would like to thank Pei-Ling Tsai for her kind help when I moved to the United States; Szu-Wei Tu for her expertise with microcopy and Pei-Hsuan Chen for being such a great travel companion during my graduate life.

Finally, my special thanks goes to the Cancer Prevention Research Institute of Texas for generous financial support of my graduate studies.

DIRECT REDOX REGULATION OF F-ACTIN ASSEMBLY AND DISASSEMBLY BY MICAL

by

RUEI-JIUN HUNG

DISSERTATION

Presented to the Faculty of the Graduate School of Biomedical Sciences

The University of Texas Southwestern Medical Center at Dallas

In Partial Fulfillment of the Requirements

For the Degree of

DOCTOR OF PHILOSOPHY

The University of Texas Southwestern Medical Center at Dallas

Dallas, Texas

May, 2013

DIRECT REDOX REGULATION OF F-ACTIN ASSEMBLY AND DISASSEMBLY BY MICAL

Publication No._____

Ruei-Jiun Hung, Ph.D.

The University of Texas Southwestern Medical Center at Dallas, 2013

Supervising Professor: Jonathan R. Terman, Ph.D.

How guidance cues present outside of cells exert their precise effects on the internal actin cytoskeleton is poorly understood. Such effects are critical for diverse cellular behaviors including polarity, morphology, adhesion, motility, process elongation, navigation, and connectivity. Semaphorins, for example, are one of the largest families of these guidance signals and play critical roles in neurobiology, angiogenesis, immunology, and cancer. One interesting characteristic of the Semaphorins is that they inhibit the movement of cells (and their membranous processes) through their ability to disrupt actin cytoskeletal organization. However, despite considerable progress in the identification of Semaphorin receptors and their signal transduction pathways, the molecules linking them to the precise control of the actin cytoskeleton have remained mysterious. During my graduate studies, I sought to better understand a family of unusual proteins called the MICALs (which includes one *Drosophila* Mical and three vertebrate MICALs), which associate with the Semaphorin cell-surface receptor

Plexin and are important for Semaphorins to exert their effects. Nothing was known, however, regarding the specific role of the MICALs in these Semaphorin-dependent events. Not long after I began my graduate work, my colleagues and I noticed that Mical was necessary for proper actin cytoskeletal organization and sufficient to reorganize the actin cytoskeleton in vivo. Therefore, to better understand the role that Mical plays in actin cytoskeletal rearrangements, I took a biochemical approach, and purified the Mical protein. Utilizing biochemical and imaging approaches with purified proteins, I found that Mical directly binds to actin filaments (F-actin) and is able to induce the rapid disassembly of F-actin. Thus, my results revealed that Mical is a novel F-actin disassembly factor that provides a molecular conduit through which F-actin disassembly can be precisely achieved in response to Semaphorins. So I next wondered how Mical induces F-actin disassembly. Interestingly, the MICALs belong to a class of flavoprotein monooxygenase/hydroxylase enzymes that associate with flavin adenine dinucleotide (FAD) and use the co-enzyme nicotinamide adenine dinucleotide phosphate (NADPH) in oxidation-reduction (Redox) reactions. Although MICALs have no known substrate/s, my in vivo and in vitro results revealed that Mical employs its Redox region to bind F-actin and disassembles filaments in an NADPH-dependent manner. Moreover, this Mical-treated actin failed to re-polymerize even after removal of Mical, indicating that Mical stably modifies actin to alter polymerization. Mass spectrometric analyses revealed that F-actin subunits were directly modified by Mical on their conserved pointed-end that is critical for filament assembly. Specifically, Mical post-translationally oxidized a conserved amino acid (Methionine 44) within a region of actin that is critical for actin-actin contacts, simultaneously severing filaments and decreasing polymerization. Thus, my thesis observations reveal a novel and specific oxidation-dependent signaling mechanism that selectively regulates actin dynamics and cellular behaviors.

TABLE OF CONTENTS

PRIOR PUBLICATIONS

Hung, RJ, laW Hsu, JL Dreiling, MJ Lee, CA Williams, MD Oberst, RB Dickson, CY Lin (2004), Assembly of adherens junctions is required for sphingosine 1-phosphate-induced matriptase accumulation and activation at mammary epithelial cell-cell contacts, ***Am J Physiol Cell Physiol***, 286(5):C1159-69.

Hung, RJ, HS Chien, RZ Lin, CT Lin, J Vatsyayan, HL Peng, HY Chang (2007), Comparative analysis of two UDP-glucose dehydrogenases in *Pseudomonas aeruginosa* PAO1, ***J Biol Chem***, 282(24):17738-48.

Hung, RJ, U Yazdani, J Yoon, H Wu, T Yang, N Gupta, Z Huang, WJH van Berkel, JR Terman (2010), Mical links semaphorins to F-actin disassembly, ***Nature***, 463(7282):823-7.

Lin, RZ, TP Wang, **RJ Hung**, YJ Chuang, CC Chien, HY Chang (2011), Tumor-induced endothelial cell apoptosis: roles of NAD(P)H oxidase-derived reactive oxygen species, ***J Cell Physiol***, 226(7):1750-62.

Hung, RJ, and JR Terman (2011), Extracellular inhibitors, repellents, and semaphorin/plexin/MICAL-mediated actin filament disassembly, ***Cytoskeleton***, 68(8):415-33. ***(Invited review)***

Hung, RJ, CW Pak, JR Terman (2011), Direct Redox regulation of F-actin assembly and disassembly by Mical, ***Science***, 334(6063): 1710-3.

LIST OF FIGURES

LIST OF APPENDICES

LIST OF DEFINITIONS

ADP – adenosine diphosphate

BDNF – brain-derived neurotrophic factor

BMP – bone morphogenetic proteins

CH – calponin homology

CIL – contact inhibition

CRMP – Collapsin Response Mediator Protein

CSPG – chondroitin sulfate proteoglycans

GPI – Glycosylphosphatidylinositol

FAD – flavin adenine dinucleotide

MAG – myelin-associated glycoprotein

Mical – Molecule Interacting with CasL

NADH – nicotinamide adenine dinucleotide

NADPH – nicotinamide adenine dinucleotide phosphate

OMgp – oligodendrocyte-myelin glycoprotein

PHBH – p-hydroxybenzonate hydroxylase

Redox – oxidation-reduction

RGMs – repulsive guidance molecules

VEGF – vascular endothelial growth factor

Wnts – wingless-ints

CHAPTER ONE

General Introduction

Actin proteins assemble together into long filaments and it is this property that underlies cellular behaviors including polarity, morphology, adhesion, motility, process elongation, navigation, and connectivity. These behaviors are precisely controlled by signals that originate from outside of cells and impinge through signal transduction pathways on the proteins that directly regulate actin dynamics. Many of these extracellular signals have now been identified including small molecules such as amino acids, metals, lipids, and cyclic nucleotides; peptides and pheromones; plant chemotropic cues; cell adhesion molecules such as CAMs and cadherins; extracellular matrix molecules such as laminin and fibronectin; growth factors such as brain-derived neurotrophic factor (BDNF) and vascular endothelial growth factor (VEGF); morphogens such as hedgehog, wingless-ints (Wnts), and bone morphogenetic proteins (BMPs); cytokines including chemokines and tumor necrosis factors; and axon guidance cues including ephrins, netrins, semaphorins, and slits. Interestingly, these extracellular regulators of actin dynamics can be generally grouped into two classes based on either their positive or negative effects on cell motility. Positive signals attract cells or provide permissive/adhesive signals to induce cell movement, whereas negative signals prevent cells from moving or repel them from inappropriate areas. In chapter one, I will review these negative or inhibitory effects on cell movement and

discuss what was known prior to the results of my thesis work about how the largest family of these repulsive cues, the semaphorins, negatively regulates actin dynamics.

Contact Inhibition and Repulsive Guidance – Historical Perspectives

In the late 1800's, Theodor Engelmann, Wilhelm Pfeffer and others working with bacteria, flagellata, leukocytes, and plant spermatozoa noticed that chemicals exhibit differences in their effects on motile processes (Eisenbach, 2004; Loeb, 1906; Porter et al., 2011; Rosen, 1962). Those chemicals triggering movement towards themselves were termed attractants, while chemicals inducing negative movements were called repellents. These positive and negative responses were also regarded as chemotaxis, if the chemical stimulated the oriented movement of an organism or cell, and chemotropism, if only parts of the organism or cell reoriented in response to the stimulus. Influenced by these seminal observations, the Spanish Nobel laureate Santiago Ramon y Cajal proposed his chemotactic (neurotropic) hypothesis to explain how a nerve cell develops, displaces its cell body and axonal and dendritic processes, and forms its connections (Cajal, 1893, 1899). At the time, observations on nerve fiber growth after injury and transplantation also brought forth the idea that inhibitory barriers ("negative neurotropism") might prevent axon regeneration (**Figure 1.1a;** (Cajal, 1893, 1919; Lugaro, 1906; Windle, 1955)). It was these extensive observations on poorly regenerating axons that "suggested that there might be some form of short-range cell interaction which limited cell movement (Abercrombie, 1970)" and influenced the seminal observations of Michael Abercrombie, Paul Weiss, and others working during that time (Abercrombie, 1970; Harris, 1974; Heaysman, 1978;

Weiss, 1958; Wolf, 1921). Specifically, Abercrombie and colleagues noted that when fibroblast cells meet each other in culture, their locomotion stops immediately in the region of contact, which is followed by a localized contraction of the cell membrane, a subsequent change in direction, and migration away from the area of contact (**Figure 1.1b**; (Abercrombie and Heaysman, 1953)). Abercrombie named this cellular behavior "contact inhibition of locomotion (CIL)" and related behaviors have also been observed using a number of cell types (reviewed in (Abercrombie, 1980; Harris, 1974; Keynes and Cook, 1995; Mayor and Carmona-Fontaine, 2010; Schwab et al., 1993)).

Over the years, these negative chemotaxic and chemotropic events have been perhaps best characterized using neurons and watching the growth of their axons. Several groups first noted that growing nerve fibers spontaneously retract both *in vivo* and *in vitro* (Burrows, 1911; Speidel, 1933), and further characterization revealed that these retractive events often occur when the growing tips of nerve fibers (growth cones) encounter obstructions including other cells and axons (Hughes, 1953; Nakai, 1964). Further analysis of these behaviors suggested that nerve fibers selectively associate according to their subtype ("selective fasciculation" (Weiss, 1947)) and that when axons make contact with one another they either grow along the other fiber or they retract (Nakajima, 1965). Therefore, it appeared that the reaction of a nerve fiber to contact was selective – either positive or negative – and in light of the similarity of these retractive events to CIL, these negative reactions were termed "contact inhibition of extension" (Dunn, 1971; Ebendal, 1976). Dennis Bray, Dick Bunge and their colleagues extended these observations when they noticed that individual fibers from the same region of the nervous system

tend to adhere or extend along one another in culture, while fibers cultured from different regions often retract upon contact and avoid one another (Bray et al., 1980). These results suggested that nerve fibers might use inhibitory or repulsive activities to prevent unwanted associations; immediately suggesting both a means to guide developing axons and a mechanism to explain substrate-dependent differences affecting regenerating axons (Aguayo et al., 1979; Berry, 1982; David and Aguayo, 1981; Reier et al., 1983; Schwab and Thoenen, 1985).

Today, it is clear that these observations on axonal selectivity and inhibitory axonal responses complement those made by others documenting that axonal behaviors vary significantly depending on cell, tissue, or substrate encounters (e.g., (Bonhoeffer and Huf, 1980; Keynes and Stern, 1984; Lawrence, 1975; Letourneau, 1975; Nuttall and Zinsmeister, 1983; Raper et al., 1983; Smalheiser et al., 1981; Sperry, 1963; Tosney and Landmesser, 1985; Wessells et al., 1980; Yoon, 1979; Zinsmeister and Nuttall, 1986)). Yet, it was mechanistically critical to confirm that these retractive events did not result from a lack of growth cone adhesion – as might occur when axons encounter a substrate that is simply non-permissive for elongation (Cajal, 1928; Carter, 1965; Keynes and Cook, 1990; Letourneau, 1987; Martz and Steinberg, 1973). Importantly, follow-up experiments further demonstrated that axons actively avoid certain cells/tissues, often taking circuitous detours around them (**Figure 1.1c-d**; e.g., (Ebendal, 1982; Peterson and Crain, 1982; Pini, 1993; Verna, 1985)), and these avoidance responses are dependent on cell/tissue viability (**Figure 1.1e**; (Ebendal, 1982; Verna, 1985; Walter et al., 1987a)). As I discuss below, inhibitory and repulsive influences are now known to regulate the motility and navigation of multiple types of axons and cells. Furthermore, inhibitors and

repellents are not only present on cell membranes, where they induce a contact-mediated effect (i.e., contact repulsion), but they are also soluble (i.e., chemorepellents) and diffuse away from the cells that secrete them (Tessier-Lavigne and Goodman, 1996).

Extracellular Repulsive and Inhibitory Cues

To identify the mechanisms underlying these inhibitory/repulsive effects, Jonathan Raper and his colleagues returned to the assays of Bray and Bunge and in a series of ground breaking studies better characterized negative axon behaviors (Fan et al., 1993; Fan and Raper, 1995; Kapfhammer et al., 1986; Kapfhammer and Raper, 1987a, b; Luo et al., 1993; Raper and Grunewald, 1990; Raper and Kapfhammer, 1990). Specifically, Raper and colleagues used time-lapse video microscopy to carefully document that neurons cultured on a uniform substrate extend growth cones at a relatively steady rate with only rare spontaneous retractions. Likewise, they observed that growth cones typically cross over other fibers without delay or retraction. Yet, they found that when different types of neurons contact one another, their growth cones rapidly decrease in size and withdraw from contact **(Figure 1.1f)**. Raper and colleagues called this phenomenon "growth cone collapse" and they noticed that within an hour the collapsed growth cone regains its typical morphology and motility. However, they also noticed that if growth cones continue to advance into unlike fibers this collapse/retraction/recovery/extension cycle repeats itself multiple times. The researchers postulated that these events revealed the existence of specific chemical labels that negatively alter axon elongation even in environments that are permissive for outgrowth.

To determine the molecular identity of this "chemical label", Raper and colleagues devised a simple and ingenuous bioassay in which they grew axons on a permissive substrate and then screened membrane fractions from different cell lines and tissue sources for growth cone collapse (Raper and Kapfhammer, 1990). Strikingly, they identified both membrane-associated and soluble fractions that induce growth cone collapse, and their results suggested that this "collapsing activity" was induced by a protein, since it was both heat and trypsin sensitive. Using successive rounds of biochemical separation, collapsing activity tests, and enrichment, the researchers went about trying to purify this mysterious "collapsing factor" (Luo et al., 1993; Raper and Kapfhammer, 1990). Their peptide sequencing results identified a specific extracellular protein that they called Collapsin that exerts negative effects on cell motility and morphology (Luo et al., 1993). Surprisingly, Collapsin was highly similar to a protein that had been identified by Alex Kolodkin, Corey Goodman and their colleagues in grasshoppers for its effects on axon guidance and named Fasciclin IV (Kolodkin et al., 1992). Today, we know that both Fasciclin IV (Sema-1a) and Collapsin (Sema3A) are the founding members of one of the largest known families of repulsive guidance cues, the Semaphorins (**Figure 1.2a**; (Kolodkin et al., 1993; Luo et al., 1995; Yazdani and Terman, 2006)). Over the years, a number of additional extracellular proteins such as ephrins, netrins, slits, repulsive guidance molecules (RGMs), Wnts, BMPs, Nogo, myelin-associated glycoprotein (MAG), oligodendrocyte-myelin glycoprotein (OMgp), and tenascin have been found that exert these same types of negative effects on cell shape and motility (**Figure 1.2b**; Reviewed in (Dickson, 2002; Giger et al., 2010; Huber et al., 2003; Keynes and Cook, 1995; Schwab et al., 1993; Tessier-Lavigne and Goodman, 1996)).

Likewise, selective neurotransmitters, amino acids, peptides, proteases, lipids, and posttranslational modifications including chondroitin sulfate proteoglycans (CSPGs) have also been described as inhibitors/repellents (Reviewed in (Fields and Nelson, 1994; Giger et al., 2010; Schwab et al., 1993)). As we highlight below for the Semaphorins (Semas), much has been learned about the mechanisms of action of these inhibitory/repulsive signals (Bashaw and Klein, 2010; Giger et al., 2010; Huber et al., 2003), yet it still remains poorly understood how they negatively alter the actin cytoskeletal machinery necessary for cell morphology and motility.

Semaphorins Negatively Regulate Cell Motility and Cytoskeletal Organization

Since the discovery of Sema-1a and Sema3A, over twenty Semas have been reported in organisms as diverse as nematode worms, insects, crustaceans, vertebrates, and viruses. Semas exist as secreted, transmembrane, and Glycosylphosphatidylinositol (GPI)-linked proteins and for these reasons and the presence of other conserved protein domains, they are grouped into eight classes (**Figure 1.2a**; (Tran et al., 2007; Yazdani and Terman, 2006)). Semas serve not only diverse functions in the nervous system but also specify the immune, cardiovascular, and musculoskeletal systems (Melani and Weinstein, 2010; Suzuki et al., 2008; Tran et al., 2007; Yazdani and Terman, 2006). Likewise, Semas have been linked to a number of pathologies including different cancers, musculoskeletal disorders, neurodegeneration, and heart disease (Mann et al., 2007; Neufeld and Kessler, 2008; Yazdani and Terman, 2006). Yet, much of our understanding of the cellular effects of Semas has come through characterizing Sema-mediated growth cone collapse. Norman Wessells, Kenneth Yamada, and their colleagues first identified

that the periphery of growth cones, including their dynamic filopodia, are highly enriched in F-actin (Yamada et al., 1970, 1971). Their observations also revealed that disrupting the actin network in axons using the actin depolymerization drug Cytochalasin B causes growth cones to "round-up" (i.e., collapse) (**Figure 1.3a**; (Wessells et al., 1971; Yamada et al., 1970)). In hindsight, these observations with actin depolymerization drugs suggested that there might exist specific "repulsive" signaling cascades that locally disassemble F-actin and negatively regulate motility. However, such an effector was unknown until Raper, Phillip Gordon-Weeks, and their colleagues observed that contact with the extracellular cue Sema3A dramatically decreases F-actin in the growth cone periphery and its filopodia (**Figure 1.3b**; (Fan et al., 1993)). Multiple Semas have now been found to induce growth cone collapse *in vivo* and *in vitro* and negatively regulate actin dynamics (e.g., reviewed in (Yazdani and Terman, 2006)). Indeed, the picture that has emerged is that Semas collapse growth cones by locally destabilizing F-actin (Brown and Bridgman, 2009; Fan and Raper, 1995) – events that are characterized by a loss of peripheral F-actin, a rapid decrease in F-actin bundles, and a reduced ability to polymerize new F-actin (Brown and Bridgman, 2009; Dent et al., 2004; Fan et al., 1993; Fournier et al., 2000; Fritsche et al., 1999; Gallo, 2006; Mikule et al., 2002; Roche et al., 2009).

Importantly, these cellular effects of Semas are not just a peculiarity of neuronal growth cones, but Semas also exert these same types of negative effects on multiple different cell types including glia, endothelial cells, platelets, different types of immune cells, mechanosensory cells, and a number of cancer cell lines (Barberis et al., 2004; Bielenberg et al., 2008; Eickholt et al., 1999; Guttmann-Raviv et al., 2007; Hung et al., 2010; Kashiwagi et al., 2005; Lepelletier et al.,

2006; Li and Lee, 2010; Miao et al., 1999; Shimizu et al., 2008; Takahashi et al., 1999; Torres-Vazquez et al., 2004; Tran-Van et al., 2011; Turner and Hall, 2006; Varshavsky et al., 2008; Walzer et al., 2005; Xu et al., 2000; Yukawa et al., 2005). In many ways, the cellular response to Semas is similar to that seen after cytochalasin treatment, yet differences have been noted including that growth cones continue to advance after treatment with cytochalasin, but not Sema3A (e.g., (Fan et al., 1993; Yamada et al., 1970)). It is thought that these differences result because Semas not only impair actin dynamics, but also negatively regulate microtubule stability (Dent et al., 2004; Fan et al., 1993; Fritsche et al., 1999) and cell-substrate interactions (Barberis et al., 2004; Gatlin et al., 2006; Kashiwagi et al., 2005; Mikule et al., 2002; Serini et al., 2003; Walzer et al., 2005; Woo and Gomez, 2006). Interestingly, these effects on microtubules and adhesion are separable from Sema-mediated F-actin disassembly (discussed in (Gallo and Letourneau, 2004)) and indicate that Semas are likely to independently regulate F-actin, microtubules, and adhesion.

Searching for the Molecular and Biochemical Basis of Sema-mediated F-actin Disassembly

Since the initial observations of Raper and colleagues over 25 years ago, the molecular mechanisms of Sema-mediated repulsion have been a question of considerable interest. Major insights into these mechanisms have come with the discovery that large, cell-surface proteins in the Plexin family are Sema receptors (**Figure 1.4a**; (Comeau et al., 1998; Takahashi et al., 1999; Tamagnone et al., 1999; Winberg et al., 1998)). Interestingly, the cytoplasmic portion of Plexins directly bind Rho and Ras family GTPases, providing a direct link between Semas/Plexins and

small GTP-binding proteins (reviewed in (Negishi et al., 2005; Puschel, 2007)). Small GTPases, although not themselves direct actin regulatory proteins, are key regulators of cytoskeletal dynamics and cell adhesion (Hall, 1998; Hall and Lalli, 2010). Moreover, Plexin receptors contain a GTPase activating protein (GAP) domain and Plexins are GAPs for specific Ras and Rap family GTPases (**Figure 1.4a**; reviewed in (Yang and Terman, 2013)). Extensive work now indicates that Plexins utilize their GAP activity to inactivate Ras/Rap family GTPases and thereby turn-off Ras^{GTP}-integrin-dependent cell-substrate adhesion (**Figure 1.4b**; reviewed in (Yang and Terman, 2013)). Progress has also been made in characterizing the means by which Sema/Plexins alter microtubule organization. The current model is that Semas differentially regulate the activities of two microtubule regulatory proteins, tau and Collapsin Response Mediator Protein (CRMP), and thereby alter microtubule dynamics (**Figure 1.4c**; (reviewed in (Hou et al., 2008; Schmidt and Strittmatter, 2007)). In contrast, much less is known of how Semas/Plexins directly connect and disassemble F-actin. Complicating these investigations are results indicating that Plexins have class-specific differences in their intracellular binding partners (reviewed in (Yazdani and Terman, 2006; Zhou et al., 2008), and so they may differ in how they induce F-actin disassembly. Likewise, an understanding of Sema/Plexin F-actin disassembly has been confounded by oberservations that Semas also induce positive effects on motility, guidance, and adhesion (reviewed in (Roth et al., 2009)) and at least some Semas can initiate "reverse signaling" through their own cytoplasmic regions or by coupling with transmembrane proteins on the same cell (reviewed in (Yazdani and Terman, 2006; Zhou et al., 2008)). So, although numerous proteins including kinases, phosphatases, and regulators of G

protein signaling play important roles in Sema-mediated repulsion (for discussion and review, see (Bechara et al., 2007; Franco and Tamagnone, 2008; Potiron et al., 2007; Yazdani and Terman, 2006; Zhou et al., 2008)), only a few of these proteins are known to directly associate with actin.

One hypothesis proposes that Sema "turns-off" actin polymerization. Specifically, Plexins associate with GTP-bound Rac, and B class Plexins prevent Rac^{GTP} from associating with its downstream effector, p21-activated kinase (PAK) (**Figure 1.4d**; (Driessens et al., 2001; Hu et al., 2001; Vikis et al., 2002)). Since PAK localizes to regions of cytoskeletal assembly and plays important roles in cell motility (Bokoch, 2003), Sema-mediated repulsion/loss of motility may be accomplished by preventing Rac from activating PAK (**Figure 1.4d)**. Yet, PAK has multiple targets (Bokoch, 2003; Hofmann et al., 2004) and it is unknown which pathway and direct actin regulatory proteins it is important to keep PAK away from in response to Semas. Moreover, in contrast to B class Plexins, Plexin A-induced repulsion does not appear to "sequester active Rac from PAK" since Plexin A requires active Rac for "collapse" (e.g., (Dalpe et al., 2004; Jin and Strittmatter, 1997; Kuhn et al., 1999; Toyofuku et al., 2005; Turner et al., 2004; Vastrik et al., 1999)). Furthermore, Plexin A - Rac^{GTP} interactions regulate Plexin GAP-mediated negative effects on adhesion (Toyofuku et al., 2005), further complicating this "sequestering" model to explain how F-actin disassembles upon Sema treatment. Indeed, Plexin A - Rac^{GTP} signaling activates an endocytic pathway that accompanies Sema-mediated growth cone collapse but is not a part of the initial F-actin disassembly process (Fournier et al., 2000; Jurney et al., 2002).

Another hypothesis first raised by Raper and colleagues (Fan et al., 1993) is that "….actin polymerizes normally in collapsing growth cones but is depolymerized at an accelerated rate…….[which] could occur if the collapsing activity induced a filament severing and capping activity or a modification of actin that facilitates depolymerization". Along these lines, key players implicated in Sema-mediated F-actin disassembly are the actin depolymerizing factor (Dransfield et al.)/Cofilins, a family of phylogenetically conserved proteins that depolymerize F-actin (Bamburg, 1999; Oser and Condeelis, 2009). However, while F-actin depolymerization is a hallmark of Sema-mediated negative motility, depolymerization of F-actin is also required for the turnover and recycling of actin that is needed for locomotion (Oser and Condeelis, 2009; Pollard and Borisy, 2003). Therefore, F-actin depolymerization induced by cofilin often favors motility, since it generates more free actin and barbed ends for polymerization (Oser and Condeelis, 2009). These positive effects on actin assembly complicate any models employing cofilin and not surprisingly, both cofilin activation (Fritsche et al., 1999; Hu et al., 2001; Kashiwagi et al., 2005; Nukazuka et al., 2008; Shimizu et al., 2008; Vikis et al., 2002) and inactivation (Aizawa et al., 2001; Scott et al., 2009; Walzer et al., 2005) have been suggested to underlie Sema-mediated repulsion (**Figure 1.4d**). Likewise, cofilin only poorly depolymerizes bundled F-actin (e.g., (Schmoller et al., 2011)), which makes up the leading edge of cells and the filopodia of growth cones, and neither cofilin activation nor inactivation is always associated with or sufficient for Sema/Plexin-mediated F-actin disassembly. Thus, further analysis of the levels, spatiotemporal activation, and regulation of cofilin (e.g., (Andrianantoandro and Pollard, 2006; Bernstein and Bamburg, 2010)) is necessary to fully

understand its role in Sema/Plexin-mediated repulsion.

MICALs are Plexin–interacting Proteins that Negatively Regulate Cell Shape and Motility

To identify new molecules underlying Sema-mediated repulsion, we and others have conducted unbiased genetic, molecular, and biochemical screens in model organisms. These screens have identified new Sema signaling components including a family of unusual proteins, the MICALs (Terman et al., 2002). The first MICAL (Human MICAL-1) was identified by Hisamaru Hirai and colleagues and named for its interaction with the SH3 domain-containing protein, CasL (Molecule Interacting with CasL; (Suzuki et al., 2002)). Cas proteins regulate integrin-mediated cell adhesion and cytoskeletal organization (Cabodi et al., 2010) and although the functional significance of this MICAL-CasL interaction remains to be determined, these biochemical observations suggested that MICAL-1 might alter cell morphology and motility. In parallel experiments, Terman, Kolodkin, and colleagues identified *Drosophila* Mical in a screen for Plexin A-interacting proteins and based on similarity, found two additional mammalian MICAL family members (MICAL-2 and MICAL-3) **(Figure 1.5a**; (Terman et al., 2002)). Subsequent work revealed that vertebrate MICALs also associate with A class Plexins; MICAL-1 immunoprecipitates with both Plexin A1 and Plexin A3, while MICAL-2 interacts with Plexin A4 (Schmidt et al., 2008; Terman et al., 2002). Interestingly, MICALs may not directly associate with B, C, or D Class Plexins (Terman et al., 2002), but the significance of these class-specific binding preferences are unclear since at least some different classes of Plexins join

together into complexes (Ayoob et al., 2006; Turner et al., 2004; Usui et al., 2003), substitute for one another (Ayoob et al., 2006), and work with MICALs *in vivo* (Ayoob et al., 2006).

MICALs are broadly expressed in many tissues and this expression varies considerably with age. For example, MICALs are highly expressed throughout the embryonic, postnatal and adult nervous systems in a variety of neuronal cell types and glia (Ashida et al., 2006; Bron et al., 2007; Fischer et al., 2005; Kirilly et al., 2009; Morinaka et al., 2011; Pasterkamp et al., 2006; Terman et al., 2002; Weide et al., 2003; Xue et al., 2010). MICALs are also highly expressed in non-neuronal tissues including within skeletal muscle (Ashida et al., 2006; Beuchle et al., 2007; Fischer et al., 2005; Terman et al., 2002; Xue et al., 2010), heart (Ashida et al., 2006; Fischer et al., 2005; Xue et al., 2010), fibroblasts (Hochman et al., 2006), lung (Ashida et al., 2006; Fischer et al., 2005; Suzuki et al., 2002), kidney (Ashida et al., 2006; Fischer et al., 2005; Suzuki et al., 2002), bone marrow (Ashida et al., 2006), thymus (Ashida et al., 2006; Suzuki et al., 2002), spleen (Suzuki et al., 2002), liver (Ashida et al., 2006; Fischer et al., 2005), testis (Ashida et al., 2006; Miura and Imaki, 2008; Suzuki et al., 2002)), and hematopoietic and fibroblast cell lines (Hochman et al., 2006; Suzuki et al., 2002). MICAL is also upregulated in several different cancer cell lines (Ashida et al., 2006) and in glia and meningeal fibroblasts after neural trauma (Pasterkamp et al., 2006). Decreased MICAL expression is also associated with neurological diseases including epilepsy (Luo et al., 2011). Subcellularly, the MICALs are associated with the cytoskeletal fraction and reside within axons, dendrites, and growth cones, along pre- and post-synaptic terminals of neuronal synapses, at the plasma membrane of muscle attachment sites, and within the growing tips of actin-rich mechanosensory bristle processes in close

association with F-actin (Beuchle et al., 2007; Fischer et al., 2005; Hung et al., 2010; Kirilly et al., 2009; Morinaka et al., 2011; Suzuki et al., 2002; Terman et al., 2002; Weide et al., 2003).

The physiological functions of the MICALs have been best characterized in Drosophila where both loss-of-function ("knockout) and gain-of-function (overexpression) studies have revealed that Sema-1a and its receptor Plexin A (PlexA) repel axons (Winberg et al., 1998; Yu et al., 1998). Likewise, *in vivo* results indicate that Mical functions with Sema-1a/PlexA to mediate axon-axon repulsion (**Figure 1.6a**; (Ayoob et al., 2004; Beuchle et al., 2007; Hung et al., 2010; Terman et al., 2002)) and Mical also has roles in Sema2/PlexB-mediated repulsion (Ayoob et al., 2006). Genetic screens have also revealed that synaptic terminals do not spread and increase in size in *Mical* mutants (**Figure 1.6b;** (Beuchle et al., 2007)), and that Mical is required to prune developing dendrites (**Figure 1.6c;** (Kirilly et al., 2009)**)**. *Drosophila* Mical is also necessary for muscle organization, larval movements, and flight (**Figure 1.6d**; (Beuchle et al., 2007; Langer et al., 2010)). Complementing these observations with *Drosophila* Mical, vertebrate MICALs also have been found to have neuronal as well as non-neuronal functions. MICAL-1 negatively alters cell morphology and axon outgrowth in culture and mediates Semas effects on axon length and growth cone collapse (Morinaka et al., 2011; Schmidt et al., 2008). Knockdown approaches have also indicated that MICAL-3 is required for Sema-mediated growth cone collapse *in vitro*, and together with Semas/Plexins, controls motor neuron migration *in vivo* (Bron et al., 2007; Morinaka et al., 2011). MICAL-2, in contrast, has not been examined in neuronal contexts, but is highly expressed in prostate cancer cells where its knockdown reduces cancer cell viability (Ashida et al., 2006).

MICALs are Multi-domain Oxidoreductase (Redox) Enzymes

MICALs are large proteins (some of which are >300kDa) with a phylogenetically conserved domain organization that undergoes alternative splicing (**Figure 1.5a**). At their C-termini, MICALs contain their plexin-interacting region, which is a coiled-coil motif that shows similarity to the alpha-helical region present in Ezrin, Radixin, and Moesin (ERM) proteins (**Figure 1.5a**; (Terman et al., 2002)). Interestingly, this plexin-interacting region autoinhibits MICAL function, and it has been proposed that Sema-induced Plexin-MICAL interactions relieve this autoinhibition and activate MICAL (Hung et al., 2010; Schmidt et al., 2008). Adjacent to the ERM alpha-like portion is a region enriched in proline residues, including multiple PxxP motifs, which are ligands for SH3 domain–containing proteins including CasL (**Figure 1.5a**; (Suzuki et al., 2002; Terman et al., 2002)). This C-terminal portion of MICAL also interacts with vimentin (Suzuki et al., 2002), Rab small GTPases including Rabs 1, 8, 10, 13, 15, 35, and 36 (Fischer et al., 2005; Fukuda et al., 2008; Grigoriev et al., 2011; Weide et al., 2003), the Rab6-interacting coiled-coil protein ELKS (Grigoriev et al., 2011), and NDR kinase (Zhou et al., 2011b). At least some of these MICAL-Rab interactions regulate vesicle fusion at the plasma membrane (Grigoriev et al., 2011). Preceding this proline-rich region is a LIM domain (**Figure 1.5a**), which is a zinc binding region that mediates protein interactions in a variety of proteins including cytoskeletal-associated proteins (Kadrmas and Beckerle, 2004). The LIM domain of MICAL-1 is important for interactions with CRMP (Schmidt et al., 2008), and these interactions regulate both MICAL-mediated repulsion (Schmidt et al., 2008) and CRMP-mediated effects on microtubules (Morinaka et al., 2011). N-terminal to the LIM

domain, MICALs contain a single calponin homology (CH) domain (**Figure 1.5a**). CH domains typically bind F-actin when they are present in tandem (Gimona et al., 2002), but Mical requires its single CH domain for proper localization *in vivo* (Hung et al., 2010) but not F-actin binding (Hung et al., 2010; Sun et al., 2006). At their N termini, MICALs contain a nucleotide-binding motif that is distinct from mononucleotide and cyclic nucleotide binding motifs. In particular, MICALs have a Rossmann fold (GxGxxG motif) that matches the consensus for binding the adenosine diphosphate (ADP)-moiety of flavin adenine dinucleotide (FAD) (**Figure 1.5a, c**; (Terman et al., 2002; Wierenga et al., 1986)). Proteins use FAD to catalyze oxidation-reduction (Redox) reactions and MICALs contain three separate motifs (GxGxxG, GD, DG) found in flavoprotein monooxygenases (also called hydroxylases), a subclass of oxidoreductase (Redox) enzymes (**Figure 1.5a, c**; (Eppink et al., 1997; Terman et al., 2002)). Flavoprotein monooxygenases (FMs) insert one atom of molecular oxygen directly into their substrate using nucleotides such as nicotinamide adenine dinucleotide phosphate (NADPH) or nicotinamide adenine dinucleotide (NADH) as electron donors. Therefore, the presence of this FM domain suggested that MICAL is a Redox enzyme. Yet, each FM has distinct substrates so predicting MICAL substrates based on FM sequence is not possible (Terman et al., 2002).

MICALs are unique among FMs in that they contain additional domains besides their Redox domain, including their CH and LIM domains that are also present in cytoskeletal-associated proteins. Likewise, the MICALs represent a new class of FMs because they contain additional motifs through which they directly associate with transmembrane proteins such as Plexins. However, the large size of the MICALs has made characterizing their biochemical

function difficult. Therefore, Terman and colleagues expressed and purified recombinant protein containing only the FM domain of Mical and found that Mical proteins exhibit the yellow color characteristic of FAD binding proteins (Terman et al., 2002). Flavins, such as FAD, contain an isoalloxazine ring (**Figure 1.5c**) that absorbs light in the ultraviolet (UV) and visible spectral range (Chapman and Reid, 1999) and is responsible for the orange appearance of proteins that bind flavins (flavoproteins). MICAL proteins also exhibit flavoprotein-like UV-Visible absorption spectra (Terman et al., 2002), and structural analysis reveals that MICAL is an FAD binding protein whose closest structural relative is the FM p-hydroxybenzoate hydroxylase (PHBH) (Nadella et al., 2005; Siebold et al., 2005). Furthermore, purified protein corresponding to the FM domain of MICAL is able to consume NADPH, indicating that like PHBH, MICAL uses NADPH as a co-enzyme (Hung et al., 2010; Nadella et al., 2005; Schmidt et al., 2008). Interestingly, MICAL is also able to produce hydrogen peroxide (H_2O_2; (Morinaka et al., 2011; Nadella et al., 2005; Schmidt et al., 2008)). Thus, H_2O_2 may be the physiological signal generated by MICAL. However, FMs such as MICAL typically directly associate and catalyze the addition of oxygen to specific substrates and produce small amounts of H_2O_2 in the absence of a substrate (Massey, 1995; Terman et al., 2002). In this way, FMs are different from oxidases, which simply produce H_2O_2. Therefore, the current model for MICALs catalytic function is that it binds and employs the cofactor/prosthetic group FAD, utilizes the coenzyme NADPH, and either directly oxidizes a specific substrate/s and/or produces H_2O_2 (**Figure 1.5c**).

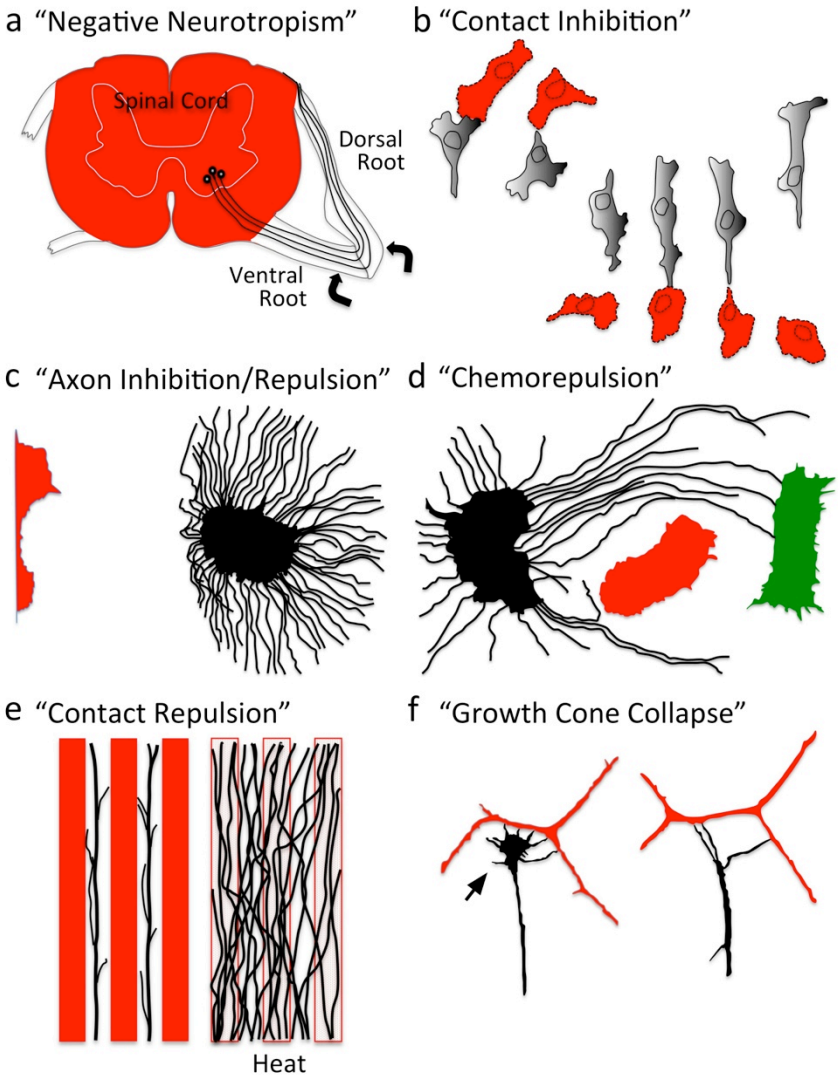

Figure 1.1. Negative Regulation of Cell Shape, Motility, and Navigation. (**a**) Regenerating axons (black) grow extensively on some substrates (ventral and dorsal roots) and not others (spinal cord, red). (Lugaro, 1906). (**b**) Cultured cells retract upon contact and change direction. (Weiss, 1958). **(c)** Neuronal fiber extension (black) is inhibited/repelled upon co-culturing in proximity to a tissue explant (red). (Ebendal, 1982). **(d)** Axons (black) circuitously grow away (red) or towards (green) different tissues explants. (Peterson and Crain, 1982). **(e)** Axons (black) avoid substrates (red), a phenomenon that is abolished upon high temperature treatment (heat); revealing that axons grow on certain substrates not because of "attraction", but because of avoidance of other substrates. (Walter et al., 1987b). **(f)** A neuronal growth cone (black) retracts upon contact with an unlike neuronal fiber (red). (Kapfhammer and Raper, 1987a).

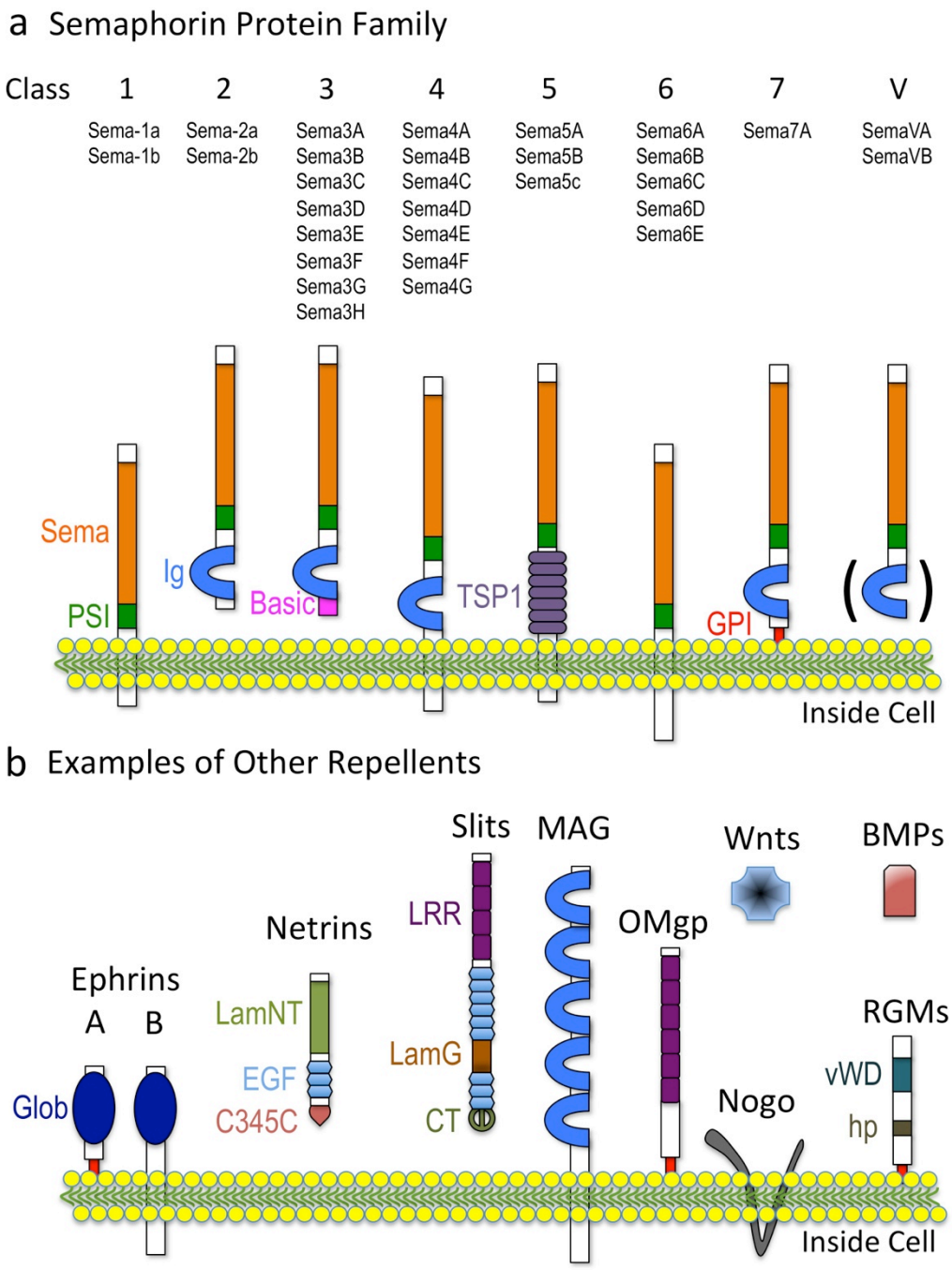

Figure 1.2. Semas and Repulsive/Inhibitory Extracellular Cues. (a) Semas. (**b**) Other well-known repulsive/inhibitory cues. Domain names are from SMART (http://smart.embl-heidelberg.de) except GPI, glycosylphosphatidylinositol; Glob, globular; hp, hydrophobic; The ( ) in (a) refers to the observation that Ig domains are present in some Class V (viral) Semas.

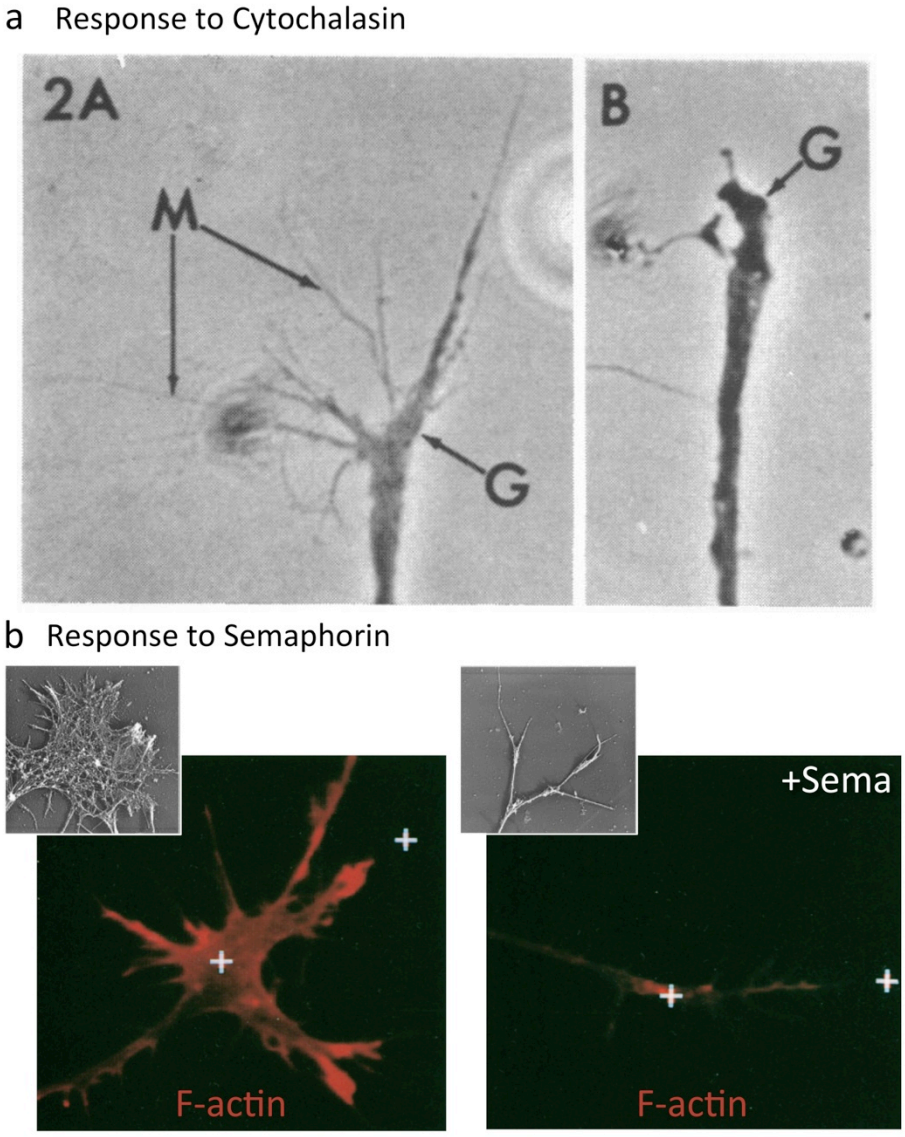

Figure 1.3. F-actin Disassembly Underlies Sema-mediated Repulsion. (a) F-actin disassembly collapses growth cones (Yamada et al., 1970). A growth cone (G) exhibits extensive filopodia (M) until cytochalasin treatment (B; 6 minute treatment) disrupts actin polymerization, disassembles F-actin, and induces collapse. (**b**) Sema treatment results in loss of F-actin (Fan et al., 1993). Rhodamine phalloidin staining reveals F-actin present in control (left) and Sema-treated growth cones (right; 5 min treatment). (**Insets**) Rotary shadow EM shows the growth cone F-actin before (left) and after Sema application (right; 30 min). Reprinted with permission of John Wiley & Sons, Inc. (Brown and Bridgman, 2009).

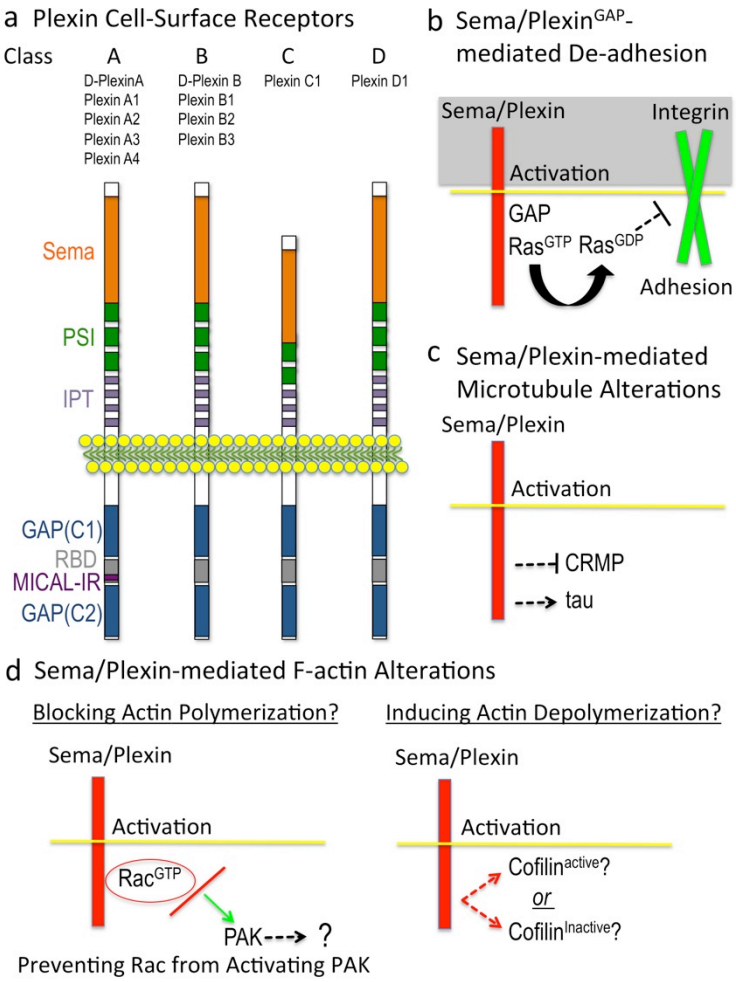

Figure 1.4. Semas Employ Plexins to Direct Repulsion. (a) Plexins. Domain names are from SMART (http://smart.embl-heidelberg.de) except GAP, GTPase activating protein; C1, conserved 1; C2, conserved 2; RBD, Rho GTPase binding domain; MICAL-IR, MICAL interacting region. (**b**) Sema/Plex-mediated effects on cell adhesion. The current model is that 1) the Plexin GAP is activated by binding of both Sema and a Rac GTPase to the Plexin extracellular and intracellular regions, respectively, 2) the Plexin GAP activity locally enriches for the GDP-bound form of Ras family GTPases, which 3) inactivates (through "inside-out" signaling) integrin-extracellular matrix-mediated adhesion. (**c**) Sema effects on microtubules. The current model is that Semas "turn-on" tau-mediated microtubule alterations and "turn-off" CRMP-mediated tubulin assembly. (**d**) Current models suggest that Sema-mediated F-actin alterations occur by limiting actin polymerization (left) and/or by inducing actin depolymerization by regulating the levels of active cofilin (right). A few other actin-associated proteins including myosin II and ERM are involved in Sema-mediated repulsion (Gallo, 2008; Mintz et al., 2008; Schlatter et al., 2008), but their effects appear secondary to directly inducing F-actin disassembly (Brown et al., 2009; Gallo, 2006; Takamatsu et al., 2010).

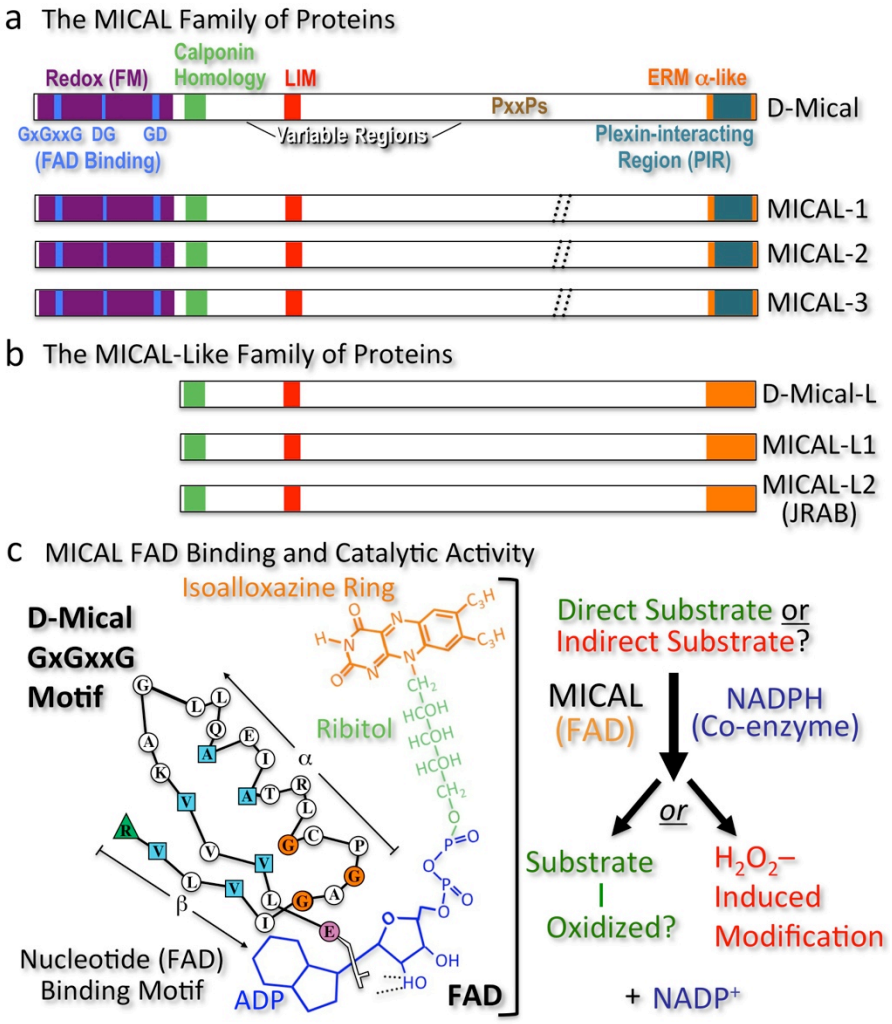

Figure 1.5. MICALs are Multi-domain Cytosolic Redox Enzymes. (**a**) MICAL family proteins are characterized by their flavoprotein monooxygenase (Redox [FM]), calponin homology, LIM, and ERM alpha-like domains. Variable regions differ in length and continuity among family members (dotted //). To conform with Drosophila nomenclature guidelines, lowercase lettering is now used when describing invertebrate MICALs (Mical), and all capitals are used when describing the vertebrate MICALs (and the MICAL family of proteins). (**b**) MICAL-Like proteins are similar to MICALs in domain organization except they lack the Redox domain. (**c**) FAD binding and MICAL enzymatic activity. (**Left**) The MICAL cofactor FAD is composed of ADP (including a pyrophosphate group), ribitol, and an isoalloxazine ring. The ADP region of FAD is bound by Mical's GxGxxG region where the critical residues are colored (Modified from (Wierenga et al., 1986)). The pyrophosphate and ribitol moiety of FAD are bound by the DG and GD regions of Mical, respectively. (**Right**) Results indicate that the Redox domain of MICAL binds FAD, consumes NADPH, and generates H_2O_2. MICAL substrate(s) are unknown. Alternatively, MICAL may have no direct substrate and may simply generate H_2O_2.

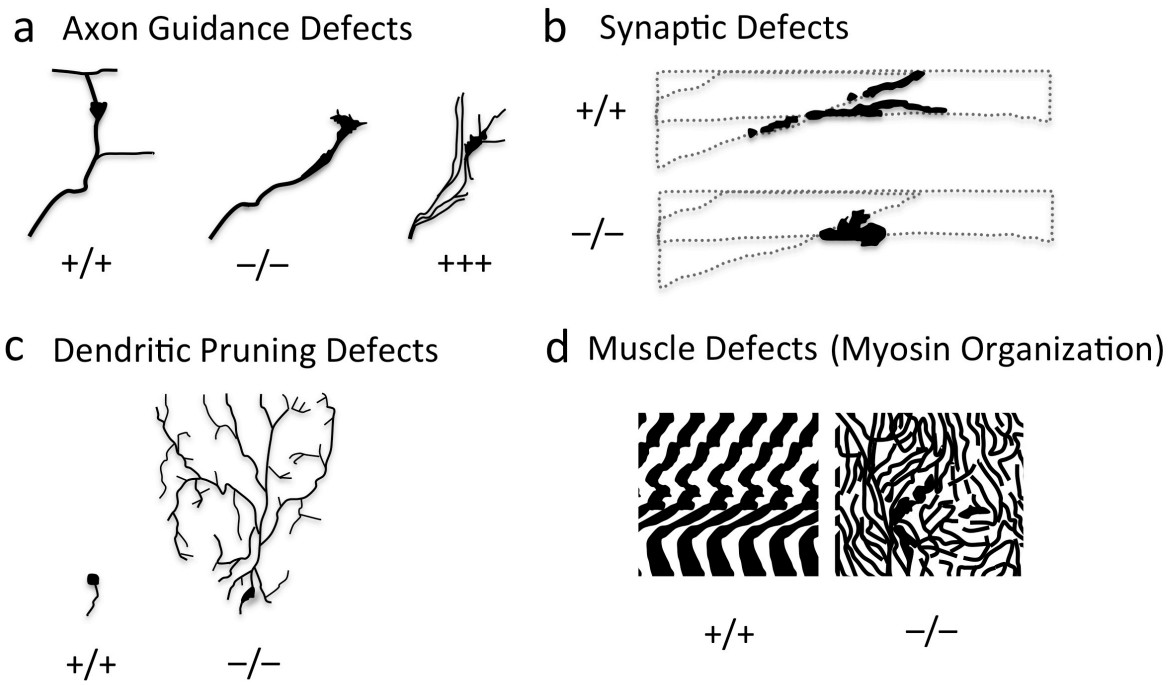

Figure 1.6. MICAL is Necessary and Sufficient to Regulate F-actin Organization *In Vivo*. (a-e) Mical is required for axon guidance (a), neuronal synapse formation (b), dendrite pruning (c), and muscle formation (d). Modified from (Beuchle et al., 2007; Hung et al., 2010; Kirilly et al., 2009; Tilney et al., 1998; Tilney et al., 1995; Yoon and Terman, submitted).

CHAPTER TWO

Mical Links Semaphorins to F-actin Disassembly

Previously published. **Hung, RJ**, U Yazdani, J Yoon, H Wu, T Yang, N Gupta, Z Huang, WJH van Berkel, JR Terman (2010), Mical links semaphorins to F-actin disassembly, ***Nature***, 463(7282):823-7. The characterization of *Drosophila* bristle morphology was performed by U Yazdani, J Yoon, and JR Terman. The axon guidance analysis was performed by T Yang and JR Terman.

Introduction

How instructive cues present on the cell surface exert their precise effects on the actin cytoskeleton is poorly understood. Semaphorins are one of the largest families of these instructive cues and are widely studied for their effects on cell movement, navigation, angiogenesis, immunology, and cancer (Tran et al., 2007). Semaphorins/Collapsins were characterized in part based on their ability to dramatically alter actin cytoskeletal dynamics in neuronal processes (Luo et al., 1993), but despite considerable progress in the identification of semaphorin receptors and their signaling pathways (Zhou et al., 2008), the molecules linking them to the precise control of cytoskeletal elements have remained a mystery. Recently, highly unusual proteins of the MICAL family of enzymes have been found to associate with the cytoplasmic portion of plexins, large cell surface semaphorin receptors, and mediate axon guidance, synaptogenesis, dendritic pruning, and other cell morphological changes (Beuchle et al., 2007; Kirilly et al., 2009; Schmidt et al., 2008; Terman et al., 2002). Interestingly, MICALs perform oxidation-reduction (Redox) enzymatic reactions (Gupta and Terman, 2008; Nadella et al., 2005; Schmidt et al., 2008; Siebold et al., 2005; Terman et al., 2002) and also contain domains found in proteins that regulate cell morphology (Suzuki et al., 2002; Terman et al., 2002). However, nothing is known of the role of MICAL or its Redox activity in mediating morphological changes. Here we report that Mical directly links semaphorins and their plexin receptors to the precise control of actin filament (F-actin) dynamics.

Results

MICAL family multi-domain cytosolic proteins (**Figure 2.1a**) mediate Semaphorin-Plexin repulsive axon guidance and cell morphological changes (Schmidt et al., 2008; Terman et al., 2002) but their role in orchestrating these events is unknown. While characterizing new hypomorphic *Mical* alleles**,** we found that surviving *Mical*$^{-/-}$ mutant adult flies exhibited abnormally shaped bristle cell processes that were straight, thick, bent, twisted, and/or had abnormal "club-like" or blunt tips (**Figures 2.1b-c; S2.1- S2.2**). These morphological defects were rescued by expressing Mical specifically in *Mical*$^{-/-}$ mutant bristles (**Figure 2.1c**), revealing that Mical is required for normal bristle process morphology. Bristle process elongation, like neuronal process extension, is actin-dependent such that bristles are formed during pupal development when a bristle cell extends an unbranched, slightly curved actin-rich cellular process (**Figure S2.2**). As development continues, a chitin cuticle external skeleton forms around the membrane of the elongated bristle, preserving a record in the adult fly of the actin organization in the developing bristle (**Figures 2.1b; S2.2**; (Tilney and DeRosier, 2005)). Consequently, the bristle process provides a simple, high-resolution model to characterize the molecules and mechanisms that regulate actin filament dynamics (Sutherland and Witke, 1999; Tilney and DeRosier, 2005). We wondered, therefore, if Mical was also sufficient to induce changes to bristle process morphology. Strikingly, Mical overexpression specifically in wild-type bristles generated branched bristles (**Figures 2.1d-e, i; S2.3**). To our knowledge, these bristle branching defects are more severe than any previously reported, and we did not find any

defects in bristle cell numbers or positioning, indicating that Mical exerts specific effects on cell morphology.

MICALs are unusual proteins that contain a Redox enzymatic domain, so we wondered if Mical's Redox activity was necessary for its specific effects on bristle shape. Indeed, point mutations that selectively disrupted the Redox domain as well as bristle-specific expression of a Mical$^{\Delta Redox}$ protein revealed that Mical's Redox activity was required for both normal bristle morphology and Mical -dependent bristle branching (**Figures 2.1f, i; S2.4**). In contrast, bristle-specific expression of the Mical Redox domain alone (Mical^{Redox}) was not sufficient for bristle branching (**Figure S2.4**), revealing Mical also requires at least some of its other domains to mediate its full effect. Interestingly, Mical also contains immediately C-terminal to its Redox domain a protein motif that is found in a number of cytoskeletal-associated proteins, a calponin homology (CH) domain (**Figure 2.1a**). Extraordinarily, bristle-specific expression of both the Mical Redox and CH domains alone (Mical^{RedoxCH}) further increased bristle branching (**Figures 2.1h-i; S2.4**), indicating that Mical^{RedoxCH} is constitutively active. These results, in combination with observations that bristle-specific expression of a Mical$^{\Delta CH}$ protein acted dominant-negatively (**Figures 2.1g, i; S2.4**), demonstrate that the Redox and CH domains of Mical are both necessary and sufficient to orchestrate specific cell morphological changes.

To better study the mechanisms underlying Mical-mediated morphological changes we directly examined developing bristles. During bristle process elongation, Mical localized to growing bristle tips in close proximity to the bristle cell membrane and at sites of bristle branching and actin localization (**Figures 2.2b, 2.3A-B**). Removing either the CH domain or the

C-terminus of Mical altered this selective localization (**Figures S2.4**), indicating that Mical might be locally regulating the actin cytoskeletal network that specifies bristle morphology. In motile cells and neuronal growth cones, the bulk of F-actin forms two types of arrays: the parallel arrays of bundled F-actin found in filopodia and the meshwork F-actin arrays found in lamellipodia. Like filopodia, Drosophila bristle processes contain pillar-like bundles of F-actin comprised of many individual actin filaments (**Figures 2.2a; S2.2**; (Tilney and DeRosier, 2005)). A record of this F-actin organization was observed in the highly ordered, parallel arrangement of grooves in adult wild-type bristles but not in *Mical*$^{-/-}$ mutants, whose adult bristles indicated disorganized, intersecting, and larger than normal F-actin bundles. Directly visualizing actin in developing bristles also revealed that the F-actin bundles in *Mical*$^{-/-}$ mutants were significantly larger than normal, abnormally positioned, and intersecting (**Figures 2.2c-d**). Interestingly, these *Mical*$^{-/-}$ mutant bristles resembled those bristles generated by overexpressing F-actin stabilizing proteins such as actin bundling/crosslinking proteins (Tilney and DeRosier, 2005), further indicating that Mical limits the size, abundance, and bundling of F-actin.

To further characterize Mical-mediated actin cytoskeletal regulation, we turned to our transgenic flies expressing different forms of Mical. In contrast to *Mical*$^{-/-}$ mutants, elevating the levels of full-length Mical or Mical^{RedoxCH} in bristles, but not Mical$^{\Delta Redox}$ or Mical$^{\Delta CH}$, generated bundles of F-actin that were significantly thinner than normal (**Figures 2.2c-d; S2.3**). Increasing Mical activity in bristles also induced a dramatic rearrangement of F-actin: a change from the normal parallel organization of bundled F-actin into a complex meshwork of short actin filaments (**Figures 2.2c; S2.3**). These Mical -mediated bristle alterations were similar to those

seen when F-actin is destabilized in bristles with either cytochalasin treatment (Geng et al., 2000; Guild et al., 2002; Tilney et al., 2000a; Turner and Adler, 1998) or with loss-of-function mutations in actin bundling/crosslinking proteins (Tilney and DeRosier, 2005). Therefore, Mical is a critical regulator of F-actin instability that is sufficient to reorganize parallel F-actin networks into complex, meshwork arrays.

Provocatively, previous results have indicated that the generation of short bundles of F-actin is required for the characteristic, slightly-curved morphology of Drosophila bristles (Tilney and DeRosier, 2005). Neuronal dendrites that extend alongside elongating bristles specify this actin arrangement and curved bristle shape (**Figure S2.2**), but little is known of the extracellular signals present on dendrites that direct these bristle alterations. Since Mical associates with the cytoplasmic portion of the semaphorin receptor, PlexA (Terman et al., 2002), we wondered if Mical-mediated actin destabilization in bristles was in response to semaphorin signals present on dendrites. Consistent with this hypothesis, we found that semaphorins localized to bristle-innervating dendrites while PlexA colocalized with Mical within bristles (**Figures 2.3a**). Likewise, increasing or decreasing PlexA levels or either of its transmembrane Sema-1a or Sema-1b ligands also resembled Mical-dependent morphological and F-actin defects (**Figures 2.2d; 2.3A; S2.5-8**). Moreover, decreasing Sema/Plexin signaling limited the actin destabilizing activity of full-length Mical, but not that of constitutively active Mical^{RedoxCH} or Mical proteins missing their plexin-interacting region (Mical$^{\Delta PIR}$; **Figures 2.3A, S2.8**). Indeed, both loss-of-function and dominant-negative Mical mutants dramatically suppressed/eliminated PlexA-

dependent bristle branching (**Figures 2.3A, S2.4**). These results indicate that Mical is both activated and required for semaphorin-induced F-actin destabilization.

Our genetic results, therefore, coupled with our observations that Mical and F-actin co-localize in vivo, indicate that Mical associates with F-actin or an F-actin regulatory protein and thereby targets the actin cytoskeleton for Semaphorin-dependent reorganization. To further address this hypothesis, we turned to in vitro assays and found that different forms of purified Mical protein ($Mical^{Redox}$ or $Mical^{RedoxCH}$), but not negative controls (BSA or the Nus solubility tag), directly associated with in vitro generated actin filaments (**Figures 2.3B; S2.9**). In contrast, neither of the purified Micals associated with in vitro generated microtubules (**Figures 3B; S2.11**), revealing that Mical selectively associates with F-actin. Likewise, the Mical-related Redox enzyme PHBH did not associate with F-actin (**Figures 2.3B; S2.9**), indicating that the Redox domain of Mical is a novel and specific F-actin binding module. In light of previous findings that Mical interacts with the cytoplasmic portion of the PlexA receptor (Schmidt et al., 2008; Terman et al., 2002), these new findings identify Mical as a direct physical link between the semaphorin receptor Plexin, present on the cell surface, and the F-actin cytoskeleton.

We next wondered if Mical directly alters actin dynamics. Mical uses the pyridine nucleotide NADPH as a required coenzyme for its Redox activity (Nadella et al., 2005; Schmidt et al., 2008) and our in vivo results reveal that Mical also requires its Redox domain to alter the actin cytoskeleton. Strikingly, activating purified $Mical^{Redox}$ or $Mical^{RedoxCH}$ protein with NADPH substantially decreased the rate, extent, and steady-state level of actin polymerization (**Figures 2.3C; S2.9**). These robust effects of Mical on actin dynamics were dependent on

NADPH concentration and were substantially reduced in the presence of the related pyridine nucleotide coenzyme NADH and eliminated in the presence of $NADP^+$ (**Figures S2.9-S2.10**). Likewise, these actin alterations were observed using very low, substoichiometric levels of Mical (**Figure S2.10**), further indicating that Mical regulates actin dynamics through its enzymatic activity. In contrast, Mical-related Redox enzymes (PHBH) and general Redox reaction products (H_2O_2 and/or $NADP^+$) showed little to no effect on actin dynamics (**Figures 2.3C,b; S2.9-S2.10**), further indicating the specificity of Mical-mediated F-actin alterations in vivo and in vitro. Moreover, activated Mical does not affect tubulin polymerization (**Figure S2.11**), revealing that Mical is a novel, specific, and selective regulator of F-actin dynamics.

Semaphorins were identified based in part on their ability to rapidly disassemble F-actin and "collapse" elongating neuronal growth cones (Fan et al., 1993; Luo et al., 1993) but the molecules directly mediating this effect have remained elusive. Employing actin depolymerization assays and EM analysis of purified proteins, we found that activated Mical directly induced actin depolymerization and significantly decreased actin filament length (**Figures 3C, b, c and 2.4A, S2.9**). These results are consistent with our in vivo observations and reveal that the critical semaphorin signaling molecule Mical is a direct effector of F-actin disassembly. In contrast, we found no evidence that activated Mical directly induced actin branching or altered the bundling ability of actin bundling/crosslinking proteins (**Figures 2.3C and 2.4A**), suggesting that Mical-dependent effects on branching and bundling in vivo are likely to be secondary to Micals ability to directly destabilize F-actin. To directly test this, we set up an in vitro assay with purified proteins that resembled the bundled organization of F-actin within

our in vivo bristle model. We found that activated Mical also directly disassembled bundled actin filaments, decreasing both their length and width (**Figures 2.4B**). Therefore, Mical is a novel F-actin disassembly factor that directly destabilizes both individual and bundled actin filaments.

Finally, we wondered if Mical was also sufficient to reorganize the actin cytoskeleton of navigating axons. Semaphorins mediate axon repulsion in part by locally disassembling the actin cytoskeleton within neuronal growth cones. Likewise, we found that Mical strongly localized to growth cones in vivo and played a critical role in the repulsion of Sema/PlexA-responsive axons (**Figures S2.12**; (Schmidt et al., 2008; Terman et al., 2002)). Furthermore, using GFP-actin to directly visualize actin cytoskeletal organization and growth cone complexity in vivo (Sanchez-Soriano and Prokop, 2005), we found that individual growth cones became significantly more complex with increased numbers of filopodia when constitutively active (but not dominant negative) forms of Mical are expressed within them (**Figure 2.4C**). These observations indicate that the redistribution of actin we see in neuronal growth cones, like what we observe in developing bristle processes and with purified Mical, is likely to result from direct Mical-mediated disassembly of actin filaments and F-actin bundles.

Discussion

We have identified here a previous unknown, Redox-dependent actin disassembly pathway that provides critical insights into the means by which semaphorins alter actin cytoskeletal dynamics and serve as navigational signals. Semaphorins have long been known to have localized

destabilizing effects on F-actin (Fan et al., 1993; Fan and Raper, 1995; Luo et al., 1993) that include a loss of F-actin (Fan et al., 1993), a decreased ability to polymerize new F-actin (Fan et al., 1993), a decrease in the number of F-actin bundles (Dent et al., 2004), and the extension of new branches (Campbell et al., 2001; Fenstermaker et al., 2004; Kapfhammer and Raper, 1987a; Liu and Halloran, 2005; Sakai and Halloran, 2006). Our results are consistent with these observations and indicate that Mical is sufficient to trigger each of these semaphorin/plexin-dependent events. Specifically, we find that Semaphorin-Plexin-Mical signaling directly destabilizes F-actin, which triggers a secondary response that produces branched meshwork actin and actin-rich extensions.

Our observations also provide a more complete understanding of the roles of repulsive guidance cues in vivo. In particular, we propose that repellents such as semaphorins disassemble or "prune back" the actin network in vivo, and that this "pruning" process initiates a cascade of events that enhances cellular complexity/plasticity. These Semaphorin-Plexin-Mical-induced actin rearrangements, therefore, in combination with what are likely to be Semaphorin-Plexin-dependent, but Mical-independent, effects on microtubules and substrate adhesion (Tran et al., 2007; Zhou et al., 2008), would enable navigating cells/axons to identify new, more permissive substrates and could underlie the directional changes associated with Semaphorin repulsive guidance. Indeed, neuronal growth cones develop complex morphologies with multiple extending filopodia when they encounter directional choice points in vivo (Broadie et al., 1993; Godement et al., 1994; Murray et al., 1998; Tosney and Landmesser, 1985), and these new filopodia probe the environment and ultimately lead the growth cone to a more permissive

substrate. Future work will seek to better understand these Mical-mediated events. These research directions are likely to be of significant biomedical importance given the roles of the more than twenty semaphorins in directing actin-dependent processes in neural connectivity, angiogenesis, immunity, and cancer.

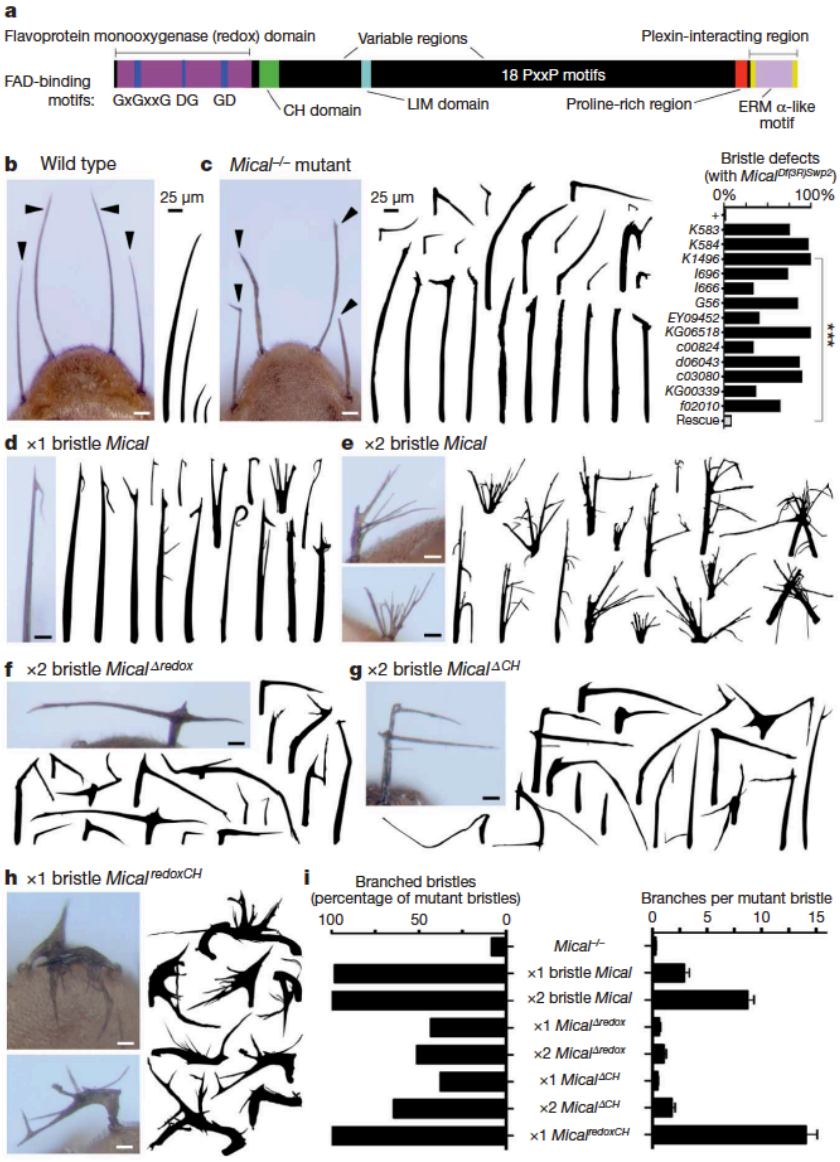

Figure 2.1. Mical regulates actin-rich cellular process morphology. **a,** Mical protein organization. FAD, flavin adenine dinucleotide; CH, calponin homology. **b,** Adult *Drosophila* bristles (arrowheads, drawings) are of varying length, unbranched, and slightly curved. **c-h,** *Mical* is necessary for normal bristle morphology and is also sufficient to alter morphology when one (x1) or two (x2) copies of different *Mical* transgenes are expressed specifically within bristles. Mutant, $Mical^{Df(3R)Swp2}$, n≥25 animals per genotype; chi-square test; *** = p<0.0001. **i**, Bristles resulting from $Mical^{-/-}$ and Mical overexpression are quantitatively distinct and the redox and CH domains of Mical are both required and together are sufficient for Mical-like bristle branching. For wild type, transgene or bristle-specific driver only, there is 0% branching. *n*≥25 bristles per genotype; data shown, mean ± s.e.m.; scale bars, 25µm.

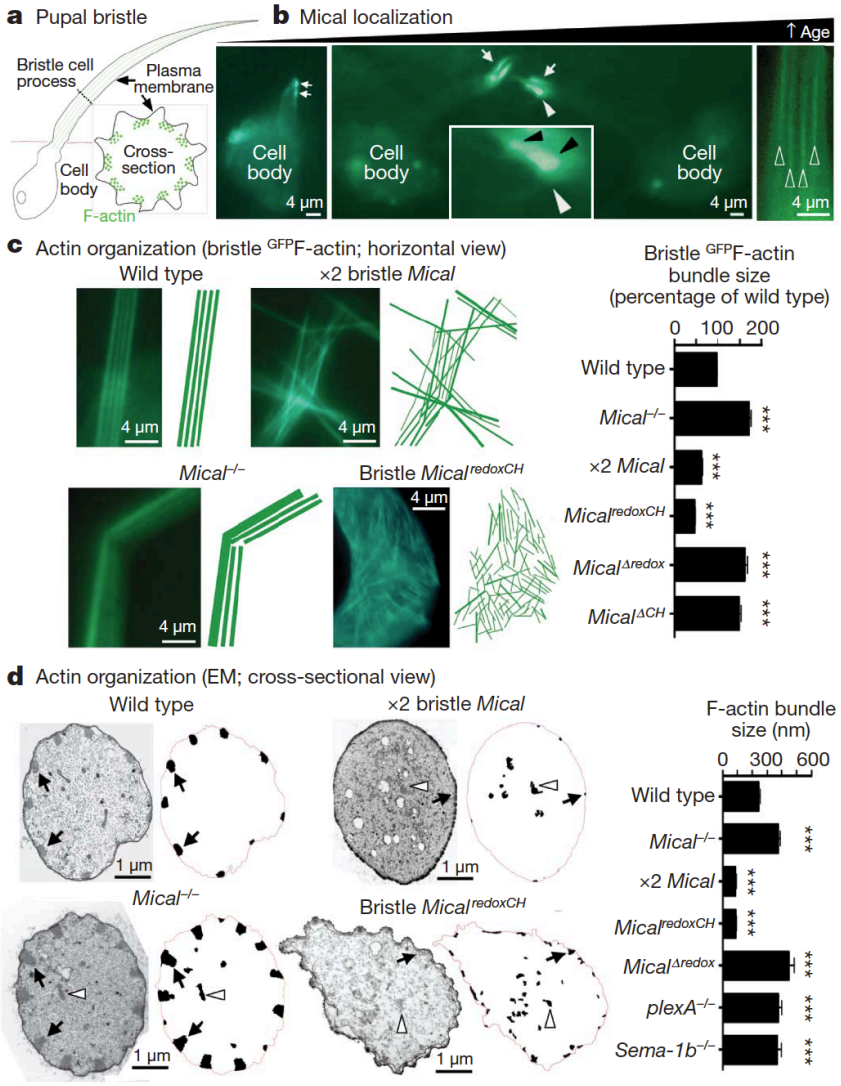

Figure 2.2. Semaphorin, plexin, and Mical control F-actin organization and bundling. a, A pupal bristle cell extends a membranous process containing F-actin (green lines, and circles seen in cross-section) bundled together adjacent to the membrane. **b,** ^{GFP}Mical (green) localizes to elongating pupal bristle tips (arrows) and adjacent (black arrowheads in a x3 magnified view, inset) to filopodial-like extensions/branches, which were not seen in wild type bristles. At older pupal ages, Mical localization forms an actin-like striped pattern (open arrowheads). The white arrowhead shows which region is seen at higher magnification in the inset. GFP, green fluorescent protein. **c, d,** Images and drawings of F-actin bundles. EM, electron microscopy. Membrane-associated (for example, arrows) and abnormally positioned (for example, arrowheads) bundles are drawn. n>80 F-actin bundles per genotype; ***, p<0.0001 (compared with wild type); data shown, mean ± s.e.m.

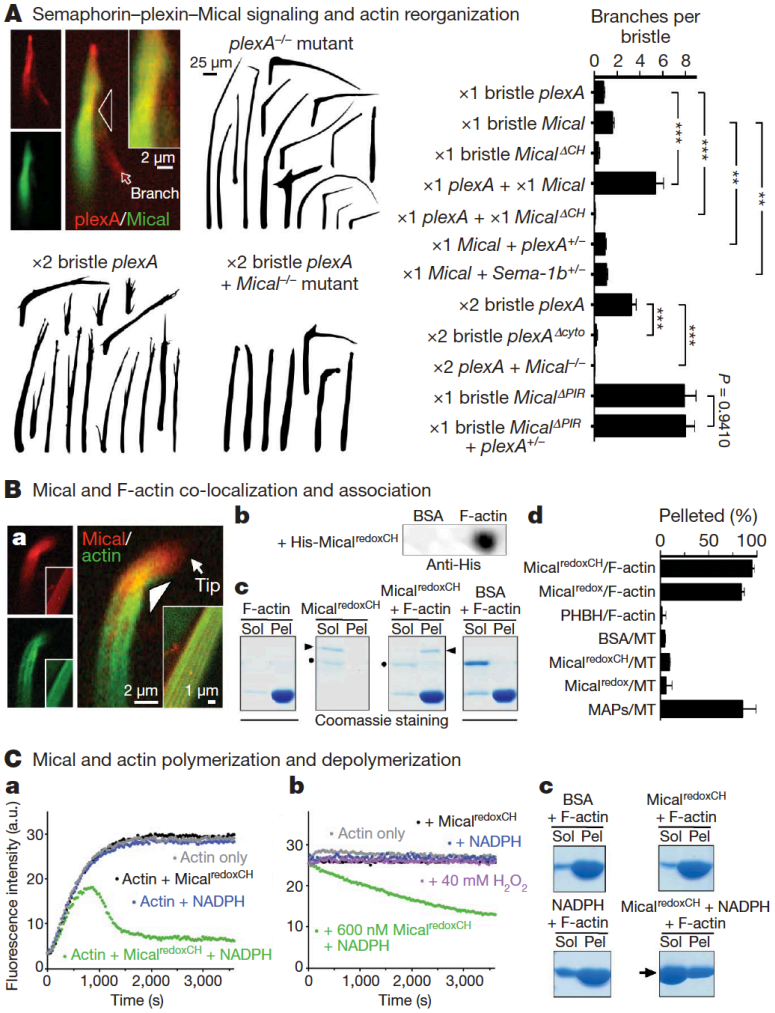

Figure 2.3. Semaphorin-plexin-mediated actin rearrangements require Mical, which binds and directly regulates actin dynamics. A, Mical (^{GFP}Mical) co-localizes (yellow) with PlexA at sites of bristle branch formation (arrowhead and inset at a x2 magnified view) and is activated and required for semaphorin-plexin-dependent branching; PIR, plexin-interacting region; cyto, cytoplasmic portion. $n \geq 28$ bristles per genotype; *t*-test; **=p<0.001, ***=p<0.0001; data shown, mean ± s.e.m. **B,** Mical co-localizes (yellow) with F-actin during early and late (inset) stages of bristle elongation (**a**). Purified Mical robustly and selectively associates with F-actin as revealed by dot-blot **(b)** and actin and microtubule co-sedimentation/pelleting (**c, d**) assays. Arrowheads, Mical^{redoxCH}; dots, Nus; MT, microtubules; BSA, bovine serum albumin; PHBH, *p*-hydroxybenzonate hydroxylase; MAPs, microtubule-associated proteins; Sol, G-actin (soluble); Pel, F-actin (pellet). $n \geq 2$ per condition; data shown, mean ± s.e.m. **C,** Pyrene-actin assays, where the fluorescence of polymerized pyrene-actin is higher than monomeric pyrene-actin, reveal that purified Mical^{redoxCH} protein + NADPH directly alters actin polymerization (**a**) and induces depolymerization (**b**), as do high-speed sedimentation/Commassie staining assays (**c**, arrow**)**. a.u., arbitrary units.

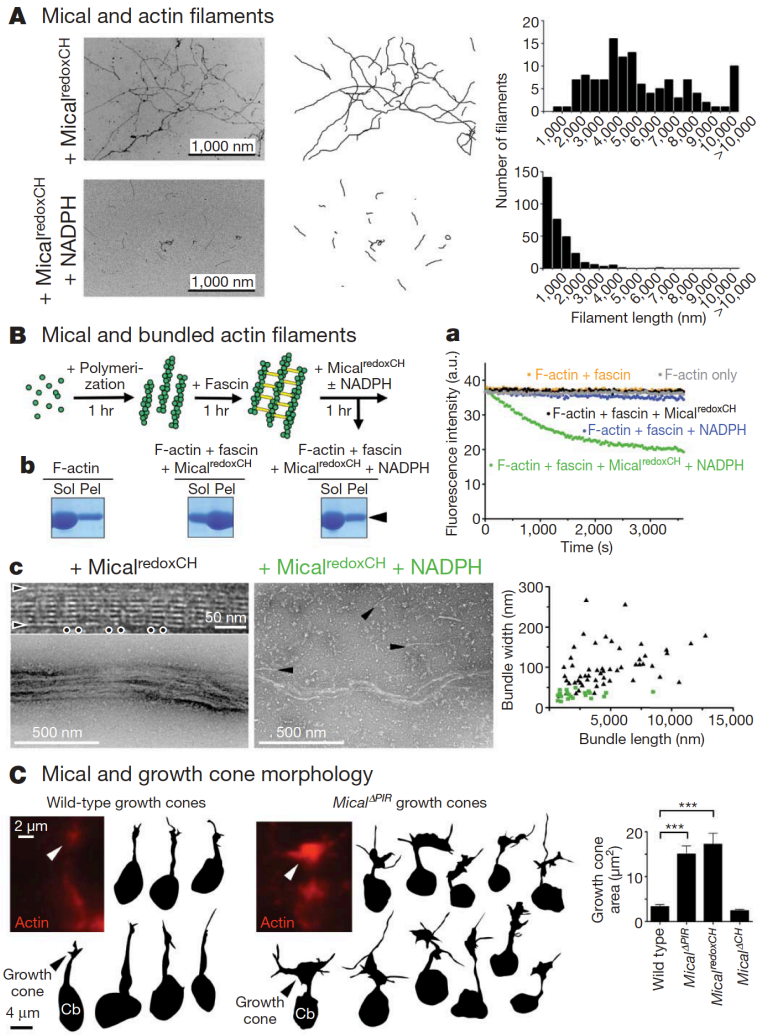

Figure 2.4. Mical directly disassembles F-actin and regulates growth cone morphology. A, Negative-staining electron microscopy shows that Mical^{redoxCH} + NADPH significantly decreases F-actin length; *n*>120 per treatment; *t*-test; p<0.0001. **B,** Actin (green) filaments bundled with fascin (yellow) are disassembled by Mical^{redoxCH} + NADPH, as seen using pyrene-labeled actin (**a**), low-speed sedimentation/Coomassie staining (**b**, arrowhead**),** and electron microscopy (**c**). Electron microscopy shows that, similar to untreated controls, F-actin bundles treated with Mical^{redoxCH} F-actin bundles (black triangles in graph) are well organized, long, and thick with "horizontally" arranged individual actin filaments (arrowheads) and repeating "vertical stripes" of fascin (dots). F-actin bundles treated with Mical^{redoxCH} + NADPH (green squares in graph) are significantly shorter and thinner (*n*>21 per treatment*; t*-test; p<0.0001) and disassemble into single actin filaments (arrowheads). **C,** Measuring the area occupied by GFP-actin (red) shows that Mical significantly alters growth cone size. Cb = neuronal cell body. *n*>40 growth cones per genotype; *t*-test; ***=p<0.0001; data shown, mean ± s.e.m.

Material and Methods

Drosophila Genetics, Molecular Biology, and Transgenic Lines

The genomic organization of the *Mical* locus and P element insertion sites were determined, with the aid of the Sequencher 4.6 program (Gene Codes, Ann Arbor, MI), using our identified cDNAs, DNA flanking the insertion sites of P elements, and publicly available Drosophila genomic DNA sequences. All complementation analysis and genetics were done using standard techniques (Terman et al., 2002; Yazdani et al., 2008). A single base-pair deletion was recently found in a previously employed (Terman et al., 2002) large, ~8.2kb, full-length *Mical* DNA and transgenic fly line (this line is now called $Mical^{N\text{-}ter}$; (Kirilly et al., 2009)), so multiple new lines of transgenic flies for both the full-length ~8.2kb "short" isoform of *Mical* (which is similar to $UAS{:}Mical^{FL}$; (Kirilly et al., 2009)) and the full-length $Mical^{G\rightarrow W}$ mutation ($Mical^{\Delta redox}$) were generated and utilized for all experiments. Similar phenotypes were seen in eight independent *UAS:Mical* transgenic lines (and these phenotypes resembled those seen after expression of the *Mical* genomic locus). Similar phenotypes were also seen in three independent $UAS{:}Mical^{\Delta redox}$ transgenic lines. The $UAS{:}^{GFP}Mical$ transgenic line was generated by inserting in-frame the full-length "short" isoform of Mical into an Xba I site of the pEGFP-C1 (Clontech) vector at the C-terminus of a GFP tag. An Nhe 1 – Xba I fragment containing GFP tagged *Mical* was then moved into an Xba I digested pUAST vector. Six independent $UAS{:}^{GFP}Mical$ transgenic lines were generated that showed a similar bristle phenotype. The $UAS{:}Mical^{\Delta CH}$ transgenic flies were generated by removing a portion of *Mical* corresponding to the calponin homology (CH)

domain of the Mical "short" isoform and moving the resultant cDNA into the pUAST vector. Five independent *UAS:Mical*$^{\Delta CH}$ transgenic lines were generated that showed similar bristle defects. The His-tagged *UAS:Mical*^{redox} and *UAS:Mical*^{redoxCH} transgenic lines were generated by excising both *Mical* cDNAs from our pET43.1bNG vector (Gupta and Terman, 2008) with KpnI and XbaI and moving them into the pUAST vector. Ten independent *UAS:Mical*^{redox} and five independent *UAS:Mical*^{redoxCH} showed similar bristle defects. The *UAS:Mical*$^{\Delta PIR}$ transgenic flies were generated by removing the region of Mical that interacts with the plexA receptor, the plexin-interacting region (PIR) (Terman et al., 2002), from the *Mical* "short" isoform and moving the resultant cDNA into the pUAST vector. Nine independent *UAS:Mical*$^{\Delta PIR}$ transgenic lines were generated that exhibited a similar bristle phenotype. Transgenic flies containing the HA-tagged plexA without its cytoplasmic portion (^{HA}*plexA*$^{\Delta cyto}$) (He et al., 2009) were generated by removing the cytoplasmic portion of the Drosophila plexA receptor (after the transmembrane portion and sequence YKKKSSE and including a restriction enzyme site and then a stop codon FR*) and it was placed in the pUAST vector. Five independent *UAS:* ^{HA}*plexA*$^{\Delta cyto}$ transgenic lines were generated that exhibited a similar bristle phenotype. All Drosophila embryo injections were done by BestGene, Inc. All other stocks are as previously described (Terman et al., 2002) or were obtained from the Bloomington Stock Center except *Mical*^{d06043}, *Mical*^{c00824}, *Mical*^{c03080}, *Mical*^{f02010}, *f01900* (Harvard Stock Collection), *UAS:GFP-Actin* and *Mical*^{GS15400} (Drosophila Genetic Resource Center, Japan), *Mical* point mutation stocks (kind gifts from Hermann Aberle),

B11-GAL4 (also called *P[GAL-4]B-11* and *B11-98*; a kind gift from John Merriam; (de la Cova et al., 2004; Guild et al., 2003; Hopmann and Miller, 2003; Tilney et al., 2003; Tilney et al., 2004; Tilney and DeRosier, 2005)), *plexA^{YD0269} and Sema-1a^{P01432}* (kind gifts from Lynn Cooley; (Kelso et al., 2004)), *UAS:Sema-1a* (a kind gift from Alex Kolodkin; (Yu et al., 1998)), and *UAS:Sema-1b* (a kind gift from Corey Goodman; (Winberg et al., 1998)).

Genotypes Employed

Only one copy of the bristle specific driver (*B11-GAL4*) was used in all experiments. *Wild-type (w^{1118})*, x1 bristle *Mical* (*UAS:Mical/+; B11-GAL4/+*), x2 bristle *Mical* (*UAS:Mical/UAS:Mical; B11-GAL4/+*), x1 bristle *Mical$^{\Delta redox}$* (*UAS:Mical$^{G\rightarrow W}$/+; B11-GAL4/+*), x2 bristle *Mical$^{\Delta redox}$* (*UAS:Mical$^{G\rightarrow W}$/UAS:Mical$^{G\rightarrow W}$; B11-GAL4/+*), x1 bristle *Mical$^{\Delta CH}$* (*UAS:Mical$^{\Delta CH}$/+; B11-GAL4/+*), x2 bristle *Mical$^{\Delta CH}$* (*UAS:Mical$^{\Delta CH}$/UAS:Mical$^{\Delta CH}$; B11-GAL4/+*), x1 bristle *Mical^{redoxCH}* (*UAS:Mical^{redoxCH}/+; B11-GAL4/+*), x1 bristle *Mical^{redox}* (*UAS:Mical^{redox}/+; B11-GAL4/+*), x2 bristle *Mical^{redox}* (*UAS:Mical^{redox}/UAS:Mical^{redox}; B11-GAL4/+*), x1 bristle *Mical$^{\Delta PIR}$* (*UAS:Mical$^{\Delta PIR}$/+; B11-GAL4/+*), x1 bristle *plexA* (*UAS:^{HA}plexA/+; B11-GAL4/+*), x2 bristle *plexA* (*UAS:^{HA}plexA/UAS:^{HA}plexA; B11-GAL4/+*), x1 bristle *plexA$^{\Delta cyto}$* (*UAS:^{HA}plexA$^{\Delta cyto}$/+; B11-GAL4/+*), x2 bristle *plexA$^{\Delta cyto}$* (*UAS:^{HA}plexA$^{\Delta cyto}$/UAS:^{HA}plexA$^{\Delta cyto}$; B11-GAL4/+*), x1 bristle *Sema-1a* (*UAS:Sema-1a/+; B11-GAL4/+*), x1 bristle *Sema-1b* (*UAS:Sema-1b/+; B11-GAL4/+*), x1 neuron/bristle *Sema-1a* (*UAS:Sema-1a/+; Sca-GAL4/+*), x1 neuron/bristle *Sema-1b* (*UAS:Sema-1b/+; Sca-GAL4/+*), x2 neuron/bristle *Sema-1b* (*UAS:Sema-1b/UAS:Sema-1b; Sca-GAL4/+*). Bristle specific rescue of *Mical$^{-/-}$* mutant experiments: (*UAS:Mical/+; Mical^{K1496}/Df(3R)swp2, B11-GAL4* or *UAS:Mical$^{\Delta CH}$/+; Mical^{K1496}/Df(3R)swp2,*

B11-GAL4). UAS-GFPactin5c/+; B11-GAL4/+ was used as "*wild-type"* to analyze developing bristle processes.

Adult Bristle Phenotype Characterization

Adult flies were examined in entirety for alterations to their large bristles (macrochaetae; Figure S2.2) since these bristles were easily visualized under a dissecting microscope. Adult bristle phenotypes were examined and quantified by crossing adults at 25°C and then flies were sorted by genotype, and then examined under a dissecting microscope (Leica Stereo Zoom S8 APO). Quantification of bristle defects was only performed on young, recently emerged adult offspring, since we noticed that adult bristles and their branches can become damaged as flies move around their surroundings and bump into each other. Bristles were scored for easily noticeable defects in morphology including splitting, branching, bending, and alterations to their tips. Adult flies containing one or more bristles showing any of these alterations were scored as containing bristle defects. It should also be noted that many mutant bristles were straighter than normal (*wild-type* bristles are slightly curved) without any other noticeable defects under the dissecting microscope. However, since the straightness of a bristle, as well as modifications to bristle length and diameter were harder to ascertain under a dissecting microscope, these particular phenotypes were not used as criteria for determining whether flies exhibited bristle morphological defects. Therefore, the percentage of mutant flies we documented containing bristle defects may under-represent the actual percentage of mutants containing these defects. Furthermore, it is likely that we under-represented the percentage of mutants containing bristle defects since mutant offspring from many of the combinations of mutant alleles for *Mical*, *plexA*,

Sema-1a, and *Sema-1b* died before adulthood and were therefore not examined.

Developmental Staging, Dissection, and Analysis of Drosophila Embryos and Pupae

Drosophila embryos were collected, processed, staged, dissected, and analyzed as previously described (Terman et al., 2002). All pupae were staged in accordance with the beginning of puparium formation (Bainbridge and Bownes, 1981). In general, bristles appear at 31 hours after puparium formation and by 60 hours the cuticle forms and the actin bundles disappear (Tilney et al., 1995). All preparation, staging, and dissection of pupae were done as described (Tilney et al., 1996; Tilney et al., 1995) with our minor modifications. In brief, white pre-pupae were collected from the sides of culture bottles for each stock, placed on double-sided tape (3M) within Petri-dishes, and returned to a 25°C incubator to allow the pupae to reach the desired stage. Pupae were then genotyped as necessary with the aid of GFP balancer chromosomes and then either prepared for whole-mount observation or dissection. Pupae were prepared for dissection by opening the outer pupal case with fine forceps (Ted Pella Inc) and placed with their ventral surface on double-sided tape. Pupae were then immersed in phosphate-buffered saline (PBS) and small incisions were made along both sides of the thorax above the wing buds. Using microscissors (Curved Gills Welsh Vannes, Storz Co.), incisions were then made at anterior and posterior positions such that the dorsal surface of the thorax could be removed for further processing. Dissected and whole-mount pupae were then fixed in 2% formaldehyde in PBS followed by washes in 0.1% Triton X-100/PBS.

Histochemical Analysis of Embryos and Pupae and Axon Guidance Assays

Dissected dorsal thoraces of pupae were fixed and stained to visualize F-actin by incubation in 0.1% Triton X-100 containing 10^{-6} M phalloidin conjugated to Alexa Fluor 594 (Molecular Probes) at 4°C overnight in the dark. Thoraces were then washed, mounted on slides in Citiflour (Ted Pella Inc. Redding, CA), and coverslipped. All embryonic (Terman et al., 2002) and pupal immunostaining (Tilney et al., 2000b) and assessment of axon guidance (Huang et al., 2007; Terman et al., 2002) was done using standard approaches. In brief, whole-mount embryos or dissected pupal thoraces were fixed, washed in PBS containing 0.1% Triton, and incubated in antibodies to Mical (1:2000; (Terman et al., 2002)), Sema-1a (1:3000; a kind gift from Alex Kolodkin (Yu et al., 1998)), plexA (1:500; a kind gift from Liqun Luo (Sweeney et al., 2007)), Fasciclin II (1:4, 1D4 supernatant, (Van Vactor et al., 1993)), GFP (1:500 ,3E6, Invitrogen or 1:3000, A-6455, Invitrogen), HA (1:200, BMG-3F10, Roche), or a 6X His-tag (1:500; 70796, Novagen or R930-25, Invitrogen).

Microscopy and Imaging, Drawings, Genetic Interaction Assays, and Quantification

Genotyping of pupae was done with the aid of GFP balancers and using a Zeiss Discovery M^2 Bio stereomicroscope fitted with a GFP filter. Adult bristles were imaged under the compound microscope by removing bristles and placing them on a slide in 70% glycerol and then coverslipping them. Pupae were imaged under the compound microscope by placing whole-mount pupae in a depression well slide (Fisher), covering them with Citifluor (Ted Pella, Inc.) or Vectashield (Vector Labs), and coverslipping them. Brightfield, darkfield, DIC, and

fluorescence visualization and imaging was done using a Zeiss Axioimager upright microscope and images were captured using a Zeiss Axiocam HR camera and Zeiss Axiovision software. The "thickness" of F-actin bundles in different genetic backgrounds (5 animals/genotype) was determined at the same level of scutellar bristles of age-matched pupae by measuring the "width" of bundled GFP-labeled actin using Zeiss Axiovision software following capturing of the images using a Zeiss Axioimager upright microscope and a Zeiss Axiocam HR camera. All co-localization analysis and imaging with multiple flurophores was done in a single plane with the aid of a Zeiss Apotome optical sectioning tool (Bauch and Schaffer, 2006) or a Zeiss LSM510 Confocal microscope. The images and drawings of the adult bristles were done with the aid of a Zeiss Discovery M^2 Bio stereomicroscope, a motorized focus and zoom, and three-dimensional reconstruction software (Zeiss Axiovision software and Extended Focus Software [a kind gift from Bernard Lee]). Quantification of the number of bristle branches was done utilizing these images and drawings such that the number of mutant bristles that contained branches was counted for each genotype and the results were presented as a percentile of the total number of mutant bristles examined. The number of branches on each mutant bristle examined was then determined for each genotype and the results were presented as the mean number of branches per bristle ($\pm$ the standard error of the mean (SEM)). All quantification used for the genetic interaction analyses (*Plexin* and *Mical* genetic interactions) was performed blinded to genotype using one of the transgenic lines that showed weaker expression of Mical (x1 *Mical*) since it was found to give rise to bristle branches of relatively similar shape, position, size, and number. In addition, the same four scutellar bristles were quantified in each animal, allowing for precise

comparison from animal to animal since the bristle morphology of the same four cells could be quantitatively assessed. Any deviation from the main shaft of the bristle was considered a branch. For example, a bent bristle would not be considered to have a branch because there was no deviation from the main shaft. The shaft was simply bent. In contrast, a "cross" shaped bristle would be considered to have a branch since the main shaft of the bristle gave rise to a new process (the "crossbar"). Quantification of axon guidance defects was done using standard approaches (Huang et al., 2007; Terman et al., 2002; Yu et al., 1998). To examine a role for Mical in mediating actin reorganization within growth cones, we utilized the developing embryonic Drosophila nervous system and expressed different proteins selectively in aCC/RP2 pioneer motor neurons using the *RN2-GAL4* driver (Fujioka et al., 2003; Sanchez-Soriano and Prokop, 2005). Determining the area of the actin containing growth cones in different genetic backgrounds was done in age-matched embryos by normalizing to a similar level of fluorescence intensity and measuring the area of GFP-actin immunostaining in the tips of axons using Zeiss Axiovision software following capturing of the images with a Zeiss Axioimager upright fluorescence microscope and a Zeiss Axiocam HR camera. All of the GFP-actin labeled aCC/RP2 growth cones in $\geq$3 age-matched animals/genotype were measured (n>40). All quantitative data was analyzed with the aid of GraphPad and Prism software packages. Brightness, contrast and color balance of images and backgrounds were adjusted using Adobe Photoshop or Microsoft Powerpoint software.

All examination of pupae using the transmission electron microscope was done using standard approaches (Tilney et al., 1998). In brief, age matched pupae from different genotypes

(2 animals/genotype) were collected, attached to double-sided tape (3M), and the pupal case was opened with fine forceps (Ted Pella Inc). Pupae were then immediately placed in fixative (2% glutaraldehyde in 0.05 M phosphate buffer at pH 6.8) at which time the posterior end of the abdomen, the wing buds, and the anterior portion of the head were cut off to allow the fixative to penetrate the pupae. After fixation, the pupae were washed in water to remove the phosphate, stained with 1% uranyl acetate, dehydrated in acetone, and embedded in the proper orientation in Epon. Sections through the pupae were then cut in the transverse or horizontal plane using a diamond knife and these sections were then stained with uranyl acetate and lead citrate and then examined and photographed using a transmission electron microscope (FEI Tecnai G2 Spirit Biotwin). The shape of the microtubules in our sections (i.e., whether they were cut transversely or angled) was also used to verify the plane of orientation. For uniformity across different genetic backgrounds, the measurements of the F-actin bundles was determined on sections through scutellar bristles cut at the same level (i.e., they were of the same diameter) at the tips of the bristles.

Protein Purification

The Mical^{redoxCH} protein was generated by PCR-amplifying the appropriate portion of *Mical* (amino acids 1-669) and inserting into the modified pET43.1bNG vector we had previously generated (Gupta and Terman, 2008). The Mical^{redoxCH} expression construct was then transformed into *Escherichia coli* Rosetta2 (DE3) (pLysS) (Novagen) and grown in TB. In general, all bacterial transformations, culturing, isopropyl-β-D-thiogalactoside (IPTG) induction,

collection of lysates, analysis of protein expression, and Ni^{2+} purification of the six histidine (His)-tagged protein were performed as previously described (Gupta et al., 2007; Terman et al., 2002). In particular, expression was induced by the addition of 0.2 mM IPTG, and cells were grown for 24 hours at 14ºC before harvesting by centrifugation. Pellets were frozen and then subjected to resuspension in lysis buffer and sonication. Sonicated lysates from $Mical^{redoxCH}$ expressing bacteria were then bound to Ni^{2+} beads, and following elution of the protein, the protein was dialyzed into a storage buffer and digested with thrombin (100 mg/mL). The digested samples were then bound again to the Ni^{2+} beads and eluted to separate $Mical^{redoxCH}$ protein from the Nus tag. After examining several different pH and ionic concentrations for storage and experimental buffers (Gupta and Terman, 2008), the $Mical^{redoxCH}$ protein was utilized for experiments. Similar methodology were utilized to purify the $Mical^{redox}$ protein following PCR-amplification of the appropriate portion of Mical (amino acids 44-531) and insertion into the pET28 vector (Gupta and Terman, 2008). These samples were analyzed for purity on Commassie stained gels and via western analysis with His-tag (1:1000; Novagen) and Nus-tag (1:10,000; Novagen) antibodies. Multiple batches of our $Mical^{redox}$ and $Mical^{redoxCH}$ protein were purified and exhibited similar results in our biochemical assays.

PHBH protein purification was as described (Eschrich et al., 1990; van Berkel et al., 1992). The Drosophila Fascin/Singed protein was generated by obtaining the full-length cDNA (RH62992; Open Biosystems), PCR-amplifying the full-length *fascin* with primers (Forward: 5'- AGCTGGATCCATGACGCGAATCATTACGTC -3', Reverse: 5'- AGTCAAGCTTCTAGAACTCCCACTGTGTGGCCGA -3'), digesting the resultant PCR

product with BamHI and HindIII and inserting it into the His-tagged bacterial expression vector ppSUMO (a kind gift from Xuewu Zhang). Fascin-ppSUMO was then transformed into competent cells and the bacteria was inoculated into 150 mL TB medium (30 μg/mL kanamycin, 2 mM $MgSO_4$, 20 μg/mL gentamycin) and shaken at 250 rpm overnight at 37°C. The 150 mL of culture medium was then divided into 6 x 1L TB medium (30 μg/mL kanamycin, 2 mL Antifoam B emulsion (Sigma, A6707-500ml) per liter). After shaking at 30°C for 8-10 hours, IPTG was added to 0.5 mM final concentration and the medium was incubated at low temperature with shaking for 24 hours. The bacteria was then pelleted and frozen in liquid nitrogen. In order to harvest the fascin protein, the pellet was thawn at RT and suspended in 100 mL lysis buffer (50 mM Tris-HCl, 500 mM NaCl, 3 mM β-mercaptoethanol, 20 mM imidazole, 1 tablet of Roche Proteinase Inhibitors Cocktail). After sonication and centrifugation, the supernatant was filtered with a 0.45 μm filter and loaded onto a 5 mL HisTrapFF- affinity column (GE) with Buffer Ni-A (10 mM Tris-HCl pH 8.0, 500 mM NaCl, 5% glycerol, 3 mM β-mercaptoethanol, 20 mM imidazole) and protein was eluted with Ni-B buffer (10 mM Tris, pH 8.0, 500 mM NaCl, 5% glycerol, 3 mM β-mercaptoethanol, 250 mM imidazole). 100 μg SUMO proteinase was added into the sample and incubated at 4°C overnight to remove the SUMO and His tags. The digested sample was then loaded on a 1 mL HisTrapFF affinity column (GE) with Ni-A and Ni-B buffers to separate out the SUMO-His tag. After desalting with Q-A Buffer (10 mM Tris-HCl, pH 8.0, 10 mM NaCl, 5% glycerol, 1 mM DTT), the sample was loaded onto a UnoQ column (Bio-Rad) with Q-A buffer and Q-B buffer (10 mM Tris-HCl, pH 8.0, 1 M NaCl, 5% glycerol, 1 mM DTT). Under these conditions, the Drosophila fascin protein does not bind very well to the UnoQ

column and the flow-through was collected that contained fascin. The Drosophila Fascin protein was then concentrated (Ultracel-10k [Millipore]) and placed in storage buffer (10 mM Tris-HCl, pH 8.0, 50 mM NaCl, 5% glycerol, 1 mM DTT), aliquoted, frozen with liquid nitrogen and stored at -80°C. The protein samples were then analyzed for purity on Coomassie stained gels and via western analysis with a Drosophila Fascin monoclonal antibody (1:50; sn 7C; Developmental Studies Hybridoma Bank; (Cant et al., 1994)). Multiple batches of the fascin protein were purified and exhibited similar results in our biochemical assays. These results are similar to those previously described with purified Drosophila fascin (Cant et al., 1994).

The Drosophila α-actinin protein was generated by obtaining the full-length cDNA from the Open Biosystems Drosophila Gene Collection 1.0 (DGC1.0) library (LD37956). α-actinin cDNA was amplified with primers (Forward: 5'-CGACAAGCTTGCATGATGATGGAGAACGGACT -3', Reverse: 5'-ACTGCTCGAGTTACAAGTCGGTCTCGCCGTAGA -3') and the PCR product was digested with HindIII and XhoI and inserted into the His-tagged ppSUMO vector. Transformation, induction, culturing, lysate preparation, Nickel-column purification, SUMO proteinase digestion, and desalting was done as described for fascin and the protein samples were analyzed for purity on Coomassie stained gels. The His-tagged α-actinin protein was also analyzed via western analysis with a His antibody (1:10,000; 70796, Novagen). The enriched sample was then loaded on a MonoQ column (GE Company) with Q-A buffer and Q-B buffer (10 mM Tris-HCl, pH8.0, 1 M NaCl, 5% glycerol, 1 mM DTT) to further enrich for α-actinin. The Drosophila α-actinin protein was then concentrated (Ultracel-50k [Millipore]), placed in storage buffer (10 mM Tris-

HCl, pH 8.0, 100 mM NaCl, 5% glycerol, 1 mM DTT), and then the α- actinin protein was aliquoted, frozen, and stored as described for fascin.

Dot Blot Assays

Standard approaches (Luna, 1998; Magi and Liberatori, 2005) were used in multiple independent experiments such that 10 μL of either a 10 μM solution of F-actin (Cytoskeleton, Inc) or BSA were spotted in the center of circles drawn on nitrocellulose membrane (Millipore) which was then air-dried for 10 minutes at room temperature, subjected to UV crosslinking for 10 seconds, and then blocked with 5% BSA in PBST (0.05% Tween 20 in PBS, pH7.4) for 1 hour at room temperature. The treated nitrocellulose membrane was then incubated with 50 μL of 2.4 μM solution of purified His-tagged Mical^{redoxCH} protein diluted in a general actin resuspension buffer (5 mM Tris-HCl pH8.0, 0.2 mM $CaCl_2$) for 30 minutes at room temperature. 5 mL of the general actin resuspension buffer was then added to the membrane and incubated for 30 minutes at room temperature with shaking followed by three, ten minute washes with PBST. The membrane was then incubated for one hour at room temperature in a His antibody (1: 1000; Novagen) diluted in 5% BSA/PBST. The membrane was then washed three times in PBST for 10 minutes each, and incubated with a HRP-conjugated secondary antibody (1:10,000; Amersham) for one hour at room temperature. Following washes with PBST (five times, ten minutes each), the membrane was incubated in a chemiluminescent detection reagent (Pierce) and exposed to film.

F-Actin and Mical High-speed Co-sedimentation Assays

Standard approaches in multiple independent experiments were used for Co-sedimentation assays (Yin and Stossel, 1979). In short, purified non-muscle actin (85% β-actin, 15% γ-actin; Cytoskeleton, Inc.) or muscle actin (Cytoskeleton, Inc.) was resuspended to 1 mg/mL in a general actin resuspension buffer (5 mM Tris-HCl pH8.0, 0.2 mM $CaCl_2$). The resuspended actin was then added to a standard actin polymerization buffer (50 mM KCl, 2 mM $MgCl_2$, and 1 mM ATP) and allowed to polymerize for 1 hour at room temperature. This generated an F-actin stock at 23 μM actin. $Mical^{redoxCH}$ protein (0.3-1 μM final concentration), $Mical^{redox}$ protein (0.3-1μM final concentration), PHBH protein (2 μM final concentration), a negative control (2 μM final concentration, bovine serum albumin (BSA), Cytoskeleton, Inc), and positive controls (the actin binding proteins rabbit α-actinin [2 μM final concentration; Cytoskeleton, Inc]; Drosophila α-actinin [2 μM final concentration] and Drosophila Fascin [2 μM final concentration]) were subjected to initial (clarification) high-speed centrifugation at 150,000 x g for 1 hour at 4°C. Test proteins were then added to separate tubes and incubated with either F-actin (the final concentration was varied from 0.5-18 μM) or with F-actin buffer only for 30 minutes at room temperature. An F-actin only tube was also incubated for 30 minutes at room temperature. All test tubes were then subjected to high-speed centrifugation at 150,000 x g for 1.5 hours at 24°C. Supernatants were carefully removed and added to sample buffer for loading on an SDS-PAGE gel. The pellet was resuspended in Milli-Q H_2O with pipetting, incubation on ice for 10 minutes, and then more pipetting before being added to sample buffer for loading on an SDS-PAGE gel. The gel was then stained with Coomassie blue using standard approaches. The intensity of each

of the stained bands in the pellet and soluble fraction was then analyzed and quantified by densitometry using Image J (NIH) and the percentage of different purified proteins with F-actin in the pelleted fraction was presented.

Actin Polymerization and Depolymerization Assays

The actin polymerization assay was performed using standard approaches ((Cooper, 1992a); Cytoskeleton, Inc.). Briefly, purified rabbit skeletal muscle actin (pyrene-labeled; Cytoskeleton, Inc) was used to monitor actin polymerization since the fluorescence intensity of the pyrene-labeled polymer is substantially higher than the pyrene-labeled monomer. G-actin (monomeric actin) was resuspended to 9.2 μM in a G-actin buffer (5 mM Tris-HCl pH 8.0, 0.2 mM $CaCl_2$, 0.2 mM ATP and 1 mM DTT) and incubated on ice for 1 hour. Before all the experiments, G-actin solution was centrifuged for 1 hour at 100, 000 x g at 4^o C to remove residual actin nucleating centers. Multiple independent experiments were performed for each condition such that $Mical^{redoxCH}$, $Mical^{redox}$, PHBH, NADPH (MP Biomedicals), NADH (MP Biomedicals), $NADP^+$ (AppliChem, GmbH), and/or hydrogen peroxide (EMD Chemicals, Inc.) was then added to the actin and polymerization was initiated at 25^o C by the addition of 5 mM Tris-HCl pH 7.5, 50 mM KCl, 2 mM $MgCl_2$, 1 mM EGTA, 0.5 mM DTT, and 0.2 mM ATP. Actin was used at a final concentration of 1.1 μM. Fluorescence intensity was immediately monitored at 407 nm with excitation at 365 nm by a fluorescence spectrophotometer (Spectra max M2; Molecular Devices).

To examine the ability of Mical to induce depolymerization in conditions that favored polymerization, multiple independent experiments were performed essentially as described for our actin co-sedimentation experiments except pyrene-labeled muscle actin was used. In brief, pyrenyl-G-actin (pyrene-labeled; Cytoskeleton, Inc) was polymerized in 5 mM Tris-HCl pH 7.5, 50 mM KCl, 2 mM $MgCl_2$, 1 mM EGTA, 0.5 mM DTT, and 0.2 mM ATP for 1 hour at room temperature resulting in a 1.1 μM concentration of F-actin. Mical^{redoxCH}, NADPH, and/or hydrogen peroxide was then added to the polymerized actin and fluorescence intensity was immediately monitored as described above.

Actin depolymerization assays were also performed using a standard dilution induced approach ((Cooper, 1992a); Cytoskeleton, Inc.). Pyrenyl-G-actin (pyrene-labeled; Cytoskeleton, Inc) was resuspended to 23 μM in the G- actin buffer described above and was polymerized in a weak polymerization buffer (1.25 mM Tris-HCl pH 7.5, 12.5 mM KCl, 0.5 mM $MgCl_2$, 0.25 mM EGTA, 0.125 mM DTT, and 0.05 mM ATP) for 1 hour at room temperature. Depolymerization was initiated by performing a five-fold dilution with G-actin buffer in the presence or absence of Mical^{redoxCH} and/or NADPH and multiple independent experiments were performed for each condition. After dilution, fluorescence intensity was immediately monitored at 407 nm with excitation at 365 nm by a fluorescence spectrophotometer (Spectra max M2; Molecular Devices).

Detecting the G- to F-actin Ratio

Purified non-muscle actin (85% β-actin, 15% γ-actin; Cytoskeleton, Inc.) was resuspended to 1 mg/mL in a general actin resuspension buffer (5 mM Tris-HCl pH8.0, 0.2 mM $CaCl_2$). The resuspended actin was then added to a standard actin polymerization buffer (50 mM KCl, 2 mM $MgCl_2$, and 1 mM ATP) and allowed to polymerize for 1 hour at room temperature. This generated an F-actin stock at 23 μM actin. Our purified Mical^{redoxCH} protein (2.4 μM final concentration), and/or NADPH (200 μM final concentration) was then added to separate tubes and incubated with this F-actin stock (18.6 μM final concentration) for 30 minutes at room temperature. All test tubes were then subjected to high-speed centrifugation at 150, 000 x g for 1.5 hours at 24^{o}C. Supernatants were carefully removed and added to sample buffer for loading on an SDS-PAGE gel. The pellet was resuspended in Milli-Q H_2O with pipetting, incubation on ice for 10 minutes, and then more pipetting before being added to sample buffer for loading on an SDS-PAGE gel. The gel was then stained with Coomassie blue.

Actin Filament Bundling Assays

Multiple independent experiments with minor variations which showed similar results were performed to characterize the ability of either purified Drosophila fascin, purified Drosophila α-actinin, or purified Mical^{redoxCH} to bundle actin filaments using standard low-speed co-sedimentation approaches (since this approach differentiates between unbundled actin filaments and bundled actin filaments). In brief, purified non-muscle (85% β-actin, 15% γ-actin; Cytoskeleton, Inc.) or muscle actin (Cytoskeleton, Inc.) was allowed to polymerize for 1 hour at room temperature as described above for all of our actin polymerization experiments. Multiple

independent experiments with a range of actin filament and test protein concentrations were then used to examine actin filament bundling and each of these experiments exhibited similar results. In particular, F-actin (4 μM - 18.6 μM final concentration) was incubated with purified Drosophila Fascin (2 μM), purified Drosophila α-actinin (2 μM), purified rabbit α-actinin (2 μM; Cytoskeleton, Inc.) or purified Mical^{redoxCH} (2.5 μM) for 30 – 60 minutes at room temperature. In some cases, with similar results, 20 mM Tris-HCl pH 6.5 was added to the bundling mixture since these conditions were recommended for use with rabbit α-actinin (Cytoskelton, Inc.). The samples were then subjected to low-speed centrifugation for 20-60 minutes at 24°C (bundled actin filaments pellet at a lower speed than unbundled actin filaments). The distribution of actin in the pellet and supernatant fraction was analyzed by SDS-PAGE and protein was visualized with Coomassie stain.

Effects of Mical on Bundled Actin

The ability of Mical to induce the disassembly of bundled actin filaments was performed as described for the actin bundling assays except bundled actin filaments were then incubated with purified Mical^{redoxCH} protein (1 μM - 2.5 μM final concentration was used with similar results), and/or NADPH (200 μM final concentration) for 1 hour at room temperature. Samples were then subjected to low-speed centrifugation and the distribution of actin in the pellet and supernatant fraction was analyzed by SDS-PAGE as described for the actin bundling assays.

The experiments designed to examine the time-course of Micals effects on bundled actin using pyrene-labeled actin was performed essentially as described for all pyrene-labeled actin

polymerization assays. In brief, pyrenyl-G-actin (pyrene-labeled; Cytoskeleton, Inc) was polymerized for 1 hour at room temperature resulting in a 1.1 μM concentration of F-actin. This F-actin (1.1 μM final concentration) was then incubated with Drosophila Fascin (0.55 μM) for 1 hour at room temperature (generating an actin/fascin molar ratio of 2). Bundled actin filaments were then incubated with Mical^{redoxCH} (600 nM final concentration), and/or NADPH (100 μM final concentration) and fluorescence intensity was immediately monitored as described above for other pyrene-labeled actin assays. To confirm the bundling ability of fascin on pyrene actin (and the disassembly of bundled filaments by Mical) standard approaches were used such that after the real-time pyrene-actin assays, the mixtures were centrifuged for 20 min at 10, 200 x g to determine the amount of bundled actin present in the samples. The distribution of actin in the pellet and supernatant fraction was analyzed by SDS-PAGE and proteins were visualized with Coomassie stain as described above (the results of these experiments [data not shown] confirmed the results of our pyrene actin assays [Figure 2.4B, a]).

Analysis of Direct Effects of Mical on Purified Bundling Proteins

To determine if Mical could directly effect the ability of fascin or α-actinin to bundle actin, we incubated Mical^{redoxCH} (2.5 μM final concentration) with fascin or α-actinin (2 μM final concentration) in a general actin resuspension buffer (5 mM Tris-HCl pH 8.0, 0.2 mM $CaCl_2$) and incubated the mixtures at room temperature for 1 hour (with or without 200 μM NADPH). In some cases, with similar results, 20 mM Tris-HCl pH 6.5 was added to the bundling mixture since these conditions were recommended for use with rabbit α-actinin (Cytoskelton, Inc.).

Samples were then subjected to filtration (Ultracel YM-30 [Millipore Corporation]) to remove the small molecule NADPH and samples were washed using a general actin resuspension buffer. The samples were then mixed separately with F-actin (15 μM final concentration) and incubated at room temperature for 1 hour. Samples were then subjected to low-speed centrifugation as described for the bundling assays and then subjected to SDS-PAGE and Coomassie blue staining to visualize the distribution of actin in the pellet and soluble fraction.

EM Analysis of Purified F-actin and Bundled F-actin

Negative staining and EM imaging of actin and bundled actin were done using standard approaches (Okada et al., 1999). In brief, rabbit skeletal muscle F-actin (4 μM; Cytoskeleton, Inc.) was polymerized using standard approaches at 4 °C overnight in low-salt conditions (12.5 mM KCl and 0.5 mM $MgCl_2$) to generate long filaments, incubated separately for 1 hour with Drosophila fascin (2 μM) and/or 1 hour with $Mical^{redoxCH}$ (1 μM) with or without NADPH (100 μM). Samples without fascin were then diluted 20 fold in the polymerization buffer (those with fascin were diluted 10 fold) immediately before placing on a glow-discharged Formvar-coated copper grid (Electron Microscopy Sciences) and negatively stained with 2% uranyl acetate for 1 min to allow EM visualization of actin. Specimens were examined on a FEI Tecnai G2 Spirit Biotwin electron microscope at an accelerating voltage of 120 kV. All measurements were carried out using Image J (NIH). The length of actin filaments was measured in the same way following each treatment and was carried out on random portions of the F-actin containing EM grids. Likewise, bundled actin filaments were sampled and imaged randomly and their length

and width were measured. Untreated fascin-bundled actin filaments showed a similar appearance to what has been described previously using purified Drosophila (Cant et al., 1994) or mammalian fascin (Ishikawa et al., 2003). It should also be noted that in order to differentiate from those actin filaments that may not have been bundled together in our bundling assays, only bundles of actin filaments (not single filaments) were measured. Therefore our results are likely to underestimate the effects of Mical on fascin bundled actin (i.e., any bundle that was completely disassembled to single actin filaments would not have been accounted for/measured).

Microtubule Polymerization and Co-sedimentation Assays

The effects of Mical^{redoxCH} on microtubule polymerization were measured using fluorescence-based standard approaches ((Bonne et al., 1985); Cytoskeleton, Inc). In brief, tubulin (bovine tubulin; Cytoskeleton, Inc) polymerization was performed in a microtubule polymerization buffer (80 mM PIPES pH 6.9, 2 mM $MgCl_2$, 0.5 mM EGTA, 15% glycerol, 1 mM GTP and 5 μM fluorescent reporter (DAPI)) containing mixed tubulin (2 mg/ml final concentration), Mical^{redoxCH} (0.6 μM or 1.2 μM final concentration) and/or NADPH (100 μM). The polymerization was initiated by raising the temperature from 4°C to 37°C. Fluorescence intensity was monitored for 1 hour at 450 nm with excitation at 360 nm by a fluorescence spectrophotometer (Spectra max M2; Molecular Devices) with temperature control.

Standard approaches (Al-Bassam et al., 2007; Gustke et al., 1994) were used for the microtubule co-sedimentation assays, such that microtubules were generated by polymerizing tubulin (from a 5 mg/ml tubulin stock containing 1mM GTP; Cytoskeleton, Inc) at 35°C for 20

min in a polymerization buffer (80 mM PIPES pH 6.9, 0.5 mM EGTA, 2 mM $MgCl_2$, 7.5% glycerol). Microtubules was then diluted 10 fold in a warm buffer (35°C) containing 80 mM PIPES pH 6.9, 0.5 mM EGTA, 2 mM $MgCl_2$, and 20 μM taxol. Test proteins including $Mical^{redoxCH}$ protein (1 μM final concentration), $Mical^{redox}$ protein (1 μM final concentration), a negative control (bovine serum albumin (BSA) [2.2 μM final concentration, Cytoskeleton, Inc]), and a positive control (microtubule associated proteins MAPs [0.64 μM final concentration; Cytoskeleton, Inc]) were added to separate tubes and incubated with either microtubules or buffer for 30 minutes at room temperature. A microtubule only tube was also incubated for 30 minutes at room temperature. Each reaction was placed on top of a cushion buffer (80 mM PIPES pH 6.9, 0.5 mM EGTA, 2 mM $MgCl_2$, 60% glycerol and 20 μM taxol), and was subjected to high-speed centrifugation at 100, 000 x g for 40 min at 24°C. Supernatants were carefully removed and added to sample buffer for loading on an SDS-PAGE gel. The cushion was removed and pellet was resuspended in Milli-Q H_2O with pipetting before being added to sample buffer for loading on an SDS-PAGE gel. The distribution of microtubule and test proteins were visualized with Coomassie blue staining and the intensity of each of the stained bands in the pellet and soluble fraction was then quantified by densitometry using Image J (NIH) and the percentage of different purified proteins with microtubules in the pelleted fraction was presented.

CHAPTER THREE

Direct Redox Regulation of F-actin Assembly and Disassembly by Mical

Previously published. **Hung, RJ**, CW Pak, JR Terman (2011), Direct Redox regulation of F-actin assembly and disassembly by Mical, ***Science***, 334(6063): 1710-3

Introduction

The actin cytoskeleton underlies a diverse array of cellular behaviors (Pollard and Cooper, 2009) but its regulatory mechanisms are incompletely understood. Recently, an actin regulator, the multidomain cytosolic protein Mical, was shown to directly bind and disassemble individual and bundled actin filaments (F-actin) (Hung et al., 2010). Although still poorly understood, Mical-mediated actin remodeling alters cell morphology and navigation in response to one of the largest families of extracellular guidance cues, the semaphorins and their plexin receptors (Hung and Terman, 2011; Hung et al., 2010; Terman et al., 2002; Tran et al., 2007). Drosophila Mical and its vertebrate family members are known as the MICAL family of proteins and belong to a class of flavoprotein monooxygenase/hydroxylase enzymes that bind flavin adenine dinucleotide (FAD) and use the co-enzyme nicotinamide adenine dinucleotide phosphate (NADPH) in oxidation-reduction (Redox) reactions (Hung and Terman, 2011; Terman et al., 2002). Although MICALs have no known substrate/s, they employ their Redox region to bind F-actin and disassemble filaments in an NADPH-dependent manner (**Figure 3.1A**; (Hung et al., 2010)). These observations suggest the intriguing possibility that MICALs are direct actin regulatory enzymes.

Results

To further address this hypothesis, we utilized in vitro actin biochemical assays and found that only very low, substochiometric levels of Mical were required for F-actin disassembly (**Figure 3.1B**), supporting the idea that a catalytic/post-translational mechanism underlies Mical-

mediated F-actin disassembly. This Mical-treated actin failed to re-polymerize even after removal of Mical/NADPH (**Figures 3.1C-D**), indicating that Mical stably modifies actin to alter polymerization. We next wondered if Mical, as an oxidoreductase enzyme, simply released diffusible oxidants to non-specifically alter polymerization. However, Mical does not alter polymerization of other proteins like tubulin (Hung et al., 2010) and preventing Mical-actin interactions abolished Mical's effects on actin (**Figures 3.1E, S3.1–2**). Indeed, unlike oxidases, which generate diffusible oxidants, most Mical-class monooxygenases/hydroxylases directly bind and are activated by their substrates (van Berkel et al., 1999). Likewise, Mical selectively binds F-actin (Hung et al., 2010) and increased its enzymatic activity by >100-fold in an F-actin-dependent manner (**Figure 3.1F**). Thus, F-actin specifically activates the Mical enzyme and exhibits the characteristics of a direct Mical substrate.

To determine if F-actin is a Mical substrate, we purified Mical/NADPH-treated actin **(Figure S3.3**) and performed intact protein mass measurements. Mical/NADPH-treated actin increased its whole mass by 32 Daltons (Da) (**Figure 3.2A**), which could represent the addition of two oxygens (16Da each) to actin. Further mass analysis revealed a substantial difference in the Mical/NADPH-treated actin peptide $_{40}$HQGVMVGMGQK$_{50}$ (**Figures S3.3-3.4**), and that actin's methionine (M) 44 and M47 amino acid residues each had a mass increase of 16Da (**Figures 3.2B, S3.5**). Moreover, Mical selectively modified only these two methionines and not any of actin's 14 other methionines **(Figures S3.3-3.4, S3.6**). Free methionine was also not a Mical substrate (**Figure 3.1F**). M44 and M47 are poorly accessible to diffusible solvents including oxidants when actin is present in filaments (Dalle-Donne et al., 2002; Guan et al.,

2003; Guan et al., 2005; Takamoto et al., 2007), further indicating that these amino acid modifications are unlikely to be non-specific. Thus, Mical selectively adds 16Da (the equivalent of one oxygen) to both actin M44 and M47.

The M44 and M47 residues of actin are phylogenetically conserved and invariant among cardiac, muscle, and cytoplasmic actins (**Figure 3.3A**), and lie within the D-loop (residues 39-51) of the subdomain 2 portion of actin (**Figure 3.3B**), a region that mediates actin-actin contacts and polymerization (Dominguez and Holmes, 2011; Sheterline, 1998). To confirm that M44 and M47 are the functionally relevant sites on Mical-modified actin, we mutated each site, substituting chemically related leucine for methionine residues (**Figure 3.3A)**. We then expressed and purified wild-type, M44L, M47L, and the double mutant M44LM47L actin proteins (**Figures S3.7-3.8**). In contrast to wild-type actin, which showed a 32Da difference after Mical treatment (**Figure 3.2A**), M44LM47L actin was resistant to Mical-modification and exhibited a whole mass similar to control actin (**Figure S3.9**). Thus, M44 and M47 are the only altered residues on Mical-treated actin and are required for Mical to post-translationally modify actin. We thus used these purified mutant actins to determine if modification of M44 and/or M47 induced Mical-mediated F-actin disassembly. All three mutant actins polymerized like wild-type actin and bound Mical (**Figure 3.3C**). In contrast, F-actin generated by either wild-type or M47L depolymerized in the presence of Mical/NADPH, but filaments formed by M44L actin were resistant to Mical/NADPH and did not depolymerize (**Figure 3.3C**). F-actin generated by M44LM47L was also resistant to Mical (**Figure 3.3C**), revealing that Mical modifies actin M44 to induce F-actin disassembly.

Methionine (2-amino-4-thiomethylbutanoic acid) is susceptible to the addition of an oxygen group on its sulfur atom, which generates methionine sulfoxide (MetO) (**Figure 3.2C**). Our results, including the identification of MetO containing peptide fragments (**Figure S3.5**), suggest that Mical directly converts M44 to MetO44, which disassembles F-actin and alters actin polymerization. The D-loop region containing M44 on the pointed-end of one actin monomer mediates the contact with the barbed-end of the adjacent actin monomer (**Figure 3.4A;** (Fujii et al., 2010; Galkin et al., 2010; Murakami et al., 2010; Oda et al., 2009; Sheterline, 1998)). The side chain of methionine is normally flexible and uncharged, but the side chain of MetO with its oxygen atom is stiff and charged (Black and Mould, 1991; Hoshi and Heinemann, 2001). Thus, M44 oxidation would be predicted to affect the interaction between the pointed- and barbed-ends of individual actin subunits (Dominguez and Holmes, 2011) and perhaps lead to F-actin disassembly. To examine if such a mechanism underlies Mical's effects, we performed additional actin biochemical assays and visualized individual actin filaments directly using both real-time Total Internal Reflection Fluorescence (TIRF) and electron (EM) microscopy. Indeed, Mical cut actin filaments into multiple smaller pieces (**Figures 3.4B, S3.10-3.11; Movies S3.1-4**), indicating that Mical-mediated M44 oxidation disrupts the association between individual actin monomers and thereby disassembles F-actin and alters re-polymerization.

MICALs control the organization of actin in neurons, muscles, and bristles in vivo and mammalian cells in vitro (**Figure S3.12;** (Hung and Terman, 2011)). A dominant mutation in the M44 residue (M44T) of skeletal muscle actin underlies a human musculoskeletal disease associated with actin accumulation and aggregation (nemaline myopathy (Laing et al., 2009)),

and we sought to determine if M44 was necessary for Mical-mediated F-actin remodeling in vivo. Mical-mediated F-actin alterations, including that Mical is both activated and required for Semaphorin/Plexin-induced F-actin disassembly and remodeling, have been well-characterized using model *Drosophila* bristle processes (Hung et al., 2010), so we generated mutant bristle cells in which we replaced wild-type actin with M44L actin (**Figures 3.4C, S3.13**). As in vitro (**Figure 3.3C**), actin M44L incorporated into filaments in vivo (**Figure S3.13**). In contrast, replacing wild-type actin with actin M44L suppressed the branching and shortening of bristles characteristic of elevated Mical activity **(Figures 3.4D-F**), and generated Mical loss-of-function-like straight and tip-altered bristles (**Figure S3.13;** (Hung et al., 2010)). Thus, Mical-mediated F-actin alterations in vivo, as in vitro, require the M44 residue of actin.

Discussion

F-actin is thus a direct and specific substrate for Mical. This biochemical reaction alters actin at a specific amino acid residue disrupting actin-actin associations and fragmenting filaments. Also, this post-translationally-modified actin no longer polymerizes normally, differentiating Mical's effects from other F-actin disassembly factors like cofilin which physically disassembles F-actin, recycles actin monomers, and promotes actin assembly (Ono, 2007). Furthermore, Mical modifies the pointed-end of actin proteins, and not the fast-growing, membrane-proximal barbed-end (**Figure 3.4A**), providing a logic by which actin reassembly and branching (Hung and Terman, 2011) follows Semaphorin/Plexin/Mical-mediated F-actin collapse (**Figure S3.14**). These results together present a specific oxidation-dependent

mechanism (**Figures 3.4A, S3.15**) that selectively regulates actin dynamics and cellular behavior.

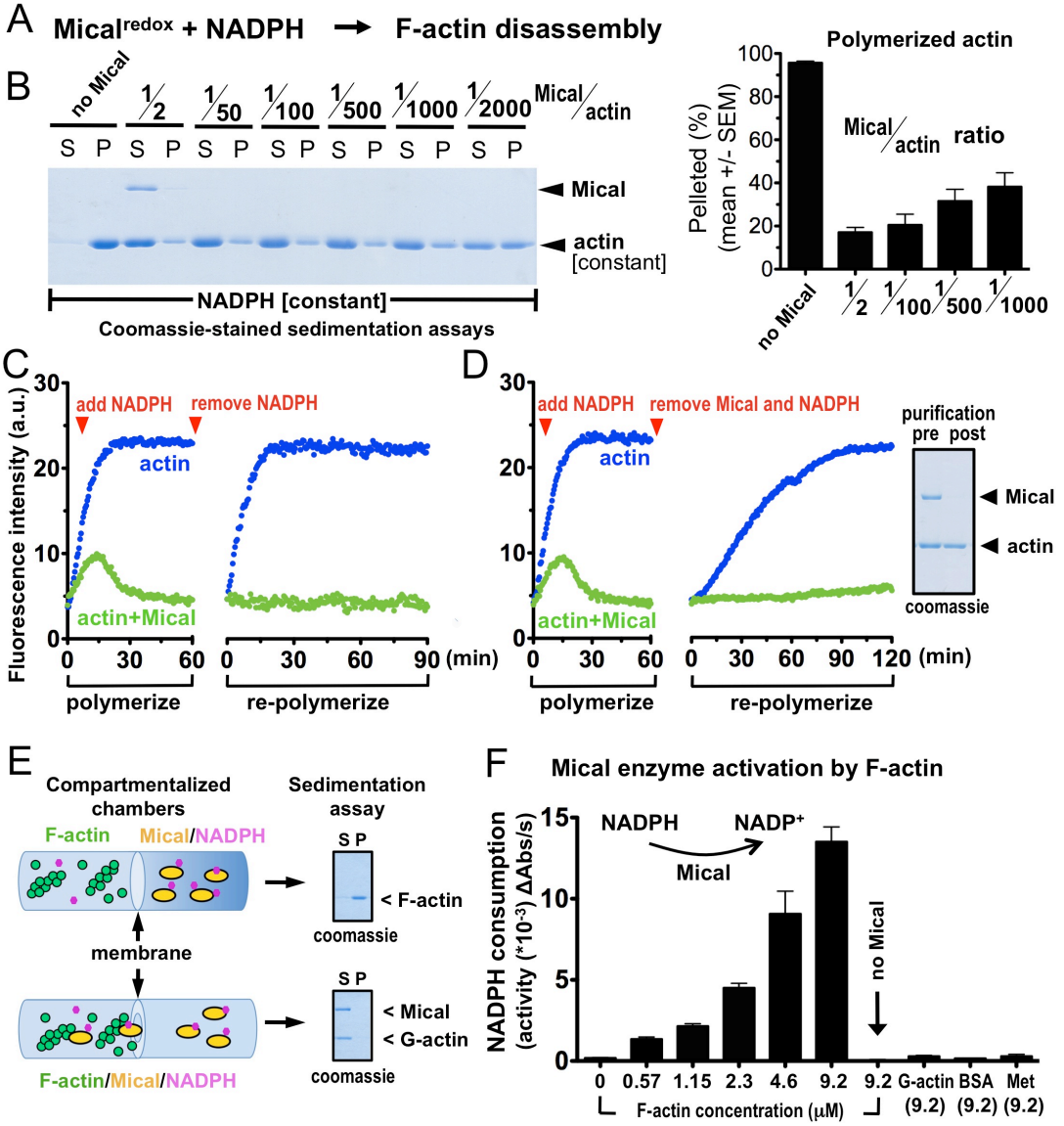

Figure 3.1. Mical directly modifies F-actin. (**A**) The Mical Redox domain alone with NADPH disassembles F-actin. (**B**) Low amounts of Mical, in comparison to actin, disassembles F-actin. S, soluble (G-actin); P, pellet (F-actin). n≥2 per condition. [Actin]=2μM; [Mical]=1μM-1nM; [NADPH]=400μM. (**C** and **D**) Mical/NADPH-treated actin (green) does not repolymerize after removal of NADPH (C) or Mical and NADPH (D). Modified actin [(D), right)] migrates normally and is not degraded. (**E**) Compartmentalized chambers with a membrane allowing small molecules, but not Mical, access to F-actin abolished disassembly (top), as compared with chambers with a punctured membrane (bottom). (**F**) Mical's enzymatic activity (as determined by conversion of NADPH to $NADP^+$), is substantially increased by F-actin, but not G-actin or other proteins [bovine serum albumin (BSA), or free methionine (Met).

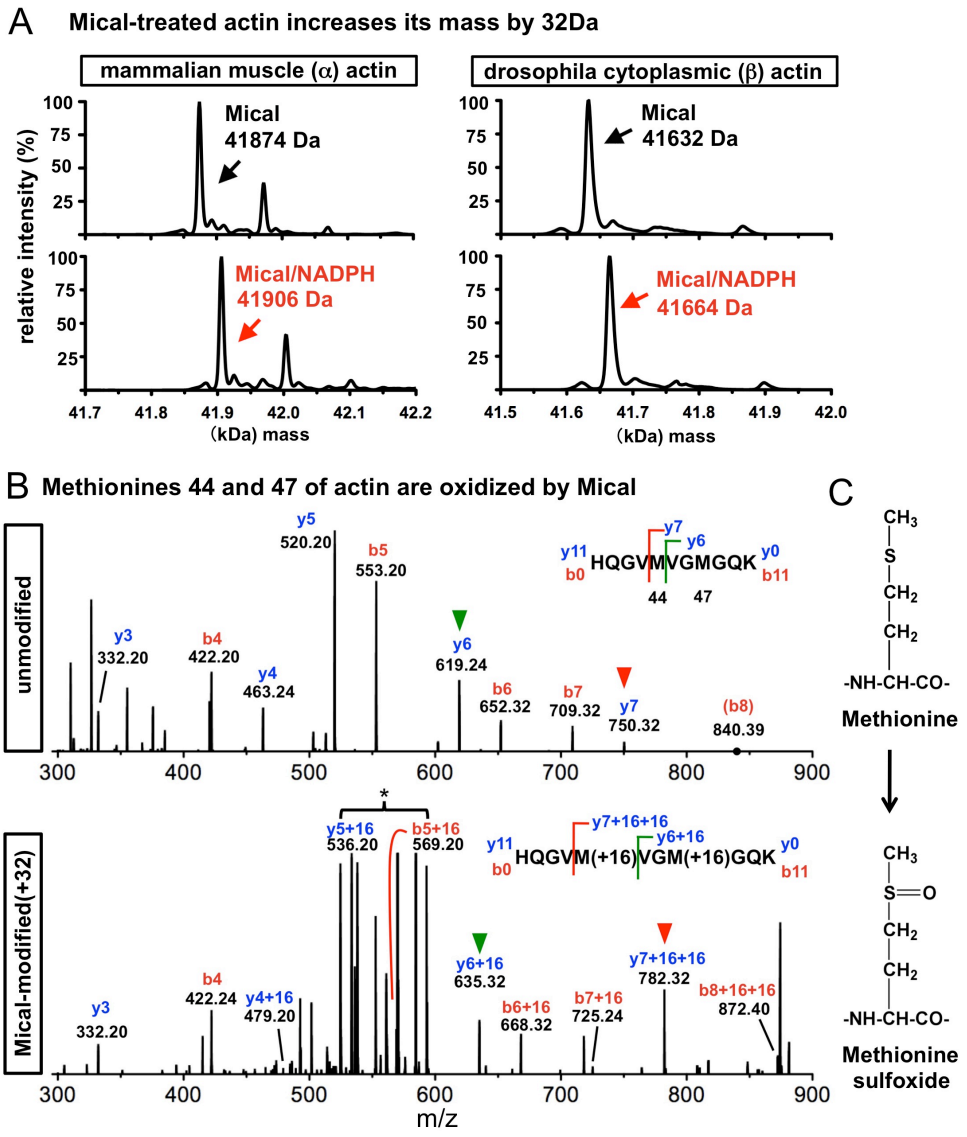

Figure 3.2. Mical oxidizes actin M44 and M47. (**A**) Mical/NADPH-treatment induces a 32Da shift in the whole mass of both α-actin and β-actin (Actin5C). (**B**) Spectra comparisons of the unmodified and modified (+32) peptide (**Figs. S3.3** and **S3.4)** reveals 16Da increases on both M44 and M47. Individual amino acid bonds were broken from both ends of the peptide chain (y^0-y^{11}, b^0-b^{11}) and the mass determined for generated fragments. For example, comparing y6 (green arrowhead) and y7 (red arrowhead) fragments between and within samples, shows a +16 mass increase on the y7 ion (M44). Comparing b ions (breaking the peptide in the opposite direction) also reveals similar M44 and M47 mass increases. This Mical-modified spectrum (e.g., asterisk) is characteristic of methionine oxidation (see **Fig. S3.5**). (**C**) Methionine and its +16 form (methionine sulfoxide).

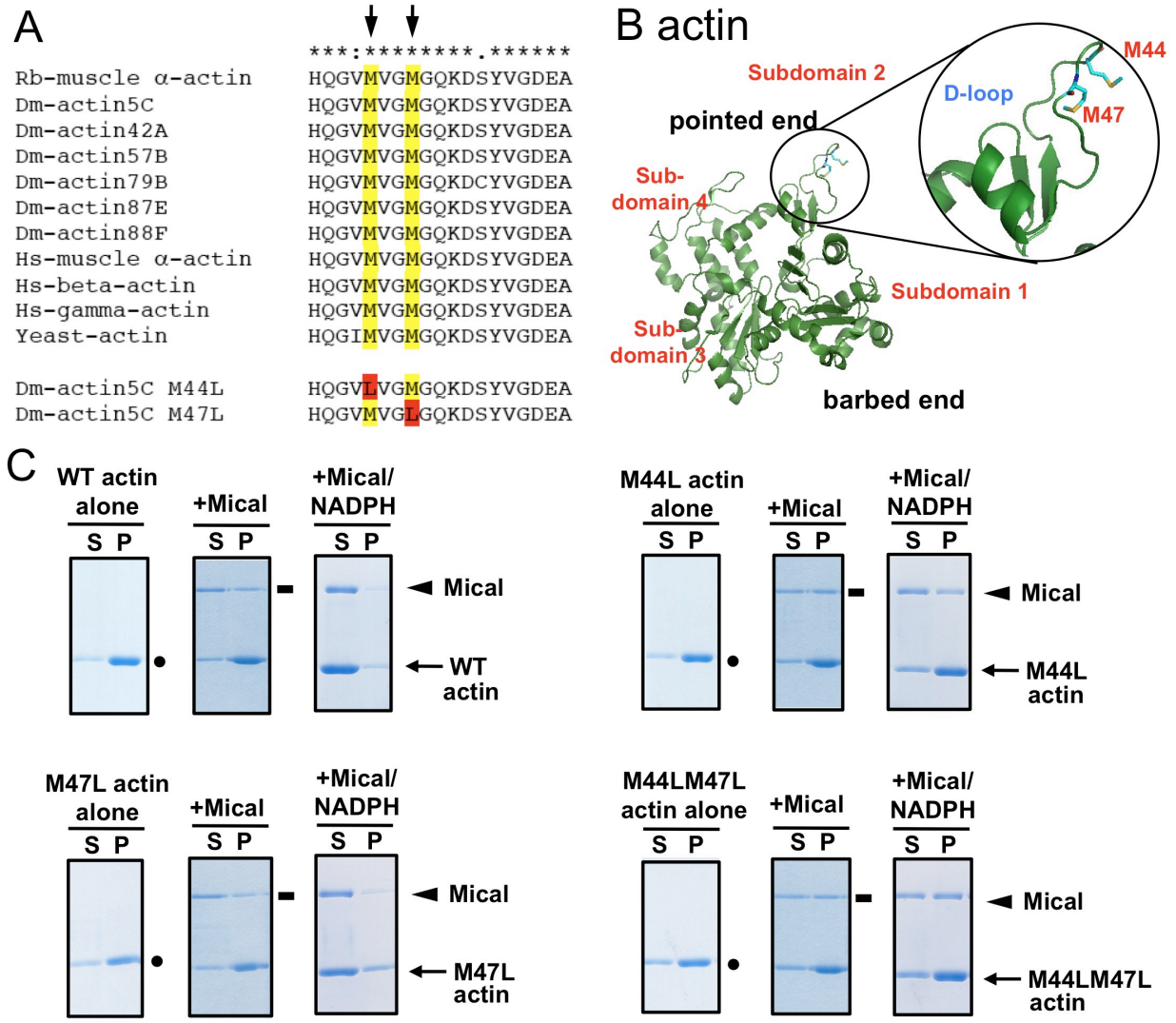

Figure 3.3. Mical disassembles F-actin by oxidizing M44. (**A**) M44 and M47 (residue numbers from Rabbit) are conserved from yeast to humans. Rb, Rabbit; Dm, Drosophila; Hs, human. (**B**) The structure of monomeric actin including M44 and M47 in the D-loop of the pointed-end of the actin monomer. PDB ID is 2ZWH (Oda et al., 2009). (**C**) Co-sedimentation reveals that WT, M47L, M44L, and M44LM47L actins polymerize (dots, P fraction) and bind Mical (rectangles, P fraction). In contrast, Mical/NADPH disassembles WT and M47L but not M44L and M44LM47L actins (arrows, P fraction).

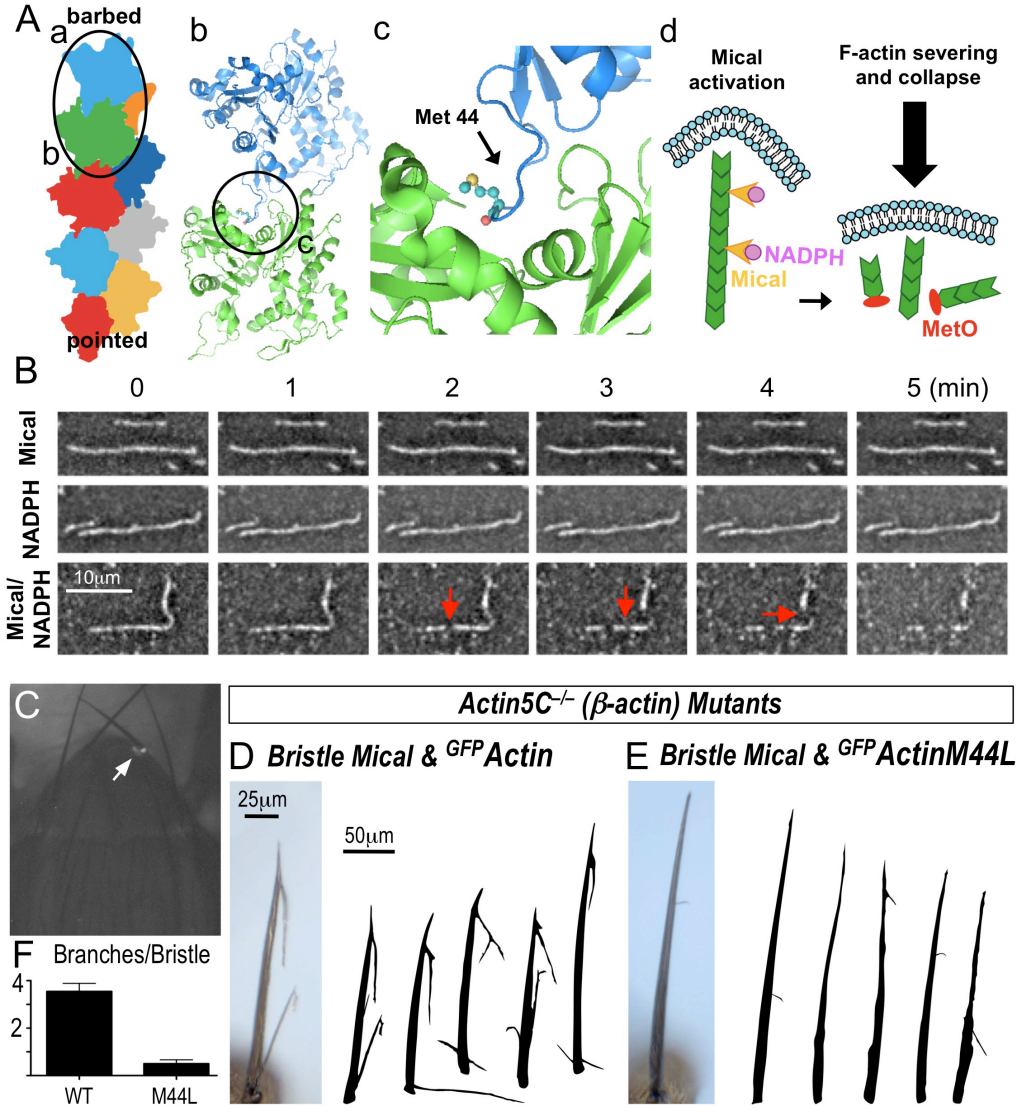

Figure 3.4. **Mical-mediated M44 oxidation severs F-actin and triggers remodeling.** (**A**) Actin filament (a) formation involves amino acids within the D-loop at the pointed-end of one actin monomer associating with residues at the barbed-end of another actin monomer (b). The M44 residue is situated in this D-loop at a critical interface between adjacent actin monomers (c). Mical (d, yellow arrowheads) activation by NADPH oxidizes M44 (MetO), disrupting actin-actin interactions to cut filaments. (**B**) Time-lapse TIRF microscopy images reveal that individual actin filaments are cut (e.g., arrows) by Mical/NADPH but not by either Mical or NADPH only (and **Movies S3.1-S3.4**). (**C** to **F**) ^{GFP}Actin5C M44L-marked single cell clone [(C), arrow] mutant for *actin5C*. [(D) to (F)] Increasing Mical in single bristle cells (D) generates F-actin reorganization and branching, which [(E) to (F)] is suppressed by actin M44L expression. Mean±SEM, n≥10 bristle cells per genotype.

Materials and Methods

Actin Polymerization, Depolymerization, and Co-sedimentation Assays

The actin polymerization assays were performed as previously described using standard approaches (Cooper, 1992b; Hung et al., 2010). Briefly, purified rabbit skeletal muscle actin (pyrene-labeled; Cytoskeleton, Inc) was used to monitor actin polymerization since the fluorescence intensity of the pyrene-labeled polymer is substantially higher than the pyrene-labeled monomer. G-actin (monomeric actin) was resuspended to 9.2 μM in a G-actin buffer (5 mM Tris-HCl pH 8.0, 0.2 mM $CaCl_2$, 0.2 mM ATP and 1 mM DTT) and incubated on ice for 1 hour. Before all experiments, the G-actin solution was centrifuged for 1 hour at 100,000 x g at 4°C to remove residual actin nucleating centers. After ultracentrifugation, the actin was further diluted to 2.3 μM with G-actin buffer. Multiple independent experiments were performed for each condition such that Drosophila Mical^{redoxCH} (Hung et al., 2010), NADPH (MP Biomedicals), catalase (from *Aspergillus niger*, Fisher) and/or hydrogen peroxide (EMD Chemicals, Inc.) was added to the actin, and polymerization was initiated at 25°C by adding an equal volume of 2X polymerization buffer (10 mM Tris-HCl pH 7.5, 100 mM KCl, 4 mM $MgCl_2$, 2 mM EGTA, 1 mM DTT, and 0.4 mM ATP) to generate a final concentration of 1.15 μM actin. Fluorescence intensity was immediately monitored at 407 nm with excitation at 365 nm by a fluorescence spectrophotometer (Spectra max M2, Molecular Devices).

To examine the ability of Mical to induce F-actin depolymerization and/or co-sediment with F-actin, multiple independent experiments were performed essentially as previously described (Cooper, 1992b; Hung et al., 2010). In brief, purified rabbit muscle actin

(Cytoskeleton, Inc.) or Drosophila Actin 5C (wild-type or different mutant forms) were resuspended in G-actin buffer to 4 μM for the Stoichiometry Assays or 2.3 μM for all other assays. The resuspended actin was then polymerized with 2X polymerization buffer in the presence of different concentrations of Mical and/or NADPH. Unless stated otherwise, we employed 600 nM of Mical^{redoxCH} and 100 μM NADPH and treated actin for 1hr. For the stoichiometry assays, F-actin was treated for two hours using different ratios of Mical^{redoxCH} (from 1 μM to 1 nM) and the NADPH was 400 μM. The mixtures were then ultracentrifuged at 150,000 x g for 20 min at 25°C. Supernatant and pellet fractions were adjusted to the same volumes, subjected to SDS-PAGE, and stained with Coomassie blue. The intensity of each of the stained bands in the pellet and soluble fraction was then analyzed and quantified by densitometry using Image J (NIH) and the percentage of actin in the pellet fraction was presented. The pyrene actin depolymerization assays were performed essentially as described (Cooper, 1992b; Hung et al., 2010) using 3 μM of actin, pre-assembled by adding polymerization salts for 1 hr (final concentration was 1.5 μM). Then, Mical^{redoxCH}, H_2O_2, and/or NADPH were added to the polymerized actin and the fluorescence intensity was monitored as described above using a fluorescence spectrophotometer. The comparison of actin depolymerization by Latrunculin B (EMD Chemicals, Inc.) and Mical/NADPH was performed in the same way as described above, but the final concentration of actin was 1.1 μM.

Removal of NADPH and Actin Re-Polymerization

Pyrene-labeled rabbit muscle actin at a concentration of 2.3 μM was treated with either 600 nM of Mical^{redoxCH} (control) or 600 nM of Mical ^{redoxCH} and 100 μM NADPH (Mical-treated actin) and polymerization was initiated at room temperature with 2X polymerization buffer as described above (final concentration of actin was 1.15 μM) and monitored by a fluorescence spectrophotometer for 1 hr as described above. Samples were then collected and exchanged with G-actin buffer several times with a centrifugal filter (Amicon Ultra, Ultracel-10K, Millipore) to disassemble actin filaments and remove the small molecule NADPH. Following collection from the centrifugal filter, polymerization of the actin was then initiated again by adding equal volumes of 2X polymerization buffer and the fluorescence intensity was monitored by a fluorescence spectrophotometer as described above.

Generation, Purification, and Utilization of Mical-treated Actin

Rabbit muscle actin, pyrene-labeled rabbit muscle actin, or Drosophila Actin 5C (wild-type or Actin 5C mutants) at concentration of 1.1 μM was treated with either 600 nM of Mical^{redoxCH} (control) or 600 nM of Mical^{redoxCH} and 200 μM NADPH (Mical-treated actin) for 90 min at room temperature in the 1X polymerization buffer. Samples were then exchanged several times with G-actin buffer using a centrifugal filter (MWCO 10K, Millipore), concentrated, and loaded into a Mono Q 5/50 GL ion exchange column (GE Healthcare) equilibrated with buffer A1 (20 mM Tris-HCl pH 7.0 at 4°C, 0.2 mM $CaCl_2$, 0.1 mM ATP and 0.1 mM DTT). The actin was then eluted with a linear gradient of 0-0.5 M NaCl in buffer A1. The most pure fraction was then

collected, exchanged to G-actin buffer, and concentrated. The actin concentration was determined by Bradford assay. Each actin sample was then directly sent to mass spectrometry for analysis or frozen with liquid nitrogen and stored at -80°C.

To look at the ability of Mical-treated actin to repolymerize, the purified actin was resuspended to 2.3 μM in G-actin buffer, and polymerization was initiated as described above with 2X polymerization buffer (final concentration of actin was 1.15 μM). The ability of actin to re-polymerize was determined as described above by either monitoring the fluorescence intensity or through a sedimentation assay. In some cases, different concentrations of unlabeled, untreated actin was added to the purified Mical-treated pyrene-labeled rabbit muscle actin and polymerization was monitored by changes in fluorescence intensity. To determine whether Mical-treated actin blocks/affects normal actin polymerization, untreated pyrene actin was induced to polymerize by adding 2X polymerization buffer as described above in the presence or absence of purified unlabeled Mical-treated actin or purified unlabeled untreated/control actin. The fluorescence intensity was then monitored using a fluorescence spectrophotometer as described above.

Compartmentalized Chamber Assays

To determine if a diffusible substance was responsible for Mical-mediated effects on F-actin, DispoEquilibrium Dialyzer Chambers (Harvard Apparatus) were employed. Specifically, the DispoEquilibrium Dialyzer Chambers we used are composed of two loading chambers separated by a membrane with a molecular weight cut-off of 5000 Da between the two chambers. The

Dialzyer Chambers were prepared according to the manufacturer's instructions. Then, 2.3 μM of pre-assembled actin filaments were placed in one chamber and the 2.4 μM of Mical^{redoxCH} and 200 μM of NADPH were placed in the other chamber. After gentle agitation for 1hr, the F-actin was subjected to sedimentation and analyzed for depolymerization as described above.

To examine the ability of H_2O_2 to cross the membrane of the DispoEquilibrium Dialyzer Chambers, 4.6 μM of pyrene Ca^{2+}-actin in G-actin buffer was placed in one chamber, and 40 mM H_2O_2 or 2.4 μM of Mical^{redoxCH} and 200 μM of NADPH were placed in the other chamber. After incubating for 1 hr, the G-actin was collected, diluted to 2.3 μM, and polymerization was initiated by adding equal volumes of 2X polymerization buffer. The fluorescence intensity was monitored immediately as described above.

NADPH Consumption

NADPH (the reduced form of the coenzyme) absorbs light at 340 nm, while the oxidized form ($NADP^+$) does not. This difference between the oxidized and reduced forms of the coenzyme makes it straightforward to measure the conversion of one to another in enzyme assays. Thus, the enzymatic activity of Mical was monitored by the rate of NADPH oxidation, which is measured by the rate of decreasing light absorbance at 340 nm (extinction coefficient 340 = 6.2 $mM^{-1}*cm^{-1}$). The basal NADPH consumption was measured in the presence of different concentration of Drosophila F-actin (Actin 5C) or methionine for the first 3 min before adding Mical^{redoxCH}. The Mical enzymatic activity was determined by subtracting the NADPH

consumption after addition of the Mical^{redoxCH} from basal NADPH consumption. The rate of NADPH consumption was determined by 10s intervals at the maximum rate.

Mass Spectrometry

The molecular weight of intact protein was measured by an ABI QStar XL mass spectrometer with a nano-electrospray ionization (ESI) source. Purified Mical-treated actin and control actin in G-actin buffer (1 mg/ml) were diluted 10 times with 1% formic acid in acetonitrile (ACN)/H_2O (50:50, v/v), and then infused into the mass spectrometer without desalting. The molecular weight of re-purified "control" muscle actin is consistent with previous reports (Bergen et al., 2003). Multiple analyses of different purified samples of both *Drosophila* and mammalian actins gave similar results.

Tandem Mass Spectrometry

The label free LC/MS/MS data were acquired on a nano-HPLC-MS system in which an UltiMate 3000 HPLC system (Dionex) was coupled to a Velos Orbitrap (Thermo Fisher Scientific) mass spectrometer. 3 µg of purified Mical-treated actin and control actin in G-actin buffer were directly digested with 200 ng of trypsin at 37 °C for 6 hr. Samples from digest (0.06 µg) were injected into the HPLC without desalting. The tryptic peptides were separated on a self-packed C18-RP-HPLC-column (ID 75 µm) using a gradient from 3% to 45% of buffer B in 22 min. The buffer composition of buffer A was 0.1% (v/v) formic acid in ACN/H_2O (5:95, v/v) and the buffer composition of buffer B was 0.1% (v/v) formic acid in ACN/H_2O (80:20, v/v). Two

LC/MS/MS runs were acquired for each sample. All data were acquired in the positive ion mode. MS data were acquired in Orbitrap at 30 K nominal resolution over an m/z range of 250-1600. The top 5 highest multiply charged ions were automatically chosen for collision-induced dissociation fragmentation. MS/MS data were acquired in Velos with enhanced resolution. Proteome Discoverer 1.2 software was used for protein identification and SIEVE 1.3 software was used for protein quantitation analysis.

Purification of Drosophila Actins from Baculovirus-infected Sf9 Insect Cells

A plasmid pAcUW2B containing the coding sequence for the Drosophila *actin 5C* gene (a generous gift from Mike Rosen (Volkman et al., 1996)) was used to express Drosophila Actin 5C essentially as previous described (Joel et al., 2004). Briefly, recombinant baculovirus encoding actin were prepared by co-transfecting *actin 5C* pAcUW2B and linearized BD BaculoGold Baculovirus DNA (BD Biosciences) into Sf9 insect cells following the manufacturer's instructions. Infected Sf9 cells (2×10^8) were then harvested 3 days after infection at multiplicities of infections (MOI) 3 and lysed in buffer containing 1 M Tris-HCl, pH 7.5 (at 4°C), 0.6 M KCl, 0.5 mM $MgCl_2$, 0.5 mM ATP, 1 mM DTT, 4% Triton X-100, 1 mg/ml Tween-20, and protease inhibitor cocktail tablet (Complete, EDTA free, Roche). The cell lysate was then clarified, dialysed against buffer A (10 mM imidazole, pH 7.5, 0.1 mM $CaCl_2$, 0.1 M KCl, 0.1 mM DTT, 0.5 mM ATP) overnight, clarified again, and loaded on a 5 ml HiTrap Q HP column (GE Healthcare). The actin was then eluted with a linear gradient of 0-0.5 M KCl in buffer A. The fractions containing actin were collected, dialysed with buffer A, and then loaded

into a Mono Q 5/50 GL ion exchange column (GE Healthcare). The actin was eluted again with a linear gradient of 0-0.5 M KCl in buffer A. The purified actin was then concentrated and dialyzed into G-buffer (5 mM Tris-HCl, pH 8.2 (at 4°C), 0.2 mM $CaCl_2$, 0.1 mM sodium azide, 0.5 mM DTT and 0.2 mM ATP). Actin concentration was determined from the absorbance at 290 nm by using an extinction coefficient of 0.63 mL mg^{-1} cm^{-1}. Actin was then snap-frozen in liquid nitrogen and stored at -80°C. Similar approaches were employed to purify the mutant Drosophila actin proteins.

Generation of Mutant Actins for the Baculovirus/Insect Cell System

To prepare for site-directed mutagenesis, a 500 bp portion of the Drosophila *actin 5C* sequence containing methionines 44 and 47 was subcloned into pOT2a vector (with restriction enzymes Bgl II and XbaI I). Primers were then designed to substitute chemically related leucine residues for methionine residues (Bartlett et al., 2003; Lipscomb et al., 1998). To make the M44L mutant, the forward primer 5'-tcaccagggtgtgttggtcggcatggg-3' and the reverse primer 5'-cccatgccgaccaacacaccctggtga-3' was used. To make the M47L mutant, the forward primer 5'-gtgtgatggtcggcttgggccagaaggac-3', and the reverse primer 5'-gtccttctggcccaagccgaccatcacac-3' was used. To make the M44LM47L double mutant, the forward primer 5'-accagggtgtgttggtcggcttgggccagaag-3', and the reverse primer 5'-cttctggcccaagccgaccaacacaccctggt-3' was used. Mutagenesis was accomplished by using the QuickChange strategy (Stratagene) and following the manufacturer's instructions. All newly generated DNA constructs were then subjected to DNA sequencing to confirm that mutations

were only present in the desired sequence. The modified partial actin sequences were then moved (using the same restriction enzymes [Bgl II and XbaI I]) to the pAcUW2B vector containing the coding sequence for Drosophila *actin 5C*. Recombinant baculovirus encoding the actin mutant constructs were then prepared as described above for the wild-type Actin 5C.

Cell Culture, Transfection, and F-actin Visualization in mammalian 3T3 cells

To look at the ability of Mical to alter F-actin in mammalian cells, Drosophila Mical and Mical^{redocCH} (Hung et al., 2010) were cloned into the mammalian expression vector pEGFP-C1 (Clonetech), which resulted in a N-terminal GFP tag on both Mical constructs. 3T3 cells (a fibroblast cell line) were maintained using standard media and protocols. 3T3 cells were then plated at a density of $6x10^5$ cells/ml in 35-mm uncoated Mattek dishes. After 24 hours, cells were transfected with EGFP, EGFP-Mical, or EGFP-Mical^{redoxCH} plasmids using Lipofectamine 2000 and following standard protocols. After 24 hours of expression, 3T3 cells were fixed using 4% paraformaldehyde in cytoskeletal-preservation buffer (138 mM KCl, 10 mM EGTA (pH 8.0), 10 mM MES (pH 6.1), 3 mM $MgCl_2$). Following several washes with PBS pH 7.2, cells were permeabilized with 0.1% Triton X 100 for 9 minutes and washed again. F-actin was stained using a 1:50 dilution of Alexa 633 phalloidin for 40 minutes. Cells were mounted using Prolong Gold (without DAPI).

Drosophila Genetics, Molecular Biology, and Transgenic Lines

Standard approaches were used to make transgenic flies containing the M44 mutation in Actin

5C (Hung et al., 2010). In particular, DNA used to generate the previously employed ^{GFP}Actin5C fly lines (Hung et al., 2010) was obtained in the pRmHa-3 vector (a kind gift from Hiroki Oda and Vladislav Verkhusha). Then, a portion of *actin 5C* containing the amino acid to be altered (M44) was subcloned into pCR2.1 (using KpnI and EcoRV restriction sites) for site-directed mutagenesis using the same set of primers and strategies described above. The mutation was then confirmed by DNA sequencing, and the sequence containing it was then moved back into the same restriction enzyme sites in the pRmHa-3 vector. Sequences corresponding to both wild-type ^{GFP}Actin5C and ^{GFP}Actin5C M44L were then moved to the pUAST vector with EcoRI and XbaI I to generate the transgenic flies. All Drosophila embryo injections were done by BestGene, Inc.

To examine the role of the actin M44 residue in Mical-mediated actin reorganization in vivo, we used standard MARCM techniques and analysis (Lee and Luo, 1999; Wu and Luo, 2006) to replace Actin5C [β-actin] with either ^{GFP}Actin5C or ^{GFP}Actin5C M44L within individual bristle cells. Specifically, increasing the levels of Mical in bristle cells using the GAL4-UAS system results in easily observable and quantifiable effects on actin organization (**Fig. S13**; (Hung et al., 2010)). These effects are completely suppressed by simultaneous expression of the GAL80 protein (data not shown), which represses the activity of the GAL4 transcription factor (Wu and Luo, 2006). Therefore, we generated flies capable of expressing Mical in all bristle cells with the B11-GAL4 promoter (a kind gift of John Merriam), but suppressed this expression with ubiquitous expression of the GAL80 protein. We then created flies containing a mutation in the *actin5C* gene (Japan (B114-409 [111-901]) along with the

ubiquitous expression of the GAL80 protein, such that when at least one copy of "wild-type" Actin5C was present, the GAL80 would suppress Mical expression. In these flies, we then used FLP-mediated mitotic recombination to generate *actin5C* homozygous mutant bristle cells and restored either wild-type ^{GFP}Actin5C or ^{GFP}Actin5C M44L using the bristle-specific promoter *B11-GAL4*. Therefore, using these genetic approaches, we generated single bristle cells that were mutant for *actin5C*, expressed Mical, and simultaneously expressed (and were marked by) either wild-type ^{GFP}Actin5C or ^{GFP}Actin5C M44L (i.e., the *actin5C* mutant cells were marked by GFP). To carry-out these experiments, female *Act5C, FRT19A/FM7; B11-GAL4, UAS:Mical/TM6B* flies were crossed to either male *hsFLP, TubGAL80, FRT19A; UAS:^{GFP}Act5C/Cyo* or male *hsFLP, TubGAL80, FRT19A; UAS:^{GFP}Act5C M44L/Cyo* flies and placed in a 25°C incubator. Then, just prior to the stages at which the posterior scutellar bristle cells are born (Poodry, 1975), vials containing offspring were heat-shocked using standard approaches (Wu and Luo, 2006) for one hour at 37°C. Heat-shocked vials were then returned to a 25°C incubator and once flies emerged, animals were sorted by genotype and those that were potentially of the correct genotype were examined for MARCM bristle cell clones (using GFP fluorescence). The genotypes in the manuscript are as follows: **Fig. 4D** = *Act5C^{mutant}, FRT19A/Act5C^{mutant}, FRT19A; UAS:^{GFP}Act5C/+; B11-GAL4, UAS:Mical/+*. **Fig. 4E** = *Act5C^{mutant}, FRT19A/Act5C^{mutant}, FRT19A; UAS:^{GFP}Act5C M44L/+; B11-GAL4, UAS:Mical/+*.

Microscopy and Imaging

Total internal reflection fluorescence (TIRF) microscopy was performed using the method of Kuhn and Pollard, 2005 (Kuhn and Pollard, 2005) with slight modifications. Specifically, unlabeled (1.05 μM) and Alexa Fluor 488-labeled rabbit muscle actin (0.45 μM) were copolymerized at room temperature for 1hr in 1X polymerization buffer. Coverslips and slides were cleaned using 95% ethanol and flamed. Flow chambers were assembled by mounting a 22 X 40 mm coverslip (number 1.5, Fisher Scientific) perpendicularly on a 25 x 75 x 1-mm slide (Fisher Scientific) with two strips of parafilm. The chamber was then quickly placed on a 100°C Heating Block (VWR Scientific) to create a seal between the parafilm and the glass. Rabbit muscle myosin (Cytoskeleton Inc.) was inactivated by incubation with 1 mM N-ethylmaleimide (NEM) for 1 hr at room temperature and the reaction was stopped with 1 mM DTT on ice for 1 hr. NEM-myosin was then placed in a storage buffer (containing 10 mM imidazole, pH 7.0, 0.5 M KCl, 10 mM EDTA, 1 mM DTT and 50% glycerol), and diluted to 0.2 μM in high salt Tris-buffered saline (50 mM Tris-HCl, pH7.6, 600 mM NaCl) before use. Flow Chambers were coated with 0.2 μM NEM-myosin for 3 min, and subsequently washed with 1% BSA in high salt Tris-buffered saline, followed by 1% BSA in low salt Tris-buffered saline (50 mM Tris-HCl, pH 7.6, 50 mM NaCl). The solution was then exchanged via capillary action (i.e., the solution was loaded on one side of the chamber and filter paper [3MM chromatography paper, Whatman] was used to draw the solution to the other side). Polymerized actin was then loaded into the chamber for 2 min and washed twice with 1X TIRF buffer (10 mM imidazole, pH 7.0; 50 mM KCl, 1 mM $MgCl_2$, 1 mM EGTA, 0.2 mM ATP, 50 mM DTT, 15 mM glucose, 100 μg/ml glucose oxidase,

20 μg/ml catalase) before imaging. The filaments were then observed using an Olympus IX71 TIRF microscope and a 60X oil objective (numerical aperture of 1.45). Images were captured every 30 sec. on a Photometrics Cascadell:512 EMCCD camera. Mical^{redocCH} and/or NADPH were diluted in 1X TIRF buffer to 600 nM and 100 μM, respectively, and were then washed/flowed into the chamber. The filaments were imaged for 10 mins.

Electron microscopy (EM) imaging of actin was done essentially as previously described using standard approaches (Hung et al., 2010; Okada et al., 1999). In brief, rabbit skeletal muscle F-actin (4 μM; Cytoskeleton, Inc.) was polymerized using standard approaches at 4 °C overnight in low-salt conditions (12.5 mM KCl and 0.5 mM $MgCl_2$) to generate long filaments, incubated separately for 40 - 60 min with Mical^{redoxCH} (1 μM) with or without NADPH (100 μM). Samples were then diluted 20 fold in 1X polymerization buffer, immediately placed on a glow-discharged Formvar-coated copper grid (Electron Microscopy Sciences), and negatively stained with 2% uranyl acetate for 1 min to allow for EM visualization of actin. Specimens were examined on a FEI Tecnai G2 Spirit Biotwin electron microscope at an accelerating voltage of 120 kV. Examination of actin filaments were performed on random portions of the EM grids as previously described (Hung et al., 2010).

Images of 3T3 cells were collected using a Zeiss LSM 510 Meta and a 63x oil objective (NA 1.40). 488 and 633 lasers were used to image EGFP and Alexa 633 respectively. All images were line-averaged 4 times and the PMT detector sensitivity was set such that all pixel intensities were below saturation. Adult bristle phenotypes of MARCM clones were examined, quantified, imaged, and drawn as previously described (Hung et al., 2010). In brief, flies were initially

sorted by genotype using a stereomicroscope (Leica Stereo Zoom S8 APO), and then examined using Brightfield and Fluorescence microscopy on a Zeiss Discovery M^2 Bio stereomicroscope. Images and drawings of the adult bristles were done with the aid of a Zeiss Discovery M^2 Bio stereomicroscope, a motorized focus and zoom, and three-dimensional reconstruction software (Extended Focus Software [a kind gift from Bernard Lee]). All analysis was done by directly comparing the posterior scutellar bristle cells of all genotypes.

CHAPTER FOUR

Discussion

Summary of the Present Work

The molecules and mechanisms linking guidance cues like semaphorins and their plexin receptors to the precise control of cytoskeletal elements have been poorly understood. Our in vivo and in vitro results now reveal a logic by which precise reorganization of the actin cytoskeleton can be achieved in a spatiotemporal manner. Our results suggest a model whereby class 1 semaphorins directly bind to the extracellular portion of plexA receptors present on the cell surface (Winberg et al., 1998) which directly interact via their cytoplasmic domain with the C-terminus of Mical present within cells (Schmidt et al., 2008; Terman et al., 2002). Mical is targeted and directly associates with F-actin via its calponin homology (CH) domain and FAD-binding (redox) domain, respectively (**Figure 4.1**). Upon association with Semaphorin-bound Plexin, Mical is activated to directly disassemble actin filaments and bundled F-actin in an NADPH/redox-dependent manner. There are also many other proteins that interact with plexin (Hung and Terman, 2011) and so understanding if and how they modulate Mical-mediated F-actin disassembly will be an important future direction

These results also indicate a novel role for specific redox signaling events in orchestrating actin dynamics. Interestingly, Mical shares many structural and biochemical properties with bacterial PHBH (Nadella et al., 2005; Siebold et al., 2005; Terman et al., 2002), a flavoprotein monooxygenase that directly hydroxylates aromatic substrates similar in chemical structure to several amino acids including tyrosine and phenylalanine. Our results, therefore, suggest a model whereby Mical binds to actin and thereby positions itself to regulate actin dynamics through NADPH-dependent posttranslational alterations of specific actin amino acid residues. In fact, my results in the chapter 3 demonstrate that Mical uses its redox activity to posttranslationally modify actin subunits to disassemble actin filaments. Specifically, Mical selectively oxidizes the methionine 44 residue (MetO) on the pointed end of individual actin proteins, disrupting the association between actin subunits and severing filaments (**Figure 4.2**). This filament severing and likely decrease in the amount of F-actin in the vicinity of activated Semaphorin/Plexin/Mical would be predicted to underlie the collapse of cells and their processes (including growth cones) that occurs in response to Semaphorins (Hung and Terman, 2011) (**Figure 4.2**). In addition, this Mical-modified actin exhibits a decreased ability to be incorporated into filaments/polymerize, a condition which might locally lower the usable pool of actin and induce further actin depolymerization/disassembly.

Mical – mediated actin reorganization: triggering branching of the actin network

Interestingly, because filaments are typically capped by abundant barbed-end capping proteins in vivo (Chhabra and Higgs, 2007), the means that Mical uses to disassemble actin (altering the

pointed-end of individual actin proteins) would also be predicted to generate more free membrane-proximal barbed ends of actin filaments. These free barbed ends would enable (or even stimulate) new actin polymerization and branching on existing filaments (Chhabra and Higgs, 2007) – through a Mical-independent secondary effect mediated by the direct action of other currently unknown actin regulatory proteins (Hung et al., 2010) (**Figure 4.2**). Thus, our present observations provide a mechanism for how Semaphorins induce both the rapid collapse and subsequent increase in complexity and "branching" of the actin network (Hung and Terman, 2011). Likewise, these new observations coupled with previous work on Mical (reviewed in (Hung and Terman, 2011)) also indicate that Mical is working with other actin regulatory proteins to regulate the actin network in vivo but at present Mical's interactions with these other actin regulatory proteins is poorly understood. For instance, in addition to working with unknown actin regulatory proteins to increase complexity and "branching" of the actin network, Mical is also able to disassemble both fascin and alpha-actinin bundled actin filaments (Hung et al., 2010), although it does not have any direct effects on either bundling protein itself (i.e., Mical treatment of fascin or alpha-actinin does not alter their ability to bundle F-actin (Hung et al., 2010)). It is also important to note that a MICAL family member, mammalian MICAL-1, associates with (Schmidt et al., 2008) and through its ability to generate H_2O_2 leads to the oxidation of CRMP family proteins (Morinaka et al., 2011), proteins known to regulate microtubule dynamics and Semaphorin-mediated growth cone collapse (reviewed in (Hung and Terman, 2011; Schmidt and Strittmatter, 2007)). Thus, MICAL family proteins have also been implicated in regulating microtubule dynamics through effects on CRMP proteins. Furthermore,

MICAL family proteins (which contain other domains besides their Redox domain) also regulate exocytosis and cell death through interactions with several other proteins including Rab GTPases and NDR kinases, respectively (reviewed in (Hung and Terman, 2011; Zhou et al., 2011a)) – although the role of the Redox domain in these processes is still poorly understood. Finally, as discussed in my introduction, Plexin also interacts with other proteins that regulate actin dynamics including Rac GTPases and so understanding how Mical works with Rac GTPases will be an important future direction.

Mical is a novel actin regulatory enzyme

Mical joins a small number of diverse enzymes including arginylation enzymes (Karakozova et al., 2006) and ADP-ribosyltransferases (Aktories et al., 1986) that directly modify actin with differing effects (Sheterline, 1998; Terman and Kashina, 2012). Specifically, Mical is a Redox enzyme and our results uncover an oxidation-dependent signaling process that selectively regulates actin dynamics and cellular behaviors. Nitric oxide synthase (NOS) is the prototypical Redox signaling enzyme and generates diffusible NO to modify protein function (Stamler et al., 2001). In contrast, little is known of Redox enzymes that physically associate and directly modify specific protein substrates. Likewise, cysteine residues are the best-known targets of Redox signaling (Rudolph and Freeman, 2009), but selective methionine oxidation events also alter protein function (Carp et al., 1982; Ciorba et al., 1997; Erickson et al., 2008; Young et al., 1999). Interestingly, monooxygenases have been characterized that directly modify free methionine, including synthetic peptides containing N-terminal methionine residues (Duescher et

al., 1994; Elfarra and Krause, 2005; Kaufman and Mason, 1982), but to our knowledge Mical is the first enzyme identified that selectively targets methionine residues on a specific protein. Furthermore, M44 is buried within F-actin and poorly accessible to diffusible oxidants (Dalle-Donne et al., 2002; Guan et al., 2003; Guan et al., 2005; Takamoto et al., 2007), suggesting a model where Mical's active site "fits" between actin monomers to access and modify its specific substrate. Our results reveal that F-actin is a direct substrate for Mical and Mical modifies individual actin subunits within F-actin on their M44 residue present within the D loop of actin. Interestingly, the D loop is one of the most flexible regions of actin and varies significantly between monomeric (G-) and polymerized (F-) actin (Egelman, 2001; Oda and Maeda, 2010). For instance, the M44 residue is solvent exposed in certain forms of G-actin (such as Ca^{2+}-G-actin), and along with other surface exposed residues undergo oxidation-induced modifications that have been linked to altered actin polymerization (Dalle-Donne et al., 2002; Guan et al., 2003; Milzani et al., 2000). However, when actin is induced to polymerize (by adding Mg^{2+}) or is present in its filamentous form (F-actin), M44 is poorly accessible to diffusible oxidants (Dalle-Donne et al., 2002; Guan et al., 2003; Guan et al., 2005; Takamoto et al., 2007). Thus, Mical must access the buried M44 residue of actin. In **Figure 4.3A**, rotating the Mical structure by 90 degrees (from the top of the page down) provides one model to envision how the active site (small arrow) of Mical accesses (large arrow) the M44 residue. In **Figure 4.3B**, the $Mical^{redox}$ catalytic reaction is based on our results and others studying p-hydroxybenzoate hydroxylase (PHBH), whose structure is most closely related to MICAL-1^{redox}. In the reductive half reaction (top step in **Figure 4.3B**), the FAD is reduced by NADPH (NADPH becomes

$NADP^+$ and FAD becomes $FADH_2$). In the oxidative half-reaction (bottom step in **Figure 4.3B**), the reduced FAD ($FADH_2$) is re-oxidized by molecular oxygen (to FAD) and inserts one oxygen atom into its substrate. Following re-oxidation to FAD, the reaction could occur again. Our results reveal that the rate of Mical's enzymatic reaction (as judged by conversion of NADPH to $NADP^+$) speeds-up with increasing concentrations of its F-actin substrate. It is also of interest whether these Mical-mediated actin alterations are reversible; perhaps by reducing enzymes like thioredoxin (Morinaka et al., 2011). Alternatively, *actin* mRNA is specifically targeted to the leading edge of motile cells and their processes (Holt and Bullock, 2009), providing unmodified actin that could be utilized following Mical activity, perhaps even in response to "attractive" guidance cues (Pak et al., 2008). Our observations also raise the possibility that certain pathologies and traumas allow reactive oxygen species abnormal access to M44 where they non-specifically work like Mical and disrupt F-actin-based cellular behaviors. Future work should be directed at investigating these important unanswered questions.

The role of Mical in bristle morphology

In motile cells and neuronal growth cones, the bulk of F-actin forms two types of arrays: the parallel arrays of bundled F-actin found in filopodia and the meshwork F-actin arrays found in lamellipodia. Like filopodia, Drosophila bristle processes are rich in bundles of F-actin and our results indicate that Mical plays an important role in specifying the size and organization of these bundles. The slightly curved shape of Drosophila bristles is not obtained from long continuous bundles of F-actin that would create a straight bristle, but from the generation and assembly of

multiple short bundles of F-actin (Tilney and DeRosier, 2005). Our experiments reveal that these Mical-mediated effects on F-actin bundling are tightly controlled since elevating the levels of Mical in bristles or introducing a hyperactive form of Mical transforms F-actin bundles into meshwork-like arrays of F-actin reminiscent of that seen in lamellipodia. Furthermore, out of these meshwork arrays arise newly oriented bundles of F-actin that generate bristle branches reminiscent of filopodia. Our results reveal that Mical normally plays a critical role in the control of this F-actin bundling through what our experiments suggest to be Semaphorin/Plexin/MICAL signaling at precise loci along the bristle.

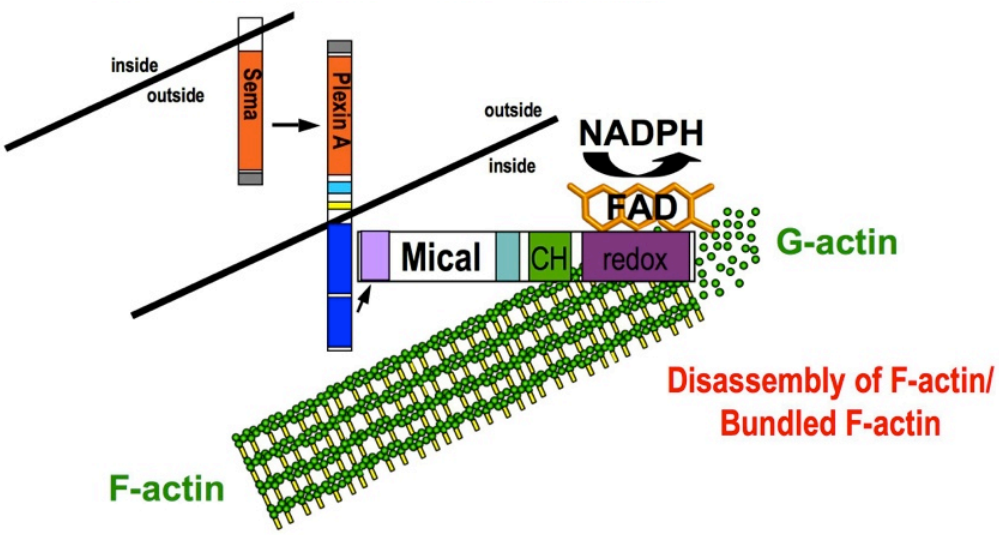

Figure 4.1. Mical directly links Semaphorins and Plexins to specific F-actin rearrangements. Illustration of the Semaphorin, Plexin, Mical signaling pathway that directly associates with and orchestrates F-actin reorganization. (see text for detailed description)

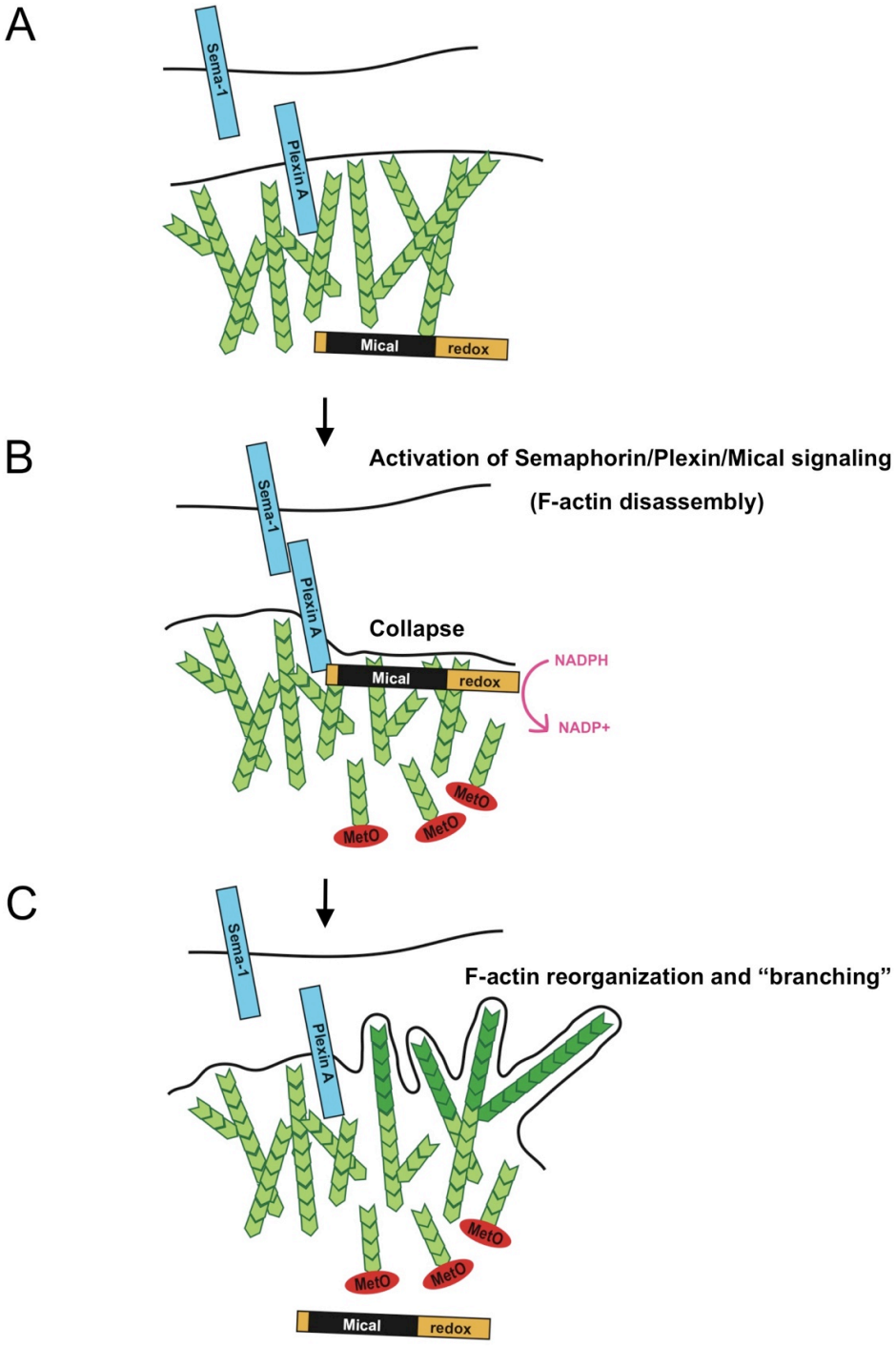

Figure 4.2. Summary of Semaphorin-plexinA-Mical mediated actin reorganization and the mechanism by which Mical disassembles actin filaments. (A) In the absence of semaphorins-plexin activation, Mical is in the cytosolic region and doesn't bind to PlexinA receptors. Results from others and ours (Hung et al., 2010; Schmidt et al., 2008) indicated that Mical in the absence

of PlexinA activation is in an inactive state that the redox enzymatic region is blocked by its C-terminus region. Furthermore, Mical enzymatic activity can be regulated by its coenzyme, NADPH. (B) This Semaphorin/Plexin association activates Mical (Hung et al., 2010; Schmidt et al., 2008) to directly associate with F-actin via its redox domain and disassemble actin filaments in an NADPH-dependent manner (Hung et al., 2010). Mical selectively oxidizes the methionine 44 residue on the pointed end of individual actin proteins (MetO), disrupting the association between actin subunits and severing filaments. (C) Mical severs actin and thus generates more free membrane-proximal barbed ends of actin filaments, allowing new actin polymerization and branching on existing filaments, (Chhabra and Higgs, 2007) – through a Mical-independent secondary effect mediated by the direct action of other currently unknown actin regulatory proteins (Hung et al., 2010).

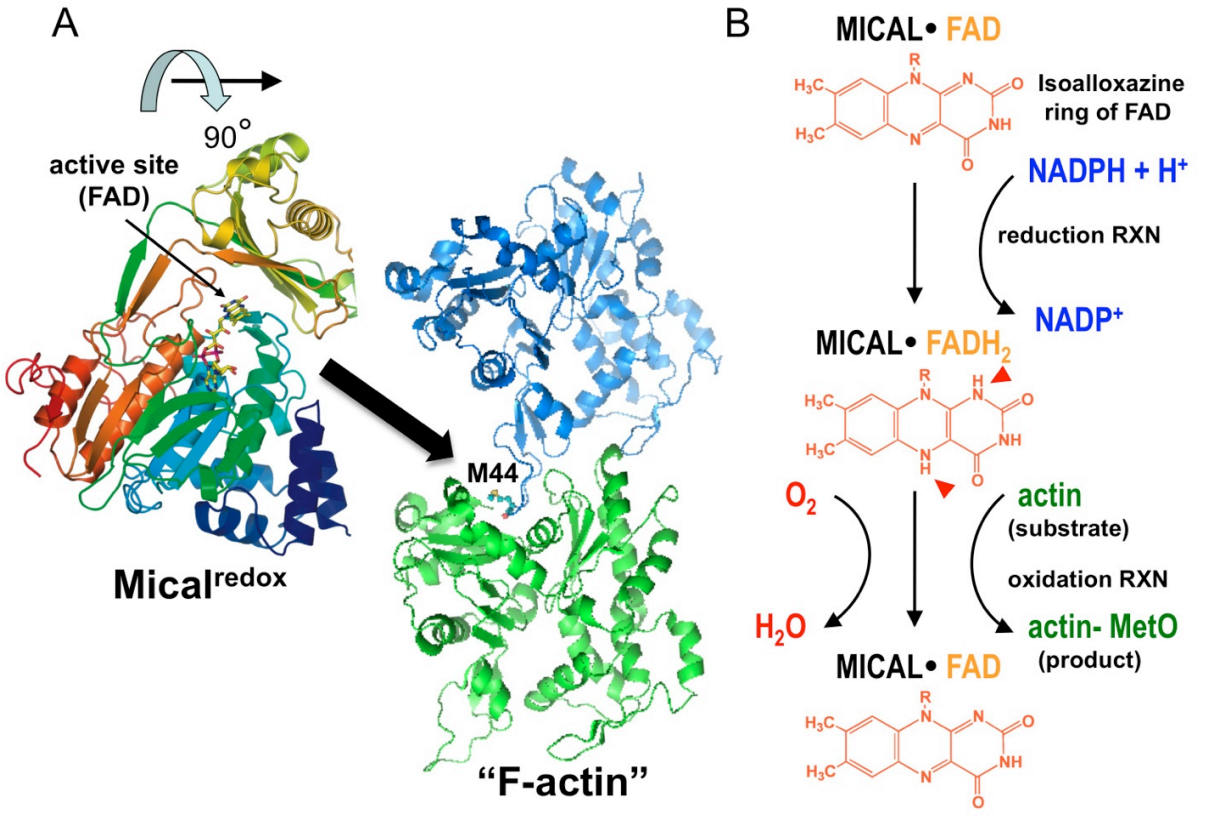

Figure S4.3. Structural representations of Mical^{redox} and F-actin and a model of Mical's catalytic reaction. (A) The structure of mouse MICAL-1^{redox} (PDB ID is 2BRY) (Siebold et al., 2005), which is 54% identical at the amino acid level to Drosophila Mical ^{redox} (Terman et al., 2002), and a dimer of actin (in the F-actin model, PDB ID is 2ZWH) are shown. Mical modifies individual actin subunits within F-actin on their M44 residue, which is poorly accessible to diffusible oxidants (Dalle-Donne et al., 2002; Guan et al., 2003; Guan et al., 2005; Takamoto et al., 2007). Thus, Mical must access the buried M44 residue of actin. In this illustration (based on published structures; PDB IDs are 2BRY, 2ZWH), rotating the Mical structure by 90 degrees (from the top of the page down) provides one model to envision how the active site (small arrow) of Mical accesses (large arrow) the M44 residue. Moreover, FAD which is bound to monooxygenases like Mical and is essential for their enzymatic activity (described in B), is present in the active site (small arrow). (B) This proposed model of the Mical^{redox} catalytic reaction is based on our results and others studying p-hydroxybenzoate hydroxylase (PHBH), whose structure is most closely related to MICAL-1^{redox}. In the reductive half reaction (top step), the FAD is reduced by NADPH (NADPH becomes $NADP^+$ and FAD becomes $FADH_2$). The arrowheads (middle structure) indicate the positions that gain hydrogens (reduced FAD). In the oxidative half-reaction (bottom step), the reduced FAD ($FADH_2$) is re-oxidized by molecular oxygen (to FAD) and inserts one oxygen atom into its substrate.

APPENDIX A

Supplemental information for chapter two

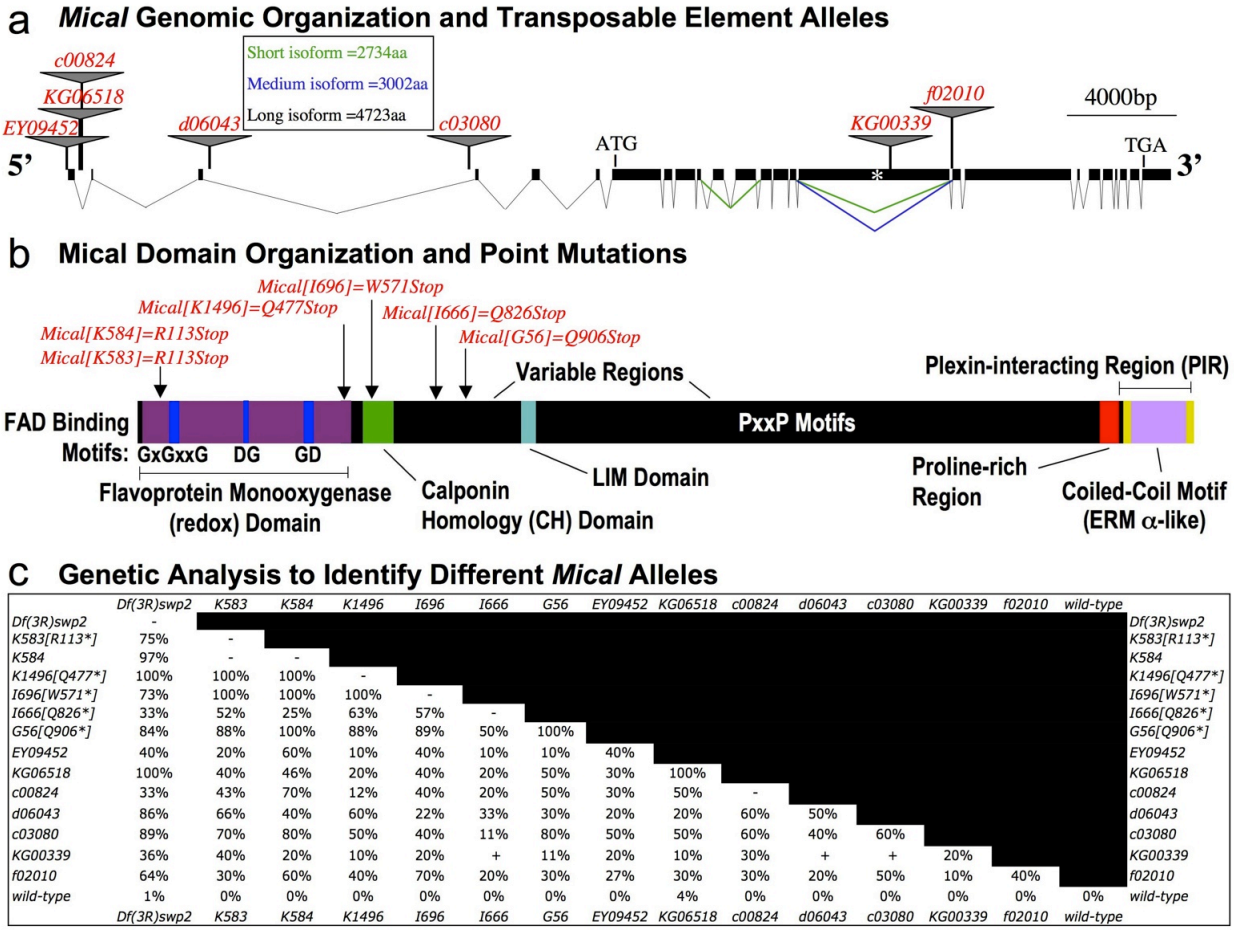

C Genetic Analysis to Identify Different *Mical* Alleles

	Df(3R)swp2	K583	K584	K1496	I696	I666	G56	EY09452	KG06518	c00824	d06043	c03080	KG00339	f02010	wild-type	
Df(3R)swp2	-															Df(3R)swp2
K583[R113*]	75%	-														K583[R113*]
K584	97%	-	-													K584
K1496[Q477*]	100%	100%	100%	-												K1496[Q477*]
I696[W571*]	73%	100%	100%	100%	-											I696[W571*]
I666[Q826*]	33%	52%	25%	63%	57%	-										I666[Q826*]
G56[Q906*]	84%	88%	100%	88%	89%	50%	100%									G56[Q906*]
EY09452	40%	20%	60%	10%	40%	10%	10%	40%								EY09452
KG06518	100%	40%	46%	20%	40%	20%	50%	30%	100%							KG06518
c00824	33%	43%	70%	12%	40%	20%	50%	30%	50%	-						c00824
d06043	86%	66%	40%	60%	22%	33%	30%	20%	20%	60%	50%					d06043
c03080	89%	70%	80%	50%	40%	11%	80%	50%	50%	60%	40%	60%				c03080
KG00339	36%	40%	20%	10%	20%	+	11%	20%	10%	30%	+	+	20%			KG00339
f02010	64%	30%	60%	40%	70%	20%	30%	27%	30%	30%	20%	50%	10%	40%		f02010
wild-type	1%	0%	0%	0%	0%	0%	0%	0%	4%	0%	0%	0%	0%	0%	0%	wild-type
	Df(3R)swp2	K583	K584	K1496	I696	I666	G56	EY09452	KG06518	c00824	d06043	c03080	KG00339	f02010	wild-type	

Figure S2.1. Adult Drosophila *Mical*$^{-/-}$ mutants exhibit abnormal bristle morphology. a, The *Mical* genomic locus. A number of P elements were identified as situated within *Mical* suggesting they might be *Mical* mutant alleles. As described previously (Terman et al., 2002), cDNA analysis of *Mical* indicated multiple splice forms including 1) a "long"; 2) a "medium" (spliced out exon is shown in blue); and 3) a "short" isoform (spliced out exons shown in green). The asterisk indicates an exon not found in the "short" or "medium" isoform and therefore the P element (KG00339) situated in this exon may not affect the expression level of the "short" or "medium" isoforms. **b,** Mical is a large multi-domain cytosolic protein characterized by an oxidoreductase (redox) enzymatic portion (containing FAD binding motifs [GxGxxG, DG, and GD] that define a flavoprotein monooxygenase domain), a calponin homology (CH) domain, a LIM domain, a number of consensus SH3 domain binding motifs (PxxP motifs), a Proline-rich region, and the Plexin-interacting region that contains a coiled-coil motif similar to the alpha region of Ezrin-Radixin-Moesin (ERM) proteins. Two regions variable in length (Variable Regions) are generated by alternative splicing (Terman et al., 2002). There is one Mical family member in Drosophila and three Mical family members in mammals that show a similar domain

organization (Terman et al., 2002). Aberle and colleagues (Beuchle et al., 2007) recently described a number of new nonsense mutations in *Mical.* The position of these point mutations within the Mical protein (and the name of the corresponding alleles) are indicated with arrows. **c**, Genetic complementation and molecular analysis were used to identify fourteen different *Mical* alleles. Most predicted severe alleles of Mical are homozygous lethal but transheterozygous combinations of these alleles generated a few escaper adults. Characterization of these fourteen *Mical* mutant alleles revealed misshapen adult bristles that were thick, bent, twisted, non-curved, and/or had abnormal "club-like" or blunt endings. –, lethal; percentage (%) = percent of flies of the corresponding genotype that contained bristle defects ($n > 10$ flies examined per genotype). *Df(3R)swp2* is the small *Mical* deletion mutant (Terman et al., 2002; Yazdani et al., 2008) and the other alleles are as listed in a and b. *Stretch* mutations (Yazdani et al., 2008) do not have noticeable bristle defects (data not shown). Several combinations of crosses that included the *KG00339* allele (which only is predicted to disrupt the "long" form of Mical) do not exhibit any noticeable defects in bristle morphology.

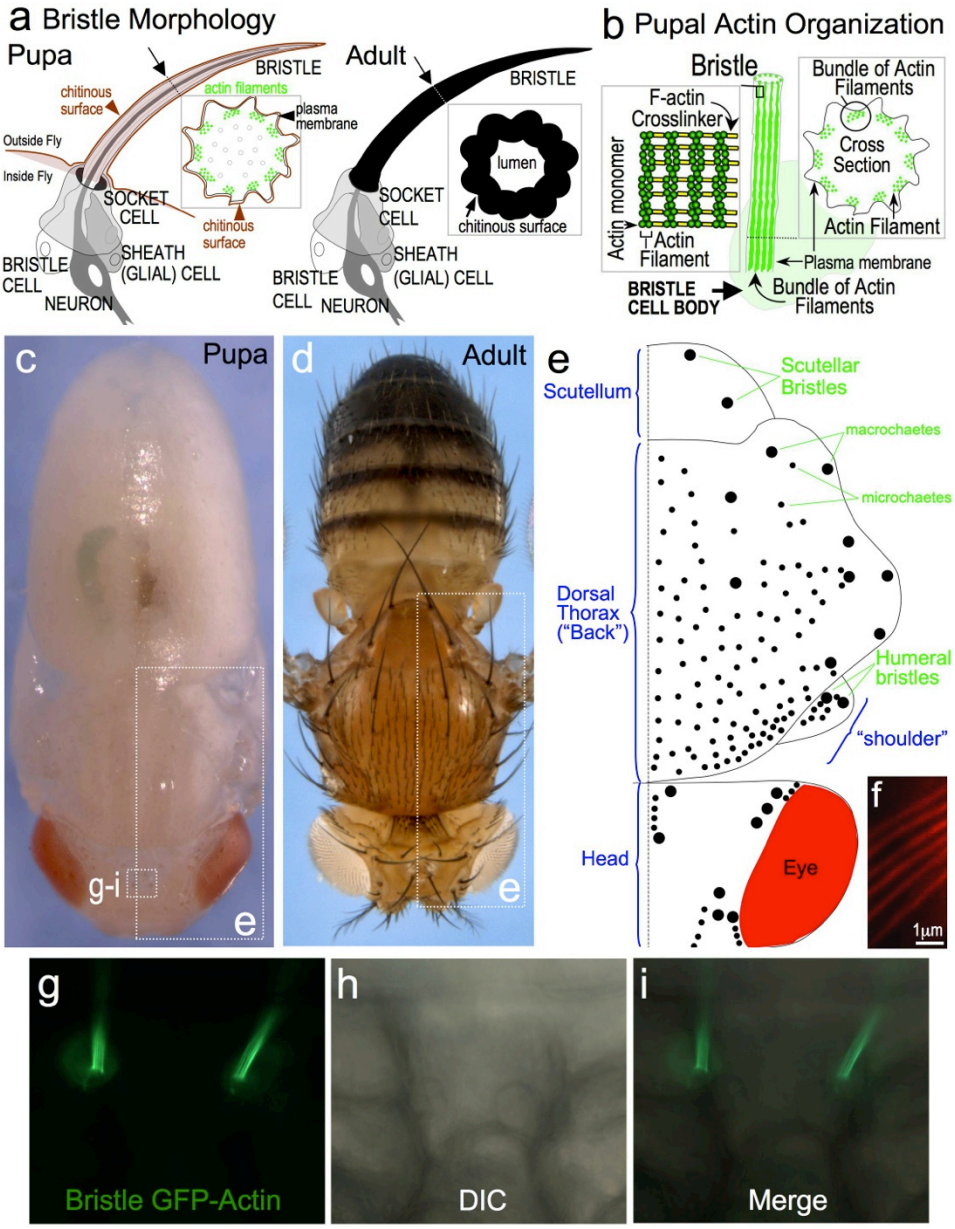

Figure S2.2. Drosophila bristle development and anatomy. Specialized cells such as neurons and bristle cells have the ability to place parts of themselves, specific cellular extensions or processes, at a distance from their cell body of origin. This process extension requires actin filament assembly in both neurons and bristle cells and modulating the organization and dynamics of these actin filaments leads to specific changes in the morphology of these processes. Neurons, for example, extend long tortuous axonal and dendritic processes with multiple branches and expansive growth cones. Bristle cells, in contrast, are much simpler and project short, unbranched, slightly curved processes. The bristle cell, therefore, provides a simple model

cell process in which to examine the molecules and mechanisms that regulate actin filament architecture (Sutherland and Witke, 1999; Tilney and DeRosier, 2005) and mutations in actin modifying proteins including actin bundling/crosslinking proteins like fascin and espin, actin regulators like cofilin, profilin, and WASP, and actin nucleators like Arp2/3 lead to altered actin filament organization in developing bristle processes and misshapen adult bristles (Tilney and DeRosier, 2005). **a,** During pupal development, each bristle cell (trichogen) extends an actin (green circles seen in the cross section) and microtubule (gray circles seen in the cross section)–filled membranous process outside the fly's body that is an extension of the bristle cell soma present within the fly (left). This membranous bristle process later retracts after chitin cuticle deposition and leaves the stiff bristle exoskeleton found in adult flies (right). Adapted from (Tilney et al., 1995) and our own observations. Like hair cells of the vertebrate inner ear (Muller and Littlewood-Evans, 2001), adult bristles are typically mechanoreceptors and neuronal dendrites attach to the upper surface of the bristle from the earliest stages of bristle elongation and are important for the characteristic, slightly-curved shape of Drosophila bristles (Tilney et al., 2004). Note that the socket (tormogen) cell surrounds the base of the bristle cell body and shaft. Previous results have indicated that actin filaments, but not microtubules, are essential for bristle elongation (Tilney et al., 2000a; Tilney and DeRosier, 2005). **b**, A drawing of the normal organization of F-actin bundles in developing *wild-type* pupal bristle processes. The drawing illustrates the presence of actin monomers (green circles) assembled into actin filaments and bundled together with actin crosslinkers/bundling proteins like fascin (yellow). These bundles of actin filaments are situated around the periphery of the bristle, closely adherent to the plasma membrane. **c-e,** Photomicrographs of a Drosophila pupa (c) during the late stages of bristle development before full chitin cuticle deposition, and a "wild-type" adult fly (d) showing the organization of the bristles on the dorsal thorax (notum) and head. Note that the specimens are shown "upside-down" to match the orientation of the bristles that are shown in this and other figures (note also that the wings are not visible to allow better visualization of the bristles). The large region outlined in c-d with the dashed box is shown in schematic form in e to provide a simple overview of the position and size of different types of bristles (also called chaetae or setae). The smaller region outlined in c is shown in g-i at higher magnification and with both fluorescence (g) and differential interference contrast (DIC; h) microscopy. Modified from (Ferris, 1950; Hartenstein and Posakony, 1989). **f-i**, F-actin can be visualized in developing bristles with fluorescently-conjugated phalloidin or bristle-specific expression of GFP-actin using the *B11-GAL4* driver (also called *P[GAL-4]B-11* and *B11-98*; a kind gift from John Merriam; (de la Cova et al., 2004; Guild et al., 2003; Hopmann and Miller, 2003; Tilney et al., 2003; Tilney et al., 2004; Tilney and DeRosier, 2005)). (**f**) The normal organization of F-actin can be visualized with fluorescently-conjugated phalloidin (red) in developing bristle processes; note the ordered, parallel arrangement of F-actin bundles (red) in developing *wild-type* bristle processes. (**g-i**) Photomicrographs of two developing bristle processes as observed in a pupa expressing GFP-actin under the bristle specific *B11-GAL4* promoter. Note that the two bristle cells and their processes are easily visualized with GFP-actin (green; g, i), even though neither their cell body nor process is readily visible with differential interference contrast (DIC) microscopy (h, i).

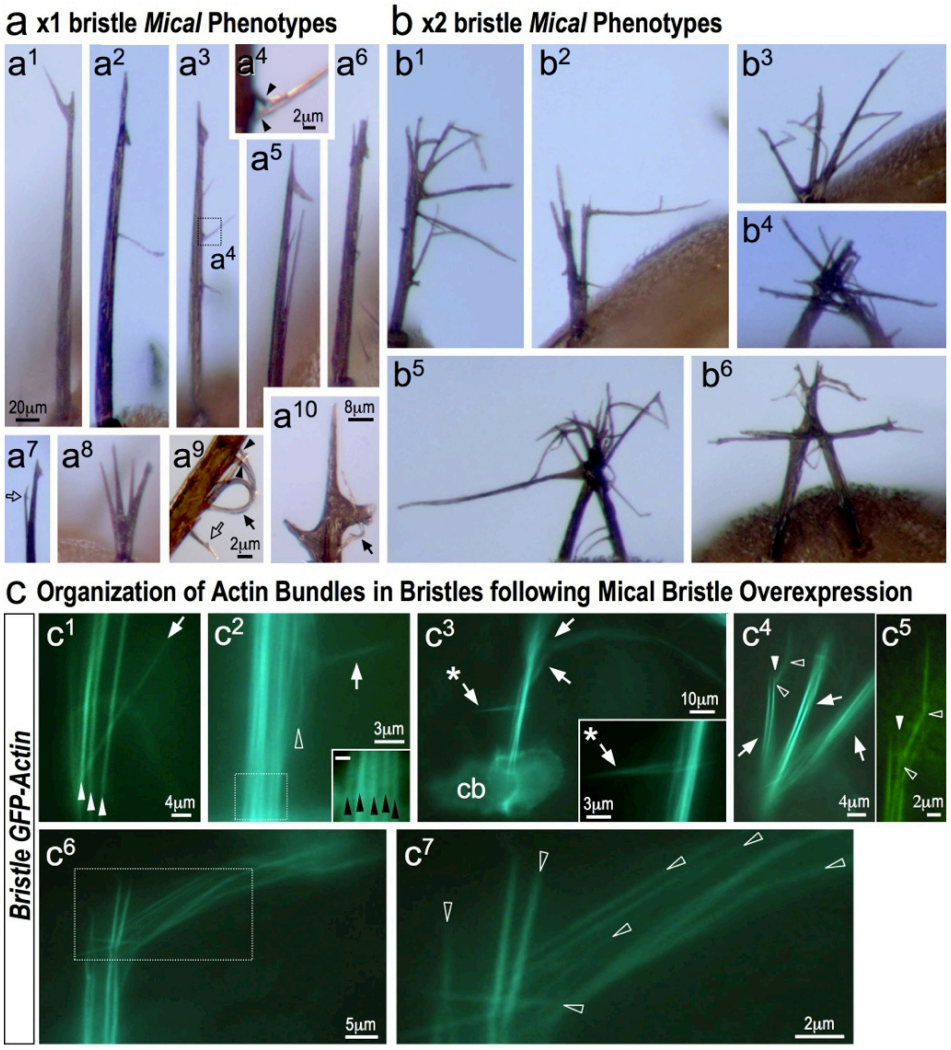

Figure S2.3. Characterization of bristle process morphology and F-actin organization following bristle-specific overexpression of Mical. a, Photomicrographs of bristles from *wild-type* adult flies overexpressing one copy of *Mical* (x1 bristle *Mical*) specifically in bristles (*UAS:Mical/+; B11-GAL4/+*) reveals the appearance of bristle branches. The images seen in a^4 (from the box outlined in a^3), a^9, and a^{10} are higher power photomicrographs that show the fine branches/protrusions (e.g., arrowheads in a^4 and a^9) exhibited by these Mical overexpression bristles. Note that some of these fine branches are curved (e.g., arrows, a^9- a^{10}) and some have their own branches (e.g., open arrow, a^7, a^9). These Mical overexpression bristles were also often shorter than normal. Scale bar: a^1 (also for a^2, a^3, $a^{5\text{-}8}$ and b). **b,** Photomicrographs of bristles from wild-type adult flies overexpressing two copies of *Mical* (x2 bristle *Mical*) specifically in bristles (*UAS:Mical/UAS:Mical; B11-GAL4/+*) reveal multiple bristle branches. In some extreme examples **(**b^4 **–** b^6**)**, branches were so prevalent that they intertwined with the branches of adjacent bristles. These interlaced branches were captured when the chitinous exoskeleton was deposited during development such that in each of these cases the two bristles

appear "fused" together. **c**, In-depth examination shows that bundles of F-actin are reorganized by overexpressing Mical selectively in bristle cells and small "finger-like" protrusions/branches containing actin filaments were observed extending out of this Mical-reorganized actin and from the sides of F-actin bundles. F-actin was visualized by expressing GFP-actin selectively in bristles. **(c^1)** In a mild Mical overexpression phenotype, a relatively ordered array of actin filaments is seen in this bristle process (arrowheads) except for the single bundle of F-actin projecting off at an angle (arrow). **(c^2)** In another bristle process from the same Mical overexpression pupa, an ordered array of actin bundles is seen in the region outlined with the dashed box (arrowheads, at higher power in the inset). However, at regions more distal to the cell body, the F-actin bundles become smaller in caliber (e.g., open arrowhead) and arranged in a disordered meshwork; a single F-actin branch (arrow) off the main bristle shaft is seen arising from this disorganized region. **(c^3)** Multiple branches are observed in this bristle (arrows) and the branch indicated with the asterisk is shown at higher power in the inset. **(c^4)** In some cases we observed that several large bristle branches had formed and each contained multiple bundles of F-actin. In this example, notice that three distinct bristle shafts are present (arrows) and the region indicated with the open and closed arrowheads can be seen in a different focal plane at higher power in c^5. In c^5, an individual F-actin bundle is indicated (closed arrowhead), while another bundle of F-actin can be seen in close association and oriented at an angle (lower open arrowhead). Note that the upper open arrowhead also demarcates a similar close association of F-actin bundles in different orientations. **(c^6 - c^7)** When higher levels of Mical are expressed, additional rearrangement of the F-actin cytoskeleton is seen. A portion of the image in c^6 (dashed box) is seen at higher power in the inset in c^7. Notice that F-actin bundles are present but have often lost their parallel arrangement. Likewise, individual bundles of F-actin vary in caliber and length (e.g., open arrowheads, **c^7**) and extend in different directions. Inset c^2= 1μm.

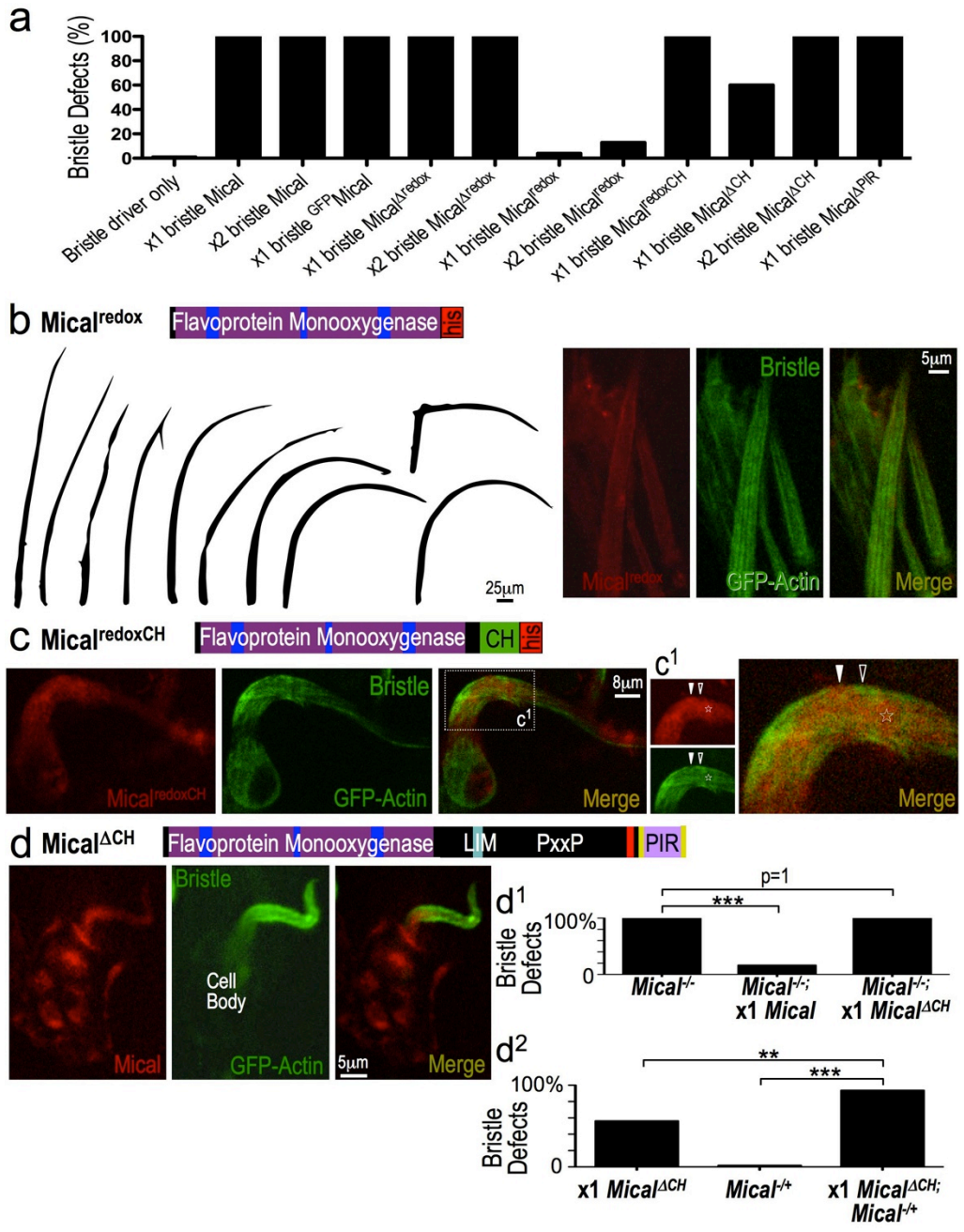

Figure S2.4. Characterization of bristle development and morphology following the expression of different forms of Mical in bristles. **a**, The percentage of adult flies containing bristle defects as a percentage of the total number of flies examined following the specific expression in bristles of one (x1 bristle) or two copies (x2 bristle) of different forms of Mical using the *B11-GAL4* bristle driver. In all cases, only one copy of the bristle driver (*B11-GAL4*) was employed. $n \geq 50$ adults per genotype. **b**, The Mical^{redox} protein is poorly localized to

bristle processes and has little effect on bristle morphology. The Mical^{redox} transgenic fly line contains only the Mical redox domain, followed by a 6 histidine (his) tag and a stop codon at the C-terminus. Very few flies expressing Mical^{redox} in all bristles (one or two copies) exhibit any bristle defects (quantified in a) but the majority of those that do, exhibit weakly branched bristles. Examination of the expression levels of Mical^{redox} protein revealed that high levels of Mical^{redox} protein is expressed (data not shown) but the majority of the Mical^{redox} protein did not localize to bristle processes (but was found in the cell body, data not shown). For example, using the bristle specific *B11-GAL4* driver, His-tagged Mical^{redox} protein (red) can be seen in Drosophila pupal bristle processes (green) but shows only a relatively diffuse pattern of localization (with only low levels present in the bristle processes) when compared to GFP-labeled F-actin and full-length Mical (Figures 2.2b, 2.3A, 2.3B). These results indicate that Mical is localized in a very specific manner within elongating bristle processes and the redox domain is not sufficient to allow for this localization. Scale bar can be used for all images in b. **c**, The Mical^{redoxCH} protein localization. The Mical^{redoxCH} transgenic fly line and protein contains the Mical redox domain and the calponin homology (CH) domain followed by a six histidine (his) tag and stop codon at the C-terminus. Bristle specific expression of Mical^{redoxCH} generates highly tortuous bristles that are even more abnormal and branched than those seen when full-length Mical is overexpressed in bristles (see Figure 2.1h - i). Mical^{redoxCH} bristles were also found resting directly on the body of the fly indicating that they could not support themselves normally (see Figure 2.1h). Confocal microscopy revealed that His-tagged Mical^{redoxCH} (red) and F-actin (green, GFP-actin) co-localize (yellow, merge) in developing bristle processes as observed in a pupa expressing GFP-actin specifically in bristles. Mical^{redoxCH} shows a puncate localization within the bristle process and the normal organization of F-actin bundles is disorganized. Notice also that Mical^{redoxCH} colocalizes with this disorganized F-actin and shows highest localization to regions of the bristle process showing the most F-actin disorganization. The region outlined with the dashed box is shown in higher power images in c^{1} where Mical^{redoxCH} and GFP-actin co-localization can be seen more clearly. Interestingly, some regions of higher Mical^{redoxCH} immunostaining (red) appeared to exhibit diffuse GFP-actin (green) immunostaining (e.g., closed arrowheads, stars) and regions showing stronger immunostained GFP-actin bundled filaments exhibited weaker Mical^{redoxCH} immunostaining (e.g., open arrowheads). These results are consistent with our results that Mical disassembles bundled actin filaments and Mical^{redoxCH} is constituitively active. Interestingly, the Mical^{redoxCH} protein while showing a punctate localization within bristle processes, and co-localization with actin, did not localize as selectively as full-length Mical to the tip of extending bristle processes or along the membrane in distinct puncta. These results indicate that Mical is localized in a very specific manner within elongating bristle processes and this localization is altered to some extent by removing portions of Mical C-terminal to the CH domain. Scale bar can be used for all images in c. **d**, Mical$^{\Delta CH}$ protein induces abnormal localization of Mical within the developing bristle process and acts like a dominant-negative Mical protein. A transgenic fly line was generated containing full-length Mical with a deletion of its CH domain (Mical$^{\Delta CH}$). Immunostaining pupae expressing Mical$^{\Delta CH}$ with a Mical antibody revealed that Mical (red) shows weaker

localization within the developing bristle process and tip in the presence of Mical$^{\Delta CH}$ protein and is highly localized within the bristle cell body and at the base of the bristle (compare with Figure 2.2b). These results indicate that Mical is localized in a very specific manner within elongating bristle processes and the CH domain of Mical is necessary for this localization. **d^{1}-d^{2}**, Several different genetic assays indicate that Mical$^{\Delta CH}$ acts as a Mical dominant negative protein. **d^{1}**, Bristle expression of Mical$^{\Delta CH}$ does not rescue the bristle defects seen in a *Mical* loss-of-function mutant. The bristle defects observed in a *Mical* loss-of-function mutant (*Mical^{K1496}/Df(3R)swp2*) can be significantly rescued with bristle expression of full-length Mical (*Mical$^{-/-}$*; x1 *Mical*; as described and also shown in Figure 2.1c) but not with bristle expression of Mical$^{\Delta CH}$ (*Mical$^{-/-}$*; x1 *Mical$^{\Delta CH}$*). Chi-Square Test; *** = $p<0.0001$. $n \geq 25$/genotype. **d^{2}**, The percentage of flies seen with bristle defects when one copy of *Mical$^{\Delta CH}$* is expressed in all bristles (x1 *Mical$^{\Delta CH}$*) in a *wild-type* background can be significantly enhanced (Chi-Square Test; *** = $p<0.0001$, ** = $p<0.01$) by removal of one copy (*Mical$^{+/-}$*) of a *Mical* loss-of-function mutation (*Df(3R)swp2*/+). $n \geq 25$/genotype. Furthermore, as shown in Figure 3A, Mical$^{\Delta CH}$, unlike full-length Mical, does not enhance (but suppresses) the branching defects seen when plexA is overexpressed in bristles. *t*-test; *** = $p<0.0001$. Scale bar can be used for all images in d.

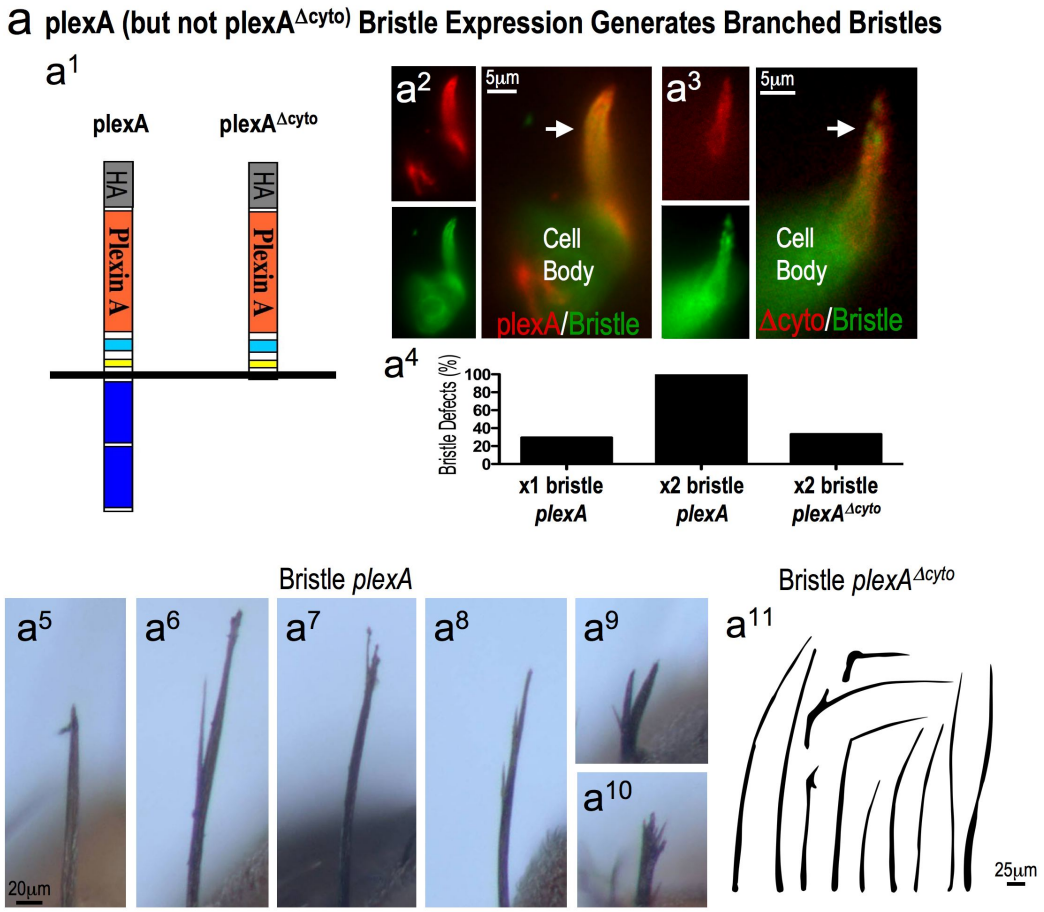

Figure S2.5. Plexin A is sufficient to alter bristle process morphology and requires its cytoplasmic portion to mediate its bristle branching effects. a, Overexpression of plexA in bristle cells (but not plexA without its cytoplasmic portion [Δcyto]) generates highly penetrant branched bristle phenotypes. **a**^{1}, To further examine if the branching effects we observed in Mical overexpression mutants were consistent with an increase in semaphorin-plexin signaling in the bristle we overexpressed plexA in all bristles with or without its cytoplasmic portion. The plexA$^{\Delta cyto}$ construct (He et al., 2009) provided the ability to examine the importance of the plexA cytoplasmic domain in altering bristle morphology and actin organization. Furthermore, Plexin A receptors without their cytoplasmic portion have been found previously to function as dominant negative Plexin receptors (e.g., (He et al., 2009; Takahashi and Strittmatter, 2001; Zhuang et al., 2009)) and so plexA$^{\Delta cyto}$ also offered an alternative approach to disrupt endogenous plexA signaling. **a**^{2} – **a**^{3}, Both ^{HA}plexA and ^{HA}plexA$^{\Delta cyto}$ localize strongly to developing bristle processes (arrows). **a**^{4}, The percentage of adult flies containing bristle defects as a percentage of the total number of flies examined following the specific expression in bristles of one (x1 bristle) or two copies (x2 bristle) of different forms of plexA using the *B11-GAL4* driver. In all cases, only one copy of the bristle driver (*B11-GAL4*) was employed. $n \geq 50$

adults/genotype. **a^5 – a^{10}**, Our results revealed that overexpression of one copy of *plexA* in all bristles led to branched Drosophila bristles. These branching phenotypes could be further increased by elevating the number of copies of *plexA* expressed in bristles. In addition to these branching defects, we also noticed that, like Mical overexpression mutants, the length of the bristles was also decreased in plexA bristle overexpression mutants. Photomicrographs of bristles from adult flies overexpressing one (a^5) or two copies of plexA in all bristles using the *B11-GA*L4 driver (*UAS:*^{HA}*plexA/+; B11-GAL4/+*; Bristle plexA). Bristles in these plexA overexpression adults exhibited branches, examples of which are shown on the scutellum (a^5- a^6, a^8), dorsal thorax/"back" (a^7, a^9), and head (a^{10}). See also Figure 3A. **a^{11}**, plexA$^{\Delta cyto}$ overexpression (one or two copies) resulted in few branched bristles and those bristle defects that we did see resembled *plexA* loss-of-function bristles. See also Figure 3A. Scale bar in a^5 can be used for a^6-a^{10}.

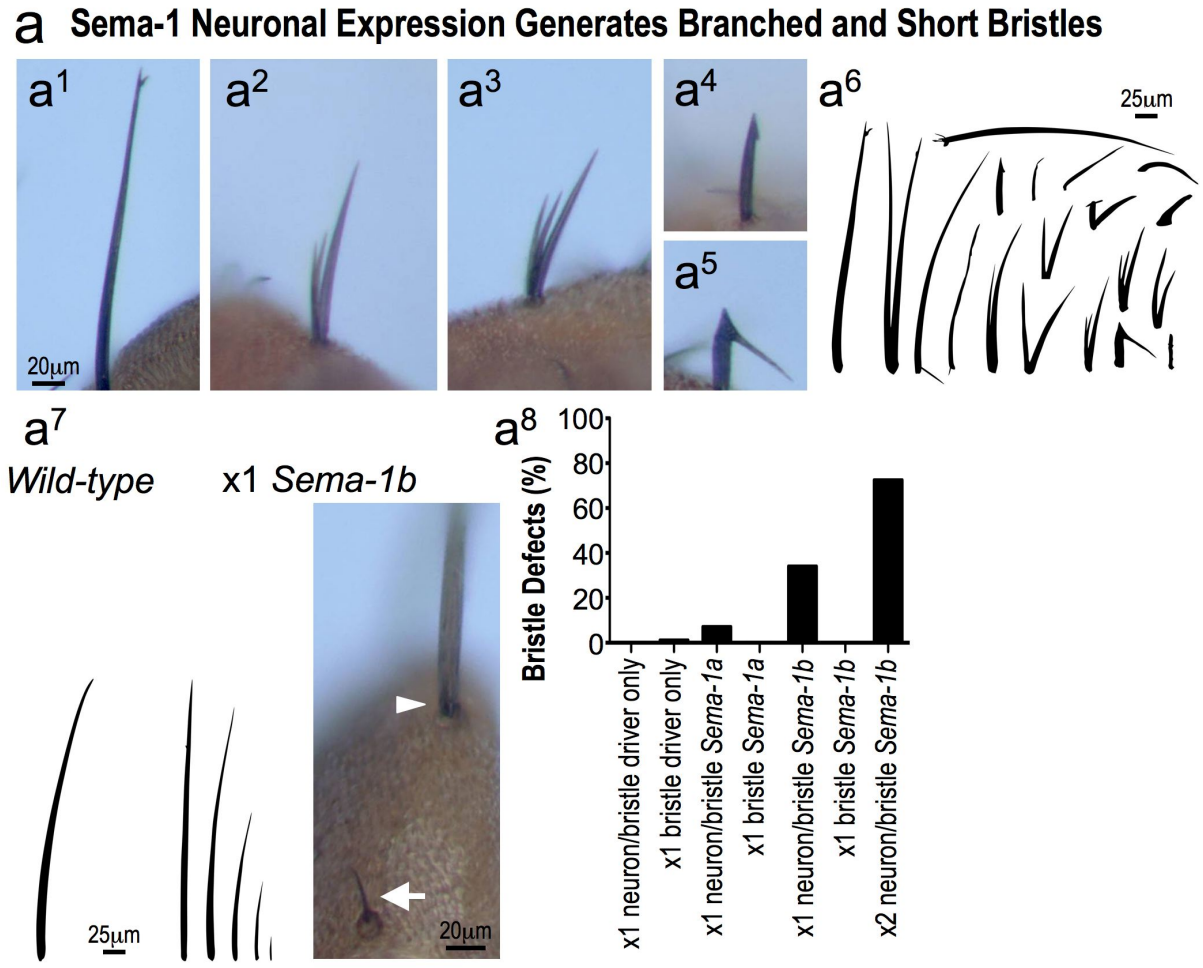

Figure S2.6. Transmembrane Semaphorins are sufficient to alter the morphology of bristle processes. a, Overexpression of transmembrane semaphorins in the neurons that innervate bristles using *Sca-GAL4* (but not in the bristle cells themselves using *B11-GAL4*) resulted in alterations to bristle morphology, and were more prevalent with Sema-1b overexpression than with Sema-1a. In light of the sufficiency of Mical and plexA to induce changes to bristle morphology, we wondered if transmembrane semaphorins were also sufficient to induce alterations to bristle morphology. Employing the *Sca-GAL4* driver to express transmembrane semaphorins primarily in neurons, we noticed alterations in the morphology of bristle processes that included selective branching of bristles as well as dramatic changes to the length and diameter of bristles. We noted, however, that these phenotypes seen when transmembrane semaphorins were overexpressed primarily in neurons were less prevalent than those seen when Mical or plexA were overexpressed in bristle processes. Among other reasons, these differences could be due to the high levels of transmembrane semaphorins already present in the innervating dendrites, that transmembrane semaphorins are not the limiting factors in inducing changes in

bristle morphology and actin reorganization (but that their receptor and downstream signaling components are), and/or the fact that the *Sca-GAL4* driver is not only expressed in neurons but also in the bristle cells themselves (and Sema-1a, for example, is known to also signal through its cytoplasmic portion [reverse signaling; (Komiyama et al., 2007)] which could complicate our experiments). **a[1] – a[5],** Photomicrographs of bristles from adult flies overexpressing Sema-1b primarily in neurons using the *Sca-GAL4* driver. Bristles in these transmembrane semaphorin overexpression adults exhibit branches, examples of which are shown on the scutellum (a[1]), and head (a[2] – a[5]). Scale bar in a[1] applies to a[2] – a[5]. **a[6],** Drawings of representative bristles from flies overexpressing Sema-1b primarily in neurons using the *Sca-GAL4* driver. Note that they are abnormally shaped and many exhibit branches of varying shapes, position, sizes, and number. **a[7]**, We also saw a class of phenotypes that were more severe in the transmembrane semaphorin overexpression lines. Overexpression of Mical or plexA in bristles using the *B11-GAL4* driver led to bristle branching defects as well as to a decrease in bristle length. Likewise, overexpression of Sema-1b in neurons using the *Sca-GAL4* driver resulted in some bristles that were much shorter and smaller in diameter than *wild-type* adult bristles. Examples of these smaller bristles are shown in the drawings of the x1 *Sema-1b* bristles: they range in size but should all be the same size as the *wild-type* bristle. A severe example of the reduced size of a bristle observed when Sema-1b was overexpressed primarily in neurons can be seen in the photomicrograph (arrow). An adjacent bristle that has a relatively normal diameter (arrowhead) is seen at the top of the image from the same fly. **a[8]**, The percentage of adult flies containing bristle defects as a percentage of the total number of flies examined following the specific expression primarily in neurons of one (x1 neuron/bristle) or two copies (x2 neuron/bristle) of *Sema-1a* or *Sema-1b* using the *Sca-GAL4* driver. In all cases, only one copy of the *Sca-GAL4* driver was employed. We saw no defective bristles when we expressed *Sema-1a* or *Sema-1b* in the bristle cells themselves using *B11-GAL4* (x1 bristle). $n \geq 50$ adults per genotype.

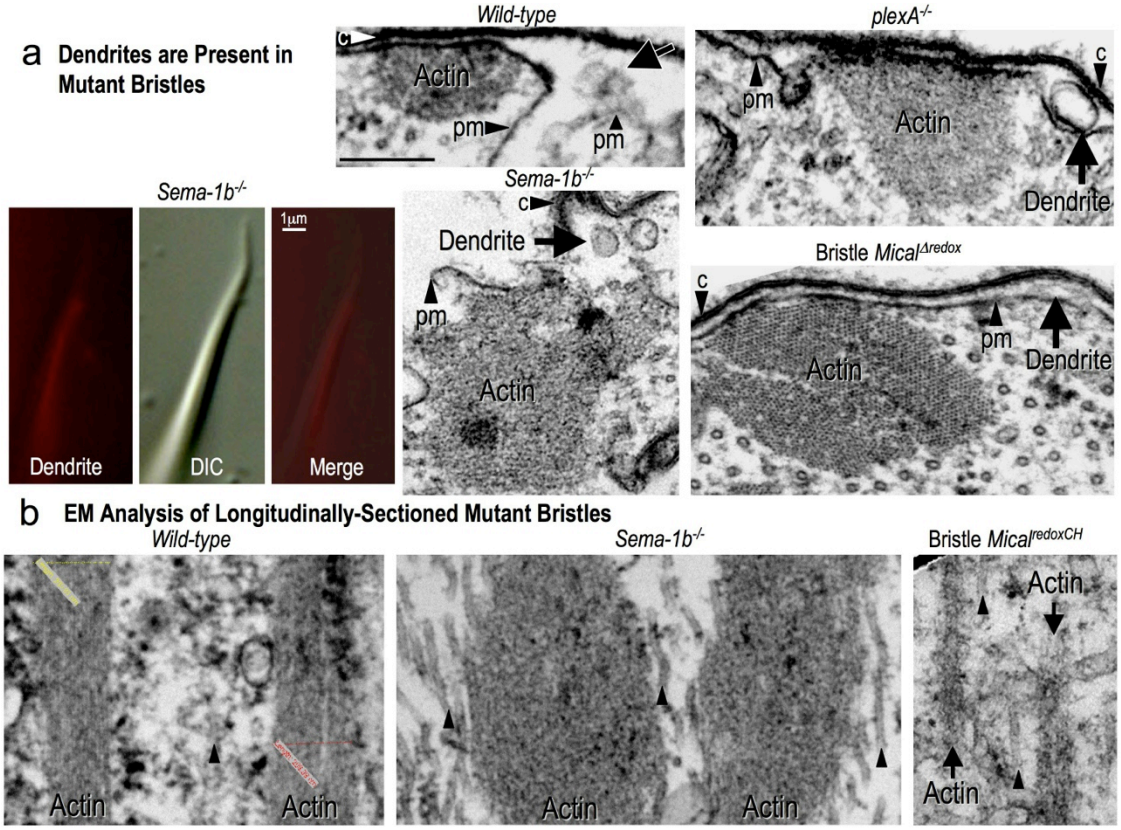

Figure S2.7. Further characterization of actin organization in *Semaphorin*, *Plexin*, and *Mical* mutants. a, We did not find any evidence indicating a lack of dendritic innervation of bristle processes in *Sema-1b*$^{-/-}$, *plexA*$^{-/-}$, or *Mical* mutants but we did find an increase in the size of F-actin bundles in the bristle processes of these mutants. Using an antibody to Sema-1a, which selectively labels the dendrites innervating bristle processes, or ultrastructural analysis we did not find any differences in the presence of dendrites within the bristle processes of *Sema-1b*, *plexA*, or *Mical* (data not shown) mutants when compared to wild-type pupae (or pupae with a Mical dominant negative protein expressed selectively in bristles [e.g., Bristle *Mical*$^{\Delta redox}$]). In these examples from a *Sema-1b*$^{-/-}$ mutant, the dendrite (red) is present within the bristle process of a late stage pupa with a tip alteration (as seen using DIC optics). Likewise, in these examples examined using EM, dendrites (arrows) could be found in the bristles of *Sema-1b*, *plexA,* and bristle-expressing Mical$^{\Delta redox}$ mutants (in close association with F-actin bundles). The plasma membrane (pm), chitin cuticle (c), and bundled F-actin (actin) are labeled for reference. These findings are supportive of our results that transmembrane semaphorins in the dendrite signal to plexA/Mical in the developing bristle process and this signaling event regulates the actin organization in the developing bristle process. These findings are also in line with our expression analysis for plexA and Mical which shows strong expression in bristle processes and no identifiable expression in the dendrites that innervate the bristles. Likewise, expression of

dominant-negative forms of either plexA (without its cytoplasmic portion) or Mical (Δredox, ΔCH) selectively in bristles generates loss-of-function-like bristle defects. These observations are also in line with the sufficiency of plexA and Mical to generate actin alterations in bristle processes when they are expressed selectively in bristle cells; while Sema-1's are sufficient to generate actin alterations in bristle processes when they are expressed in neurons but not in bristle cells. Furthermore, our observations that indicate a requirement for Sema–Plex–Mical signaling in bristle cells are supported by our ability to rescue the *Mical*$^{-/-}$ mutant bristle defects by restoring Mical selectively in bristle cells and with our in vitro results showing that Mical can directly regulate actin filament dynamics (**Figures 2.3** and **2.4**). Notice also the increase in size of the bundles of F-actin (Actin) present in *Sema-1b*$^{-/-}$, *plexA*$^{-/-}$, and bristle-expressing Mical$^{\Delta redox}$ bristles when compared to the bundles of F-actin found in wild-type bristles (see also **Figure 2.2d** and **S2.7b**). **b**, Ultrastructural analyses on longitudinal/horizontal sections of the developing bristle process viewed at the same magnification (and also the same magnification as in (a)) and cut through the "widest" portion of the actin bundle for each genotype also reveals that transmembrane Semas, plexA, and Mical regulate actin filament distribution and bundling in vivo. Longitudinally cut microtubules can also be seen (e.g., arrowheads). For example, (**Wild-type**) a longitudinal section cut through two bundles of a normal developing bristle process and examined using transmission EM reveals bundled actin filaments. **(*Sema-1b*$^{-/-}$)** An increase in the size of the bundles of F-actin was observed in *Sema-1b* mutant bristle processes. **(Bristle *Mical*^{redoxCH})** Only small bundles of F-actin (arrows) are present at the membrane and within the interior of the bristle process when Mical^{redoxCH} is expressed selectively in bristle cells (**Figure 2.2d**, Bristle *Mical*^{redoxCH}). Interestingly, when full-length Mical is overexpressed in developing bristles, only small bundles of F-actin are present at the membrane (e.g., see **Figure 2.2d**, x2 bristle *Mical*, arrow) but larger bundles of F-actin are present in the interior of the bristle process (e.g., see **Figure 2.2d**, x2 bristle *Mical*, arrowhead). These results suggest that full-length Mical specifically regulates F-actin bundling in close association to the membrane while Mical^{redoxCH} regulates F-actin bundling throughout the bristle process (i.e., at the membrane and in the interior of the bristle process)**.** The scale bar in the Wild-type ultrastructural image (250nm) applies to all EM images.

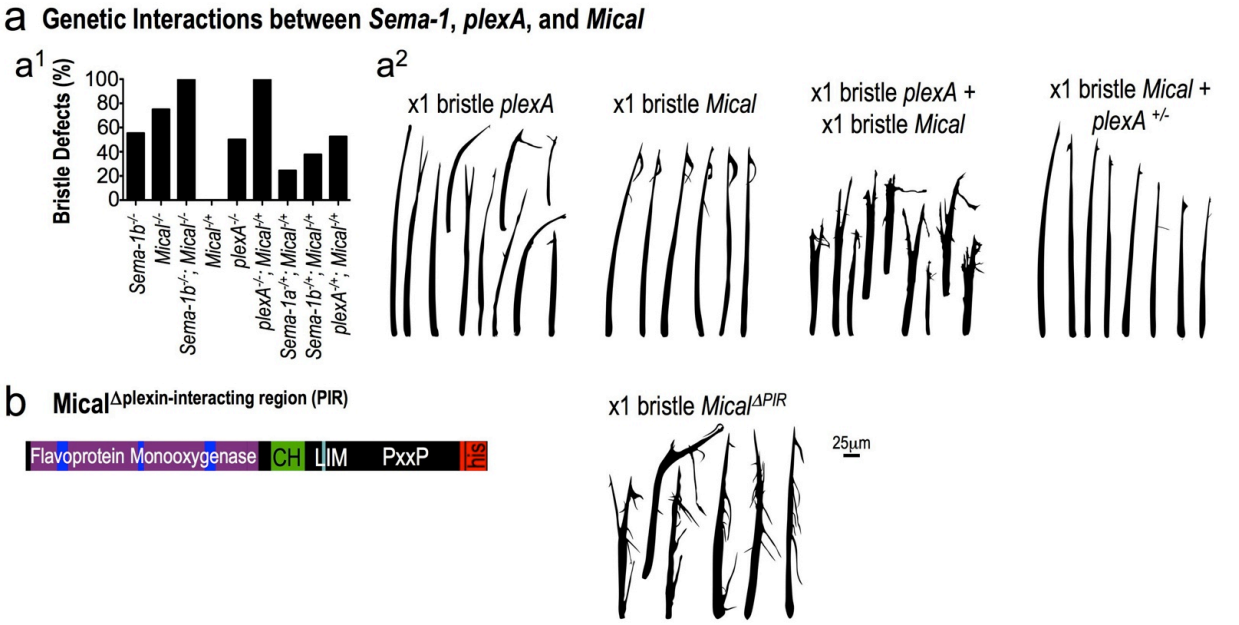

Figure S2.8. Mical works with Sema–plexA signaling to direct modifications to bristle morphology. **a,** Genetic interaction analysis reveals that Mical works with Sema–plexA signaling to direct modifications to bristle morphology. See also **Figure 2.3A**. Genetic interaction analyses between *Mical, Sema-1a, Sema-1b, and plexA*. **a[1],** Compared to either mutation alone, the percentage of flies with defective bristles increased to 100% when we made flies containing hypomorphic mutations in both *Sema-1b* and *Mical*. Likewise, compared to flies containing a homozygous mutation in *plexA*, the percentage of flies with defective bristles increased to 100% when we made flies containing a homozygous mutation in *plexA* as well as a heterozygous mutation for *Mical*. In addition, as we were attempting to make different double mutant combinations we noticed weak but consistent dominant genetic interactions between mutant alleles of *Mical* and mutant alleles *Sema-1a*, *Sema-1b*, and *plexA*. Compared with flies containing heterozygous mutations in either *Mical*, *Sema-1a*, *Sema-1b*, or *plexA* (which showed little to no bristle defects [<2%]), transheterozygous flies containing P element or small deficiency mutations in *Sema-1a* and *Mical* (*Df(2L)Exel7039/+; Df(3R)swp2/+*), *Sema-1b* and *Mical* (*Sema-1b*^{EY21782}*/+; Df(3R)swp2/+*), or *Mical* and *plexA* (*Df(3R)swp2/+; Df(4)C3/+*) exhibit bristle defects and these differences were statistically significant (Chi-Square Test; $p<0.0001$). $n \geq 16$ adults/genotype. **a[2]**, Genetic interaction assays reveal that Mical is sufficient to enhance the bristle branching effects of plexA overexpression and that Mical-mediated bristle branching is regulated by plexA. To determine if Mical works with plexA to generate F-actin reorganization and bristle branching we overexpressed plexA in the presence or absence of Mical. For the overexpression studies, one of the transgenic lines that showed weaker expression of Mical (x1 *Mical*) was used since it was found to give rise to bristle branches of relatively similar shape, position, size, and number. Expressing both one copy of *plexA* and one copy of *Mical* in all bristles (x1 bristle *plexA* + x1 bristle *Mical*) revealed a pronounced enhancement of bristle branching when compared to animals expressing either one of the transgene's alone (see also **Figure 2.3A**). In contrast, removing one copy of *plexA* in the Mical bristle overexpression

background suppressed Mical-mediated bristle branching indicating that plexA is an activator of Mical (see also **Figure 2.3A**). **b**, A transgenic fly line was generated containing full-length Mical with a deletion of only its plexin-interacting region (PIR) domain followed by a 6 histidine (his) tag and a stop codon at the C-terminus (Mical$^{\Delta PIR}$). Bristle specific expression of this Mical$^{\Delta PIR}$ protein results in a hyperactive form of Mical and generates multiple bristle branches. Furthermore, decreasing Sema–Plexin signaling limited the actin destabilizing activity of full-length Mical (see **Figures 2.3A**, **S2.8a**[2]), but not that of this constitutively active Mical$^{\Delta PIR}$ (see **Figure 2.3A**) or Mical^{redoxCH} (data not shown). These findings with Mical$^{\Delta PIR}$, coupled with our Mical^{redoxCH} data, our genetic analysis, and previous results (Schmidt et al., 2008; Terman et al., 2002) indicate that Mical's ability to control F-actin organization is tightly regulated by other regions of the large Mical protein. These results also reveal that Mical plays a positive (and necessary) role in Sema–plexA signaling and suggest that the Plexin-interacting region of Mical serves to autoinhibit Mical activity and that binding of Mical to Sema-activated Plexin releases this Mical autoinhibition and activates Mical. This mechanism would enable the localized activation of Mical in response to extracellular signals carried by semaphorins. All together, these results are consistent with a model in which Plexin is typically in an inactive conformation (e.g., (He et al., 2009; Negishi et al., 2005; Oinuma et al., 2004; Takahashi and Strittmatter, 2001)), and upon binding to Sema, Plexin becomes active and then binds and activates Mical. The scale bar can be used for all of the bristle drawings.

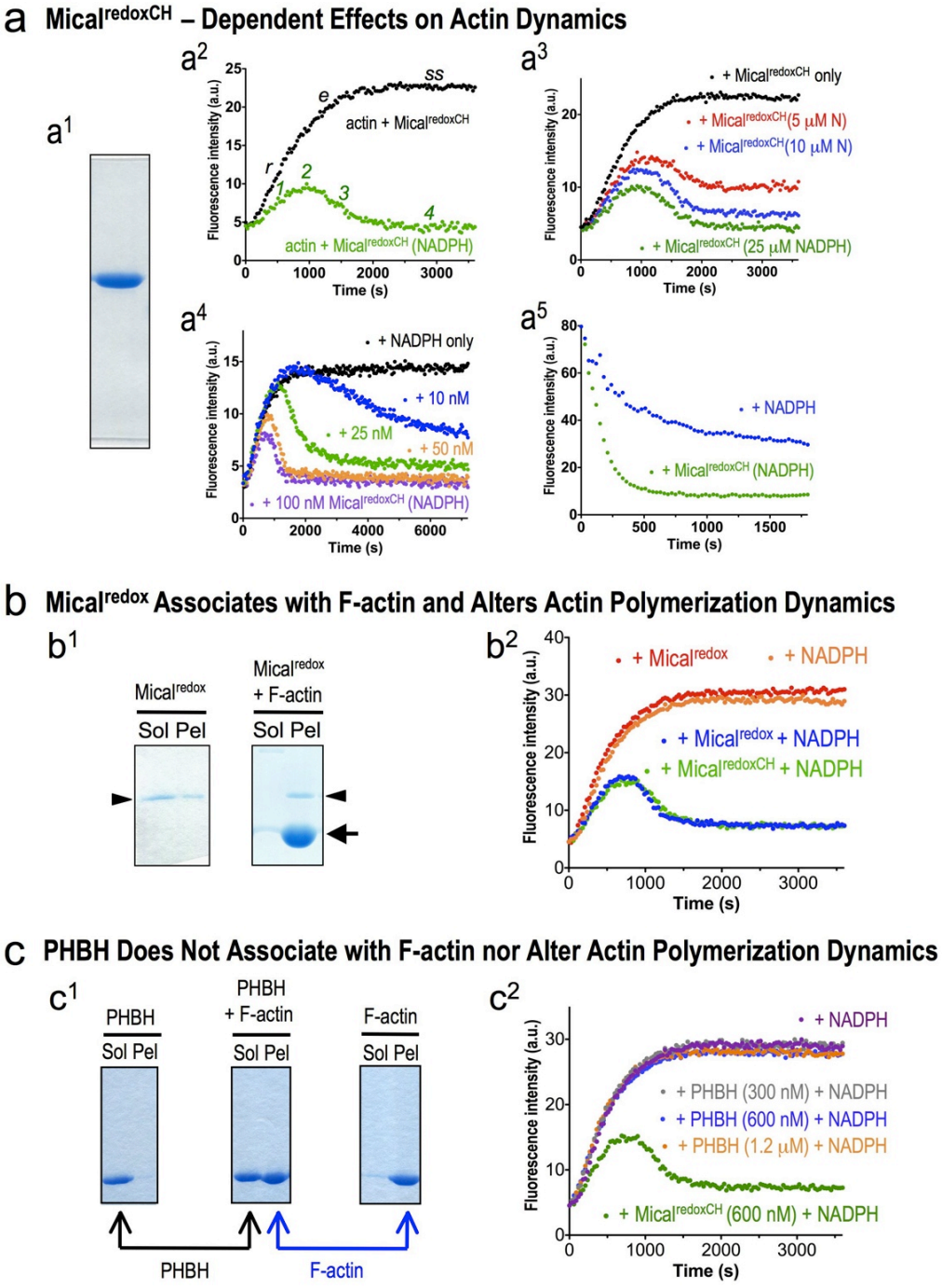

Figure S2.9. The Mical redox enzyme, but not the related redox enzyme PHBH, co-sediments with F-actin and alters actin dynamics. a, Further analysis of the effects of Mical on actin polymerization and depolymerization. **a[1]**, A Coomassie blue stained gel revealing the purity of the Mical^{redoxCH} protein that was used for the biochemistry experiments. **a[2]**, Mical^{redoxCH} alters actin polymerization in an NADPH dependent manner. As can be observed by following

the characteristic increase in fluorescence intensity over time, the addition of 600 nM Mical^{redoxCH} (black dots) does not affect the rate (*r*), extent (*e*), or steady-state level (*ss*) of actin polymerization. However, the addition 600 nM Mical^{redoxCH} in the presence of 50 μM of its NADPH coenzyme (Mical^{redoxCH} (NADPH), green dots) results in specific alterations to the ability of actin to polymerize such that actin polymerization slows-down over time (*1*), which is followed by a substantial decrease in the extent of polymerization (*2*), the rapid depolymerization of F-actin (*3*), and the inability of actin to reinitiate polymer formation (*4*). **a^{3} – a^{4}**, Mical's ability to alter actin polymerization shows a dosage response that depends on the concentration of both NADPH and Mical^{redoxCH}. **a^{3}**, The effect of Mical^{redoxCH} (600 nM) on actin polymerization weakens as the concentration of the NADPH (N) coenzyme decreases from 25 μM (green) to 5 μM (red). **a^{4}**, Likewise, the effect of Mical on actin polymerization appears catalytic since Mical alters actin polymerization at very low, substoichiometric concentrations (relative to the concentration of actin which was 1.1 μM in all experiments). The concentration of the NADPH coenzyme was fixed at 400 μM to maximize the number of activated Mical^{redoxCH} proteins. **a^{5}**, A dilution-induced actin depolymerization assay was also used to determine the effect of purified Mical^{redoxCH} protein on actin depolymerization. Depolymerization was induced by diluting pre-assembled pyrene labeled actin filaments so that there was a gradual disassembly of actin filaments (decreasing fluorescence intensity) as seen in our control experiment (100 μM NADPH; blue dots). In contrast, Mical^{redoxCH} (600 nM) in the presence of NADPH (100 μM) rapidly accelerates the rate and extent of this depolymerization (green dots). **b**, Mical^{redox} co-sediments with F-actin and regulates actin polymerization. **b^{1}**, Co-sedimentation analysis reveals that purified Mical^{redox} associates with actin filaments. Some calponin homology (CH) domains are involved in actin filament binding and are present in a number of F-actin bundling proteins. Likewise, the redox domain of Mical also contains an extensive patch of positive charge that may provide a binding surface for negatively charged actin filaments (Siebold et al., 2005). We therefore tested whether the CH domain was necessary for the association we had seen between Mical^{redoxCH} and F-actin (see also **Figures 2.3B**, **c-d**). F-actin was assembled from purified actin in vitro. In the presence of purified actin filaments, purified Mical^{redox} protein (arrowhead) is present in the pellet (Mical^{redox} + F-actin) indicating that the redox portion of Mical associates with F-actin. Sol, G-actin (soluble); Pel, F-actin (pellet). Mical^{redox} did not co-sediment with microtubules (**Figures 2.3B**, **d**; **S2.11**) indicating that Mical^{redox} selectively associates with actin. **b^{2}**, Mical^{redox} directly affects actin polymerization in the presence of NADPH. Pyrene-actin was polymerized in the presence of Mical^{redox} (600 nM), NADPH (100 μM), or either Mical^{redox} or Mical^{redoxCH} (600 nM) in the presence of NADPH. Mical^{redox}, in the presence of NADPH, exerts a similar effect on actin polymerization as Mical^{redoxCH} (in the presence of NADPH). These in vitro results, therefore, coupled with our in vivo observations (**Figure S2.4**), indicate that the CH domain of Mical is necessary for the proper localization of Mical in vivo, but is dispensable for Mical's ability to directly alter actin dynamics. **c,** *p*-hydroxybenzoate hydroxylase (PHBH), an enzyme related to Mical, does not co-sediment with F-actin or regulate actin polymerization. **c^{1}**, Standard actin co-sedimentation assays reveal no association between PHBH and F-actin. Images of Coomassie blue stained gels are shown after subjecting the samples to high-speed centrifugation. Filamentous actin was assembled from purified actin in vitro (F-actin); notice

that after high-speed centrifugation the majority of actin is present in the pellet (Pel). In contrast, after high-speed centrifugation, purified PHBH protein (PHBH) is present in the soluble (Sol) fraction. In the presence of purified actin filaments, purified PHBH protein remains in the soluble fraction (PHBH + F-actin) indicating that PHBH does not associate with F-actin. Note that PHBH and actin migrate at a similar molecular weight and since there is little to no change in the size of the PHBH band in the soluble fraction in the presence or absence of F-actin (black arrows), we conclude that little to no PHBH co-sediments with F-actin. Also notice there is little to no change in the size of the F-actin band in the pellet in the presence or absence of PHBH (blue arrows) further supporting our conclusion that PHBH does not co-sediment with F-actin. **c[2],** PHBH does not affect actin polymerization in the presence of NADPH. PHBH, an enzyme related to the Mical oxidoreductase domain, was used to examine the specificity of Mical's effects on actin polymerization. Like Mical, PHBH also utilizes NADPH, and generates $NADP^+$ and H_2O_2 in the absence of its substrate. Therefore, pyrene-labeled actin was polymerized in the presence of either NADPH (100 μM) alone, or with either PHBH (NADPH) or $Mical^{redoxCH}$ (NADPH). Unlike either $Mical^{redoxCH}$ or $Mical^{redox}$ in the presence of NADPH, PHBH in the presence of NADPH exerted no effect on actin polymerization.

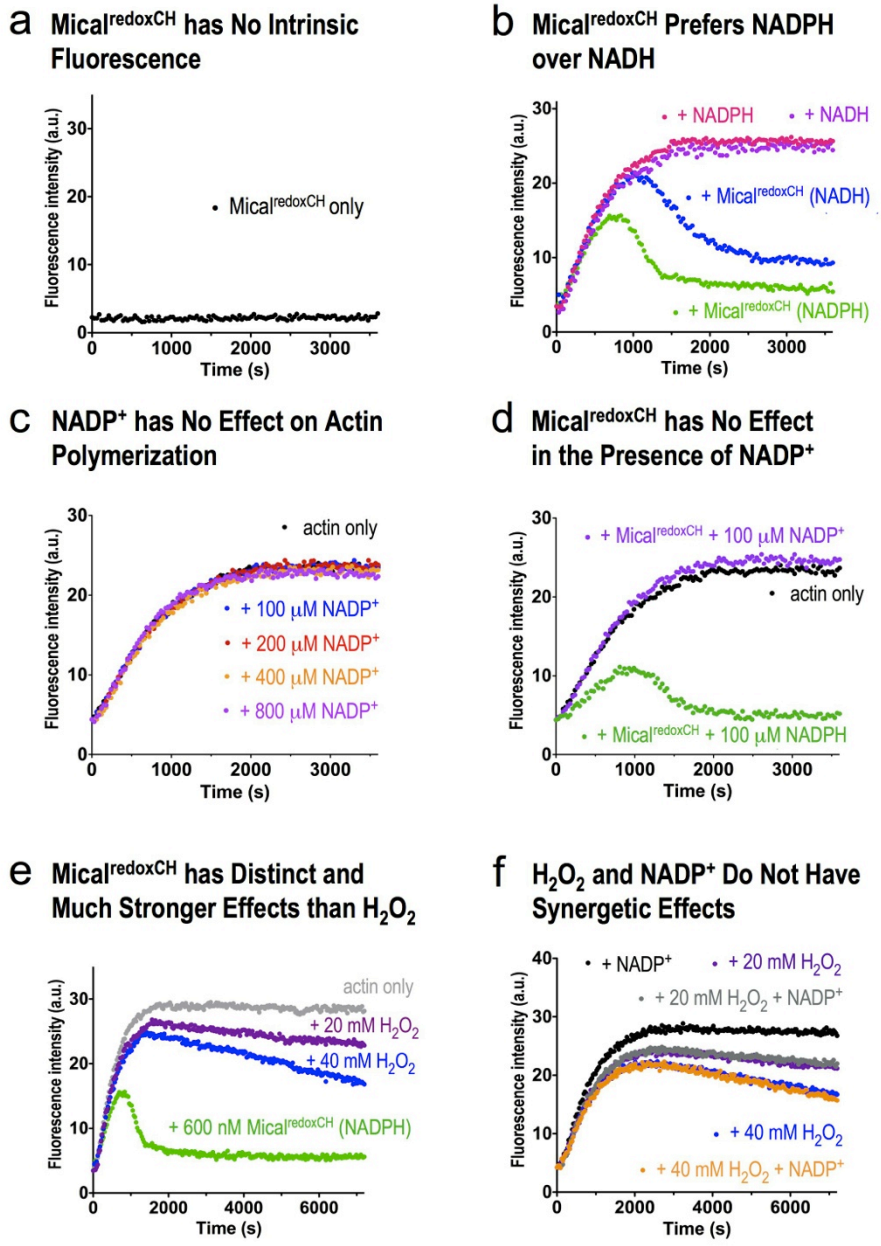

Figure S2.10. Further characterization of the effects of MICAL on actin. a, Purified Mical^{redoxCH} (600 nM) protein has no intrinsic fluorescence that can be monitored at the same wavelength as pyrene actin. **b**, Mical^{redoxCH} (600 nM) alters the rate and extent of both actin polymerization and depolymerization more effectively in the presence of NADPH (100 μM NADPH; green dots) than with the related pyridine nucleotide coenzyme NADH (100 μM NADH; blue dots). **c**, $NADP^+$, which is a product of the reaction when Mical^{redoxCH} consumes NADPH, does not affect actin polymerization. **d**, Mical^{redoxCH} has no effect on actin polymerization in the presence of $NADP^+$. This further indicates the specificity of the pyridine

nucleotide coenzyme utilized by Mical and that $NADP^+$ does not work in combination with Mical to affect actin polymerization. **e**, $Mical^{redoxCH}$ induces effects on actin polymerization that are distinct and much stronger than those induced by hydrogen peroxide (H_2O_2). The addition of extremely high concentrations of H_2O_2 (purple dots, 20 mM; blue dots, 40 mM) results in a decrease in the extent of actin polymerization and also induces a gradual depolymerization of actin. The scope and time course of these H_2O_2-mediated effects, however, are much weaker (>1 million times lower) than those induced by small concentrations of $Mical^{redoxCH}$ protein (i.e., 40 mM H_2O_2 compared to 25 nM $Mical^{redoxCH}$), revealing that Mical's effects on actin dynamics are not likely to result from non-specific production of H_2O_2. High levels of H_2O_2 also have no appreciable effects on actin depolymerization as determined using a pyrene actin depolymerization assay (see **Figure 2.3C, b**). **f**, Products of the Mical reaction ($NADP^+$ and H_2O_2) do not work in synergy to alter actin polymerization. $NADP^+$ concentration = 100 μM.

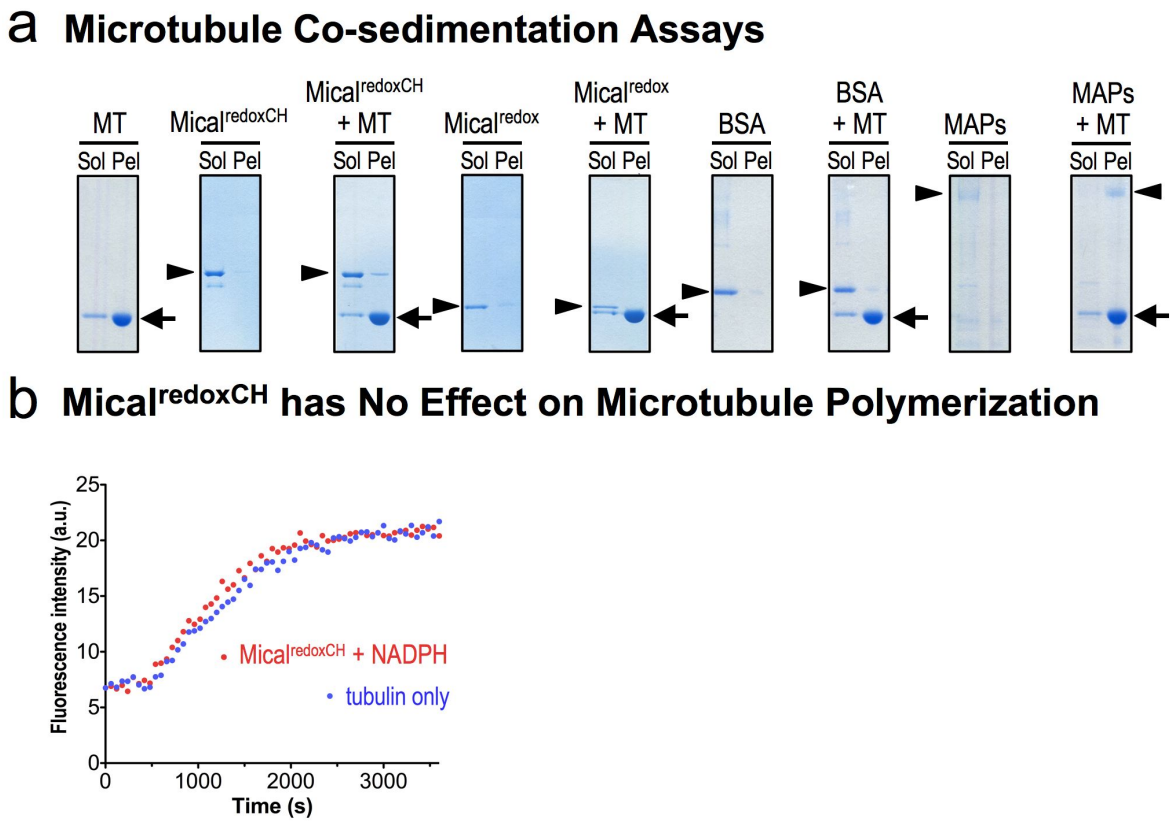

Figure S2.11. Purified Mical protein shows little to no association with microtubules and does not alter tubulin polymerization dynamics. **a**, Co-sedimentation analysis was used to examine the association between Mical and microtubules. Images of Coomassie blue stained gels are shown. Microtubules were assembled in vitro from purified tubulin (α and β subunits); notice that after high-speed centrifugation the majority of microtubules (MT) are present in the pellet (Pel, arrows). In contrast, after high-speed centrifugation the majority of purified Mical^{redoxCH} or Mical^{redox} is present in the soluble (Sol) fraction (arrowheads). Likewise, in the presence of purified microtubules, the majority of Mical^{redoxCH} or Mical^{redox} protein (and a negative control, BSA) is present in the soluble fraction indicating that both Mical^{redoxCH} and Mical^{redox} have little to no association with microtubules. Notice that microtubule associated proteins (MAPs, arrowhead), known microtubule binding proteins that were used as a positive control, change their distribution from the soluble fraction to pellet fraction in the presence of microtubules. **b**, The effect of Mical^{redoxCH} on tubulin polymerization was examined. A fluorescence-based tubulin polymerization assay was employed using standard approaches, where the fluorescence intensity (a.u. (arbitrary units)) of microtubules is substantially higher than tubulin monomers. Mical^{redoxCH} and NADPH were added in the tubulin solution and polymerization was initiated by increasing the temperature from 4°C to 37°C. There is no appreciable difference between tubulin polymerization alone (tubulin only) and tubulin polymerization in the presence of Mical^{redoxCH} with NADPH.

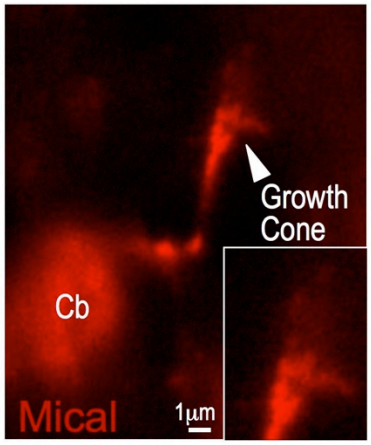

Figure S2.12. Mical localizes to neuronal growth cones in vivo. ^{GFP}Mical expressed specifically in aCC/RP2 pioneer motor neurons using the RN2-GAL4 driver (Fujioka et al., 2003; Sanchez-Soriano and Prokop, 2005) localizes strongly to the growth cone (arrow) and is present in a punctate pattern within the central portion of the growth cone and extends into filopodia. Cb, neuronal cell body.

APPENDIX B

Supplemental Information for Chapter Three

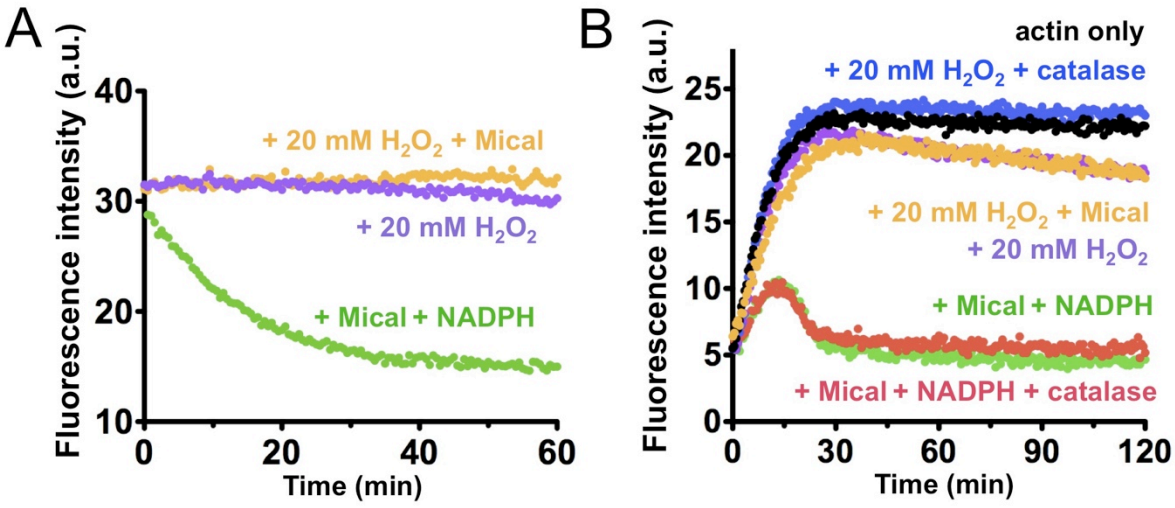

Figure S3.1. Further characterization of Mical, H_2O_2, and their effects on actin polymerization/depolymerization. (A-B) Drosophila Mical in the presence of NADPH produces small amounts of H_2O_2. However, Mical/NADPH, but not high concentrations of H_2O_2 (>1000 fold more than produced by Drosophila Mical/hour), robustly alters actin depolymerization (A) and polymerization (B). Therefore, we wondered if Mical, through its ability to bind to actin (Hung et al., 2010), makes actin responsive to H_2O_2. However, Mical (without NADPH) and H_2O_2 do not combine to affect actin dynamics (A-B), nor does Catalase, (24U; an H_2O_2 scavenger which reverses H_2O_2 effects on actin) alter Mical/NADPH effects on actin (B). These results are also consistent with our previous experiments that reveal that p-hydroxybenzoate hydroxylase (PHBH), another Redox enzyme that is related to Mical and also generates some H_2O_2, has no effect on actin polymerization or depolymerization (Hung et al., 2010). Therefore, these results indicate that Mical is not altering actin dynamics through H_2O_2 production (see also **Fig. S3.2**).

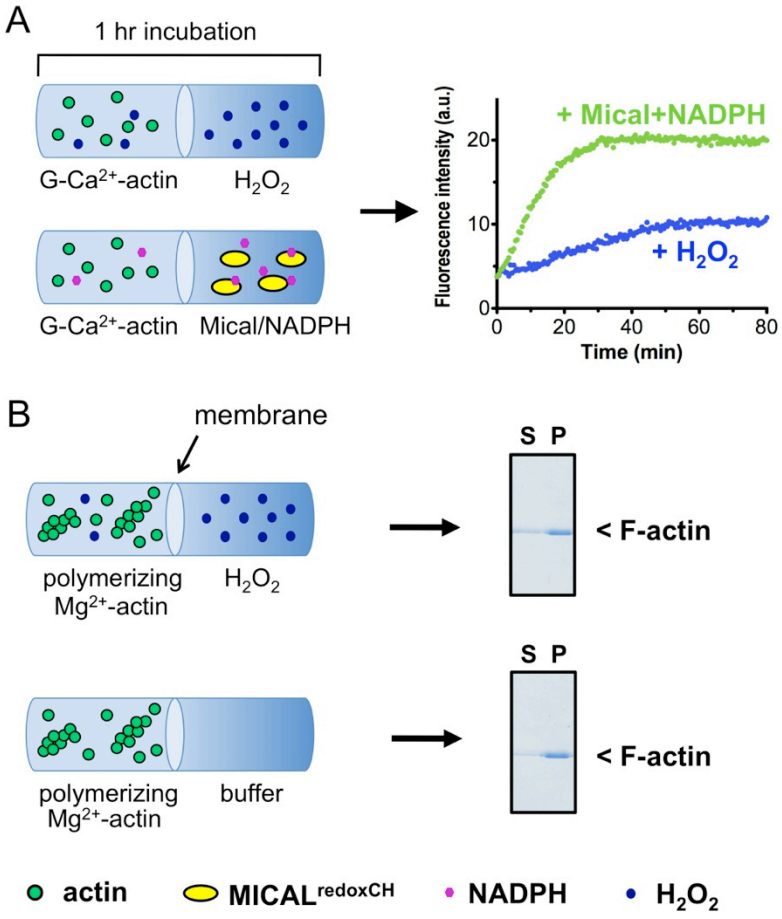

Figure S3.2. Compartmentalized chambers allow oxidants to pass through the membrane and further reveal that Mical does not alter actin dynamics by releasing diffusible oxidants. The cartoon diagrams illustrate the DispoEquilibrium Dialyzer Chambers that were employed for these experiments so as to prevent Mical (yellow) and actin (green), but not small molecules like NADPH (magenta) and oxidants including H_2O_2 (Blue), from contacting one another. (A) Left side: Pyrene labeled actin monomers (G-actin in the presence of Ca^{2+}) were placed in one chamber, and 40 mM of H_2O_2 (or 2.4 μM of $Mical^{redoxCH}$ and 200 μM of NADPH) were placed in the other chamber. H_2O_2 (and other small molecules) were allowed to diffuse across the membrane for 1 hr. Right Side: Actin was then collected, and its polymerization was initiated and monitored using standard pyrene actin approaches. As judged by the decrease in H_2O_2-treated actin's ability to polymerize in this pyrene-actin polymerization assay, H_2O_2 diffuses between the membrane separating the chambers of the compartmentalized Dialyzer apparatus and affects G-Ca^{2+}-actin. In contrast, when a membrane separates Mical from actin, Mical does not alter actin polymerization (see also **Figure 3.1E**), indicating that Mical does not use a diffusible oxidant like H_2O_2 to alter actin. (B) Left Side: Actin monomers were polymerized (with Mg^{2+}) in one chamber, and 40 mM of H_2O_2 was placed in the other chamber. As in A, we

allowed H_2O_2 to diffuse across the membrane for 1 hr. Right Side: Actin was then collected, subjected to sedimentation, and then analyzed for depolymerization (as in **Figure 3.1E**). Consistent with our previous results ((Hung et al., 2010) and also **Figure S3.1)**, H_2O_2 has little effect on actin polymerization or depolymerization when actin is polymerized using standard conditions (polymerized in the presence of Mg^{2+} [Mg^{2+}-actin] (Cooper, 1992b)). For additional clarification, it should also be noted, that these results are consistent with those of others examining the effects of H_2O_2 and other oxidants on actin, where it has been found that oxidants alter actin dynamics only under certain conditions (e.g., G-actin prepared in the presence of Ca^{2+} [e.g., **Figure S3.2A**; (Dalle-Donne et al., 2002; DalleDonne et al., 1995; Guan et al., 2003; Lassing et al., 2007; Milzani et al., 2000)]), and have little to no effect on actin polymerization and depolymerization using standard conditions (e.g., **Figures S3.1, S3.2B**; (Dalle-Donne et al., 2002; Guan et al., 2003; Guan et al., 2005; Takamoto et al., 2007)). These differences appear due to changes in the conformation and surface exposed residues present when actin is polymerized in the presence of Ca^{2+} vs. Mg^{2+} and those exposed in G-actin vs. F-actin (e.g., (Dalle-Donne et al., 2002; Guan et al., 2003; Guan et al., 2005; Hung et al., 2010; Takamoto et al., 2007)). In contrast, Mical robustly alters actin polymerization under standard conditions (in the presence of Mg^{2+}) and induces F-actin disassembly (**Figures 3.1B, S3.1**;(Hung et al., 2010)). Therefore, Mical exhibits effects on actin dynamics that differ from diffusible oxidants.

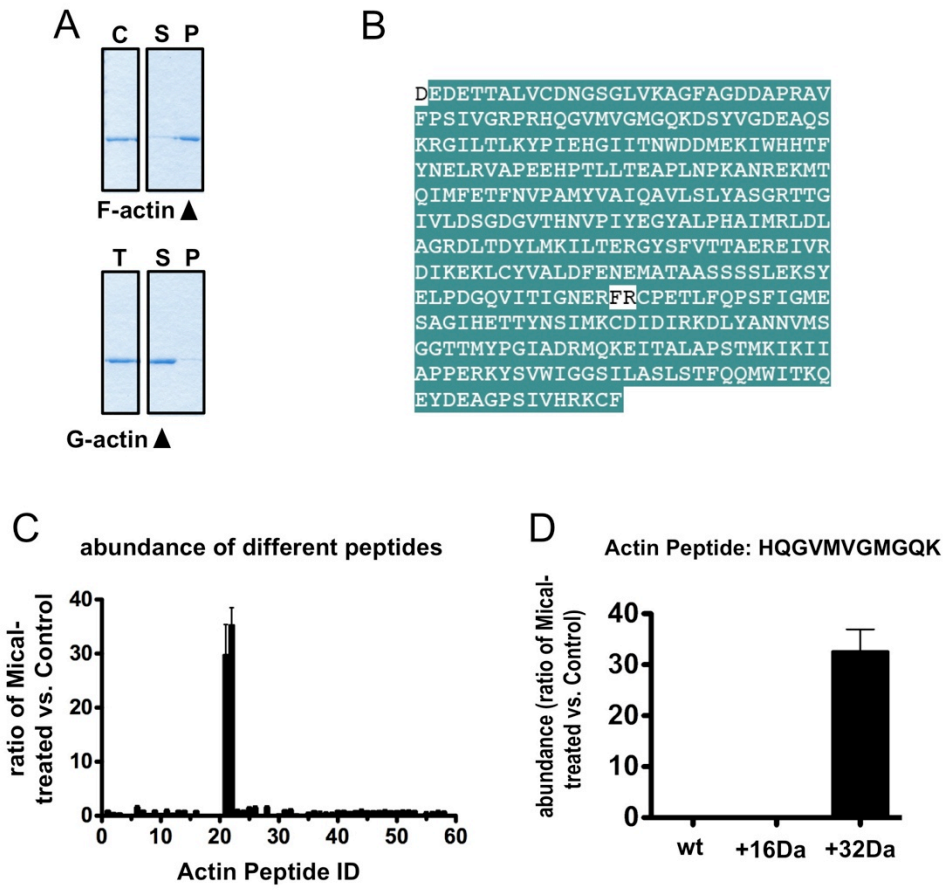

Figure S3.3. Further characterization of Mical-treated actin and mass spectrometry analysis. (A) Ion exchange chromatography was used to separate purified rabbit actin from Mical after incubation with either Mical only controls (Control [C]) or Mical and NADPH (Treated [T]). Re-purified "control" actin robustly polymerizes (Top, F-actin in P) while Mical-treated actin does not (Bottom, G-actin in S), as determined using actin sedimentation assays and Coomassie-stained gels. (B) Control and Mical-treated actins (from A) were cleaved using different proteases (both trypsin and AspN in different experiments), and the resulting peptides covering 99.2% of the amino acids in actin (highlighted in green) were subjected to Mass Spectrometry. (C-D) A single actin peptide exhibits mass differences between the Mical- and control-treated samples. Trypsin-generated actin peptides (from B) were subjected to LC/MS/MS to quantify mass differences between the peptides present in the Mical/NADPH-treated versus (vs.) the Control-treated samples. Each generated peptide (including those with a different mass or charge) is listed (Actin Peptide ID; see **Figure S3.4**), as is the ratio of its abundance in the Mical- vs. the control-treated samples. Only one actin peptide is substantially more abundant in the Mical-treated than in the control samples and its identity (including both sequence and mass (+32Da)) is shown in (D). Error bars = standard deviation between different analyzed samples (n=2).

Peptide ID	Peptide sequence	Form	Ratio of Mical-treated vs. Control	SD	M/Z	Time (mins)
1	AGFAGDDAPR	wt	0.93	0.13	488.73	19.03
2	AVFPSIVGRPR	wt	0.51	0.08	400.24	28.31
3	AVFPSIVGRPR	wt	0.49	0.06	599.86	28.31
4	CDVDIRKDLYANTVLSGGTTMYPGIADR	plus 16 Da	0.07	0.01	765.87	31.91
5	CDVDIRKDLYANTVLSGGTTMYPGIADR	plus 16 Da	0.06	0.01	1020.83	31.91
6	CPEALFQPSFLGMEACGIHETTYNSIMK	plus 16 Da	1.62	0.25	784.11	35.61
7	DLTDYLMK	wt	0.96	0.08	499.75	35.20
8	DLTDYLMK	plus 16 Da	0.38	0.04	507.74	31.78
9	DLYANTVLSGGTTMYPGIADR	wt	0.95	0.12	1108.04	37.15
10	DLYANTVLSGGTTMYPGIADR	plus 16 Da	0.40	0.04	1116.04	35.29
11	DLYANTVLSGGTTMYPGIADR	wt	0.99	0.22	739.03	37.17
12	DLYANTVLSGGTTMYPGIADR	plus 16 Da	0.44	0.04	744.36	35.29
13	DSYVGDEAQSK	wt	0.94	0.08	599.76	18.29
14	EITALAPSTMK	wt	0.93	0.10	581.31	27.60
15	EITALAPSTMK	plus 16 Da	0.26	0.02	589.31	23.50
16	GYSFTTTAER	wt	0.88	0.11	566.77	23.35
17	HQGVMVGMGQK	wt	0.00	0.00	586.29	18.53
18	HQGVMVGMGQK	wt	0.00	0.00	391.20	18.53
19	HQGVMVGMGQK	plus 16 Da	0.04	0.01	594.29	17.85
20	HQGVMVGMGQK	plus 16 Da	0.07	0.02	396.53	17.86
21	HQGVMVGMGQK	plus 32 Da	29.82	5.58	401.86	13.13
22	HQGVMVGMGQK	plus 32 Da	35.32	3.17	602.28	13.13
23	IIAPPER	wt	0.99	0.19	398.24	19.63
24	ILTER	wt	0.95	0.11	316.19	16.40
25	IWHHTFYNELR	wt	1.47	0.18	505.92	26.23
26	IWHHTFYNELR	wt	1.52	0.27	379.69	26.20
27	IWHHTFYNELR	plus 16 Da	0.15	0.03	511.25	24.10
28	IWHHTFYNELR	wt	1.61	0.22	758.38	26.15
29	IWHHTFYNELR	plus 16 Da	0.08	0.01	766.38	24.07
30	IWHHTFYNELR	plus 16 Da	0.27	0.08	383.69	25.08
31	KDLYANTVLSGGTTMYPGIADR	wt	1.01	0.13	781.73	33.32
32	KDLYANTVLSGGTTMYPGIADR	wt	1.10	0.18	1172.09	33.32
33	KDLYANTVLSGGTTMYPGIADR	plus 16 Da	0.33	0.02	787.06	31.57
34	KDLYANTVLSGGTTMYPGIADR	plus 16 Da	0.24	0.02	1180.08	31.54
35	KYSVWIGGSILASLSTFQQMWISK	wt	0.44	0.20	910.82	40.62
36	LDLAGR	wt	0.88	0.10	322.69	20.08
37	MTQIMFETFNTPAMYVAIQAVLSLYASGR	wt	0.52	0.32	1085.21	41.09
38	MTQIMFETFNTPAMYVAIQAVLSLYASGR	plus 16 Da	0.54	0.16	1090.54	40.98
39	MTQIMFETFNTPAMYVAIQAVLSLYASGR	plus 32 Da	0.48	0.17	1095.87	40.62
40	QEYDESGPSIVHR	wt	0.93	0.10	506.24	20.93
41	QEYDESGPSIVHR	wt	0.91	0.10	758.85	20.89
42	RGILTLK	wt	0.70	0.08	400.77	22.21
43	SYELPDGQVITIGNER	wt	0.88	0.08	895.95	34.78
44	SYELPDGQVITIGNER	wt	0.99	0.22	597.64	34.78

45	TTGIVLDSGDGVSHTVPIYEGYALPHAILR	wt	0.85	0.10	788.67	36.36
46	TTGIVLDSGDGVSHTVPIYEGYALPHAILR	wt	0.85	0.10	1051.22	36.36
47	TTGIVLDSGDGVSHTVPIYEGYALPHAILR	wt	0.88	0.12	1576.32	36.37
48	TTGIVLDSGDGVSHTVPIYEGYALPHAILR	wt	0.98	0.16	631.13	36.41
49	VAPEEHPVLLTEAPLNPK	wt	0.87	0.08	652.03	30.30
50	VAPEEHPVLLTEAPLNPK	wt	0.89	0.08	977.54	30.30
51	YPIEHGIVTNWDDMEK	wt	0.94	0.13	649.64	32.01
52	YPIEHGIVTNWDDMEK	wt	0.95	0.13	973.95	32.01
53	YPIEHGIVTNWDDMEK	plus 16 Da	0.90	0.10	654.98	32.21
54	YPIEHGIVTNWDDMEK	plus 16 Da	0.26	0.02	981.95	30.00
55	YSVWIGGSILASLSTFQQMWISK	wt	0.53	0.22	1301.67	40.92
56	YSVWIGGSILASLSTFQQMWISK	wt	0.54	0.25	868.12	40.92
57	YSVWIGGSILASLSTFQQMWISK	plus 16 Da	0.80	0.22	873.45	40.75
58	YSVWIGGSILASLSTFQQMWISK	plus 16 Da	0.70	0.19	1309.67	40.75

Figure S3.4. The actin peptides (peptide sequence) that are observed following Mical-treatment or control-treatment and trypsin digestion. Some sequences are shown more than once because they are detected at different masses (Form) and charge states (M/Z). Each row corresponds to the Actin Peptide ID shown in **Figure S3.3C**. The abundance of each particular peptide following Mical-treatment or control-treatment is presented as the Ratio of Mical-treated vs. Control (i.e., a ratio of 1 would indicate that equal amounts of that particular peptide are present in the Mical-treated and the Control samples). The Ratio of Mical-treated vs. Control is presented as the average of two independent analyses. SD = Standard deviation between the values obtained from the two different analyses.

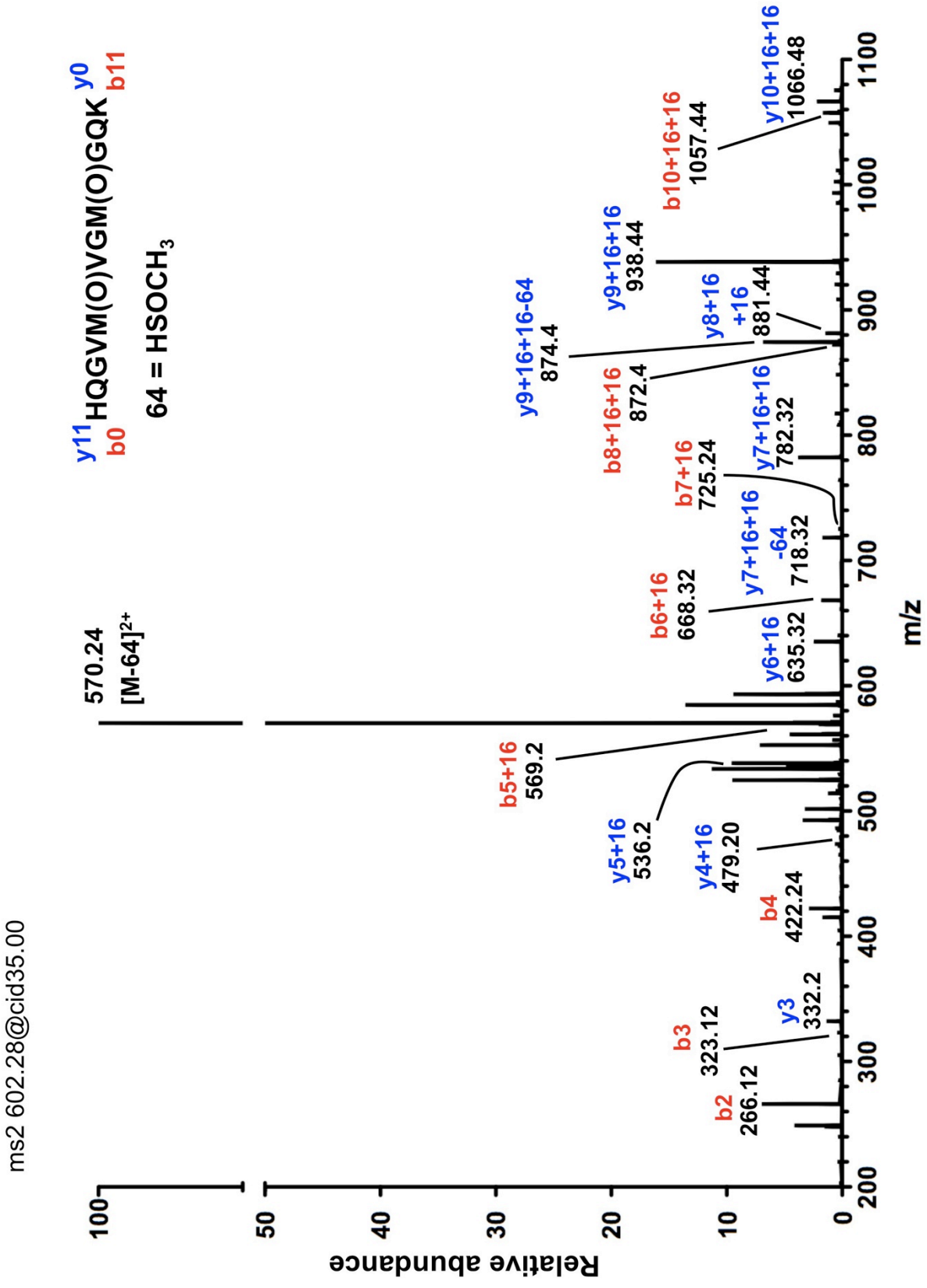
ms2 602.28@cid35.00
y11
b0
HQGVM(O)VGM(O)GQK
y0
b11
64 = HSOCH3
570.24
[M-64]2+
y9+16+16-64
874.4
y9+16+16
938.44
b10+16+16
1057.44
y10+16+16
1066.48
b8+16+16
872.4
y8+16
+16
881.44
b7+16
725.24
y7+16+16
782.32
b6+16
668.32
y7+16+16
-64
718.32
y6+16
635.32
b5+16
569.2
y5+16
536.2
y4+16
479.20
b4
422.24
b3
323.12
y3
332.2
b2
266.12
Relative abundance
m/z
100
50
40
30
20
10
0
200
300
400
500
600
700
800
900
1000
1100

Figure S3.5. Whole MS/MS spectra of peptide HQGVM(O)VGM(O)GQK. One characteristic of fragments containing methionine sulfoxide (MetO) is the neutral loss of 64 Da ($HSOCH_3$) from the b or y ion (e.g., (Khor et al., 2004)). For instance, note that the most abundant peak in this sample is 570.24 $[M-64]^{2+}$. This peak corresponds to the full-length (unfragmented) peptide HQGVM(O)VGM(O)GQK which has lost 64 Da. That peptide's total mass should equal 1204.56 (or 602.28^{2+} where 2+ equals a double charge)). However, this full-length peptide has lost 64 Da and thus its mass is 1204.56 – 64 = 1140.56 (or 570.28 $\pm$ 0.1 (double charged)).

α-actin (muscle actin)

DEDETTALVCDNGSGLVKAGFAGDDAPRAVFPSIVGRPRHQGVM44VGM47GQ
KDSYVGDEAQSKRGILTLKYPIEXGIITNWDDM82EKIWHHTFYNELRVAPEE
HPTLLTEAPLNPKANREKM119TQIM123FETFNVPAM132YVAIQAVLSLYA
SGRTTGIVLDSGDGVTHNVPIYEGYALPHAIM176RLDLAGRDLTDYLM190K
ILTERGYSFVTTAEREIVRDIKEKLCYVALDFENEM227ATAASSSSLEKSYE
LPDGQVITIGNERFRCPETLFQPSFIGM269ESAGIHETTYNSIM283KCDID
IRKDLYANNVM299SGGTTM305YPGIADRM313QKEITALAPSTM325KIKI
IAPPERKYSVWIGGSILASLSTFQQM355WITKQEYDEAGPSIVHRKCF

β-actin (cytoplasmic actin)

CDEEVAALVVDNGSGM16CKAGFAGDDAPRAVFPSIVGRPRHQGVM44VGM47
GQKDSYVGDEAQSKRGILTLKYPIEHGIVTNWDDM82EKIWHHTFYNELRVAP
EEHPVLLTEAPLNPKANREKM119TQIM123FETFNTPAM132YVAIQAVLSL
YASGRTTGIVLDSGDGVSHTVPIYEGYALPHAILRLDLAGRDLTDYLM190KI
LTERGYSFTTTAEREIVRDIKEKLCYVALDFEQEM227ATAASSSSLEKSYEL
PDGQVITIGNERFRCPEALFQPSFLGM269EACGIHETTYNSIM283KCDVDI
RKDLYANTVLSGGTTM305YPGIADRM313QKEITALAPSTM325KIKIIAPP
ERKYSVWIGGSILASLSTFQQM355WISKQEYDESGPSIVHRKCF

Figure S3.6. The methionine residues present in selected muscle and cytoplasmic actins. The mature protein sequences of rabbit muscle (α) and Drosophila (Actin 5C) cytoplasmic (β) actins are shown. There are a total of 16 and 15 methionine residues, respectively, in these muscle and cytoplasmic actins. Interestingly, the Met44 residue is not phylogenetically conserved in actin-related proteins like Arp2 and Arp3.

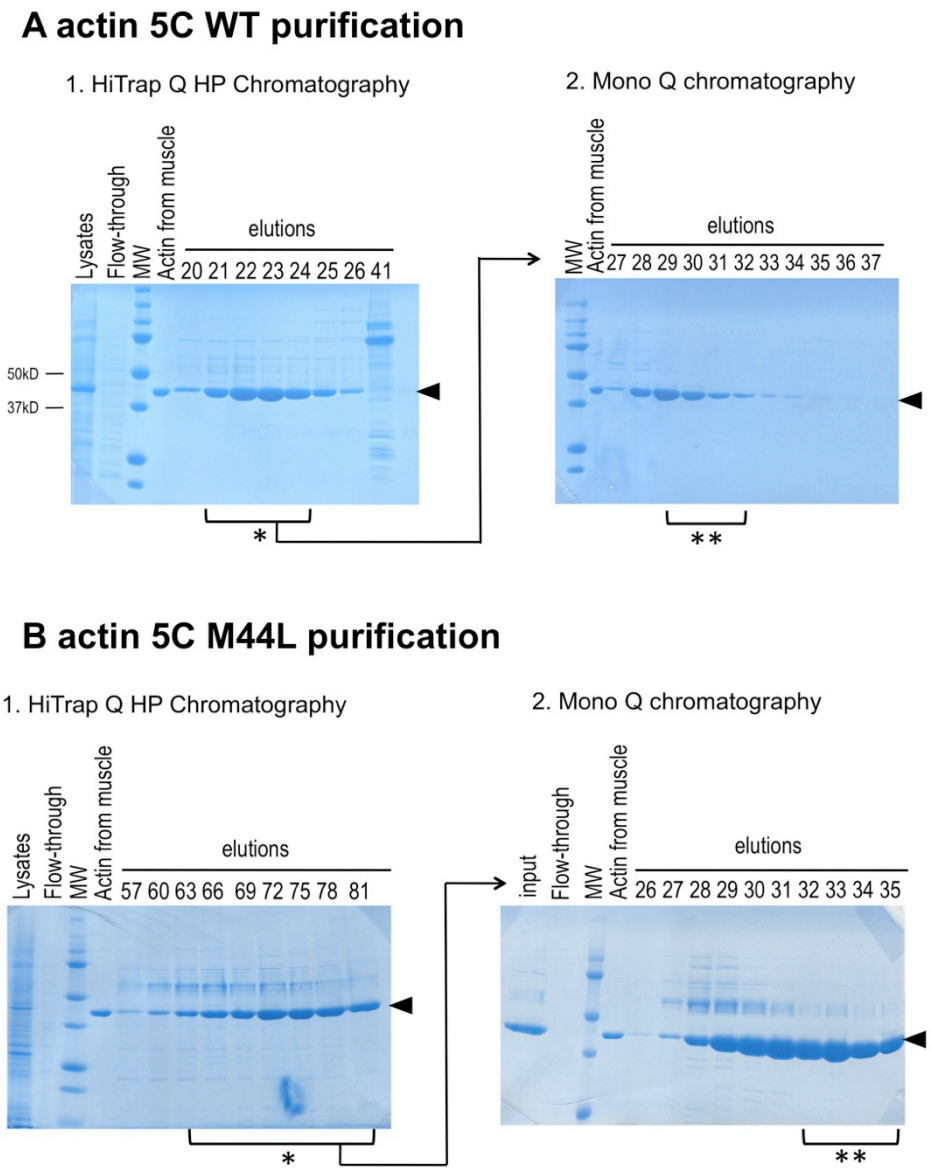

Figure S3.7. Purification of WT (A) and M44L (B) actins from insect cells. Coomassie stained gels are shown and the arrowheads point to the actin protein in all gels. The protein markers in all gels are the same. Standard approaches were used (Joel et al., 2004) such that insect (Sf9) cells infected with baculovirus encoding actin were lysed, dialyzed and clarified. The lysates were then loaded on a HiTrap Q HP ion exchange column [1]. Following elution from the HiTrap Q HP column, the enriched fractions were collected (*), dialyzed, and loaded on a Mono Q ion exchange column [2] to further purify the actin. The fractions collected for each of the actin's are marked with double asterisks (**) and were dialyzed against G-actin buffer prior to storage and use.

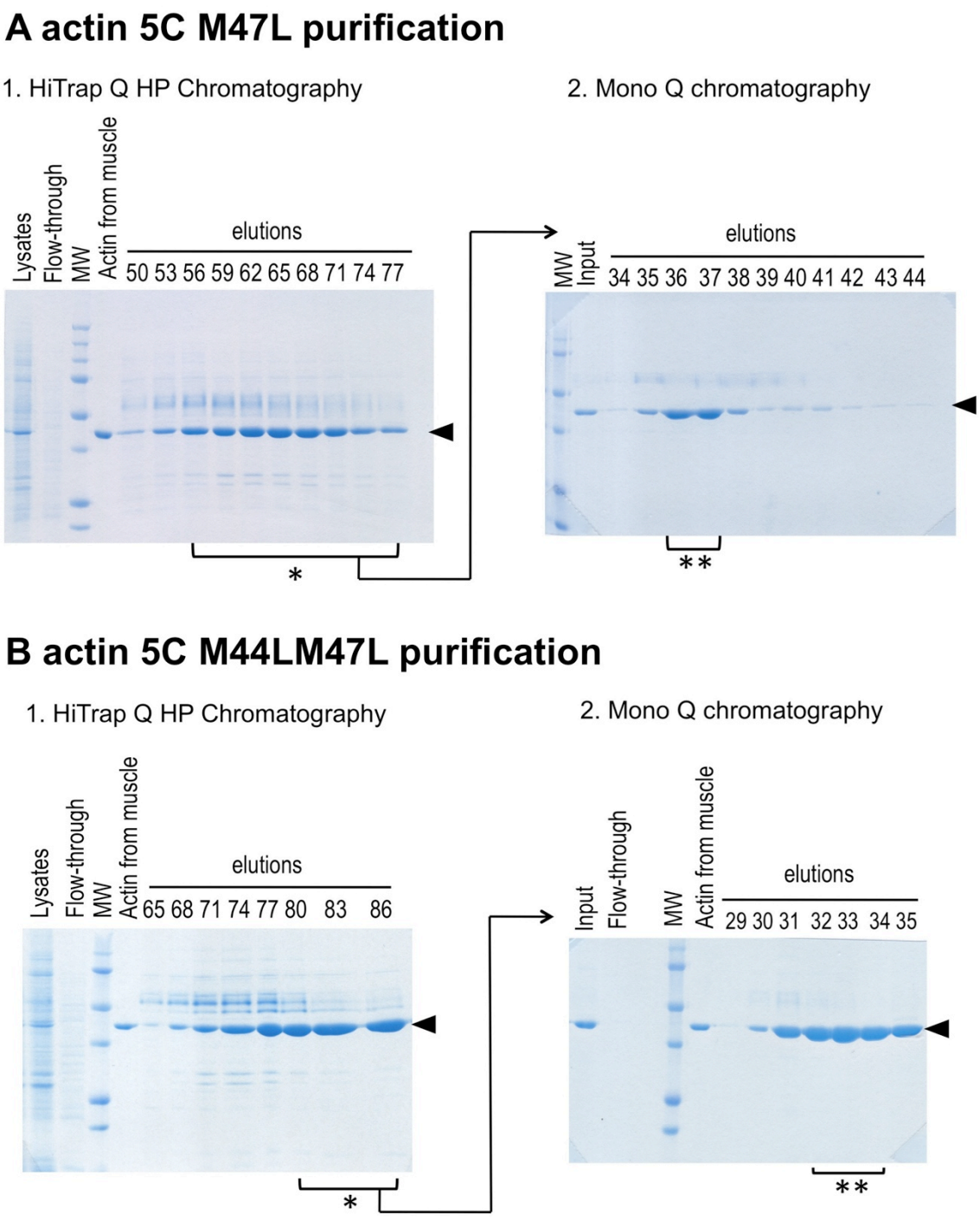

Figure S3.8. Purification of M47L (A) and M44LM47L double mutant (B) actins from insect cells using approaches described in Fig. S3.7.

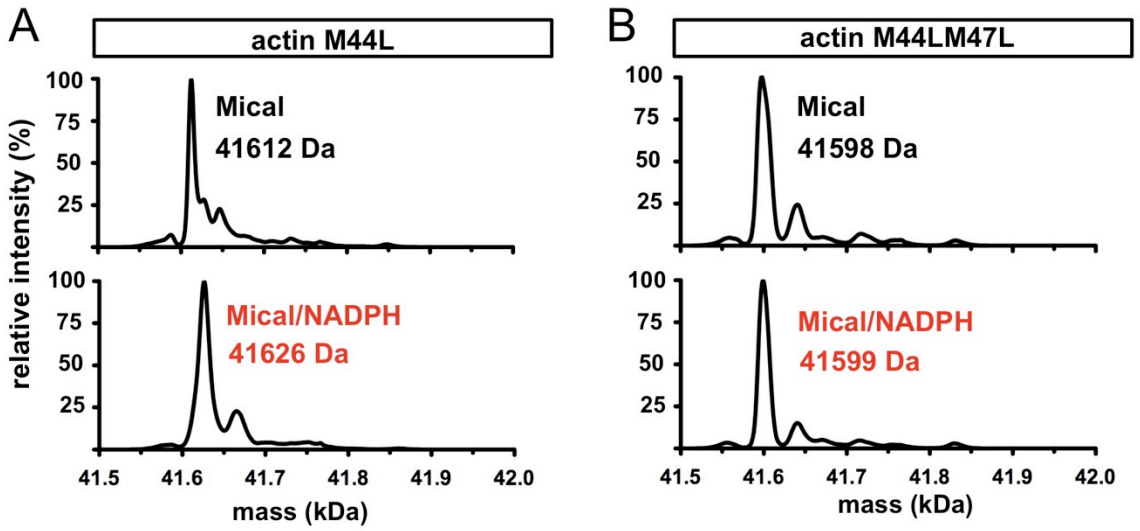

Figure S3.9. Whole mass measurement of single mutation M44L and double mutation M44LM47L. Mutating the M44 and M47 residues of actin prevents Mical-mediated 32Da increases in actin mass. The methionine (M) 44 and/or M47 residues of actin were mutated to chemically similar leucine (L) residues (Bartlett et al., 2003; Lipscomb et al., 1998) and mutant actin proteins were expressed and purified (see **Figures S3.7-3.8**), and then polymerized, subjected to Mical treatment (with or without NADPH), and re-purified. Mical treated (Mical/NADPH) and control (Mical only) samples were then subjected to ESI-MS (as in **Figure 3.2A**) to compare the whole mass of actin M44L (A) and actin M44LM47L (B); revealing that both M residues are required for Mical-mediated alterations to the mass of actin. Note that the slight differences in mass (+1 in B) are not significant, and that endogenous wild-type actin is present in insect cells and small amounts will be purified along with the mutant actins (also in **Figure 3.3C**).

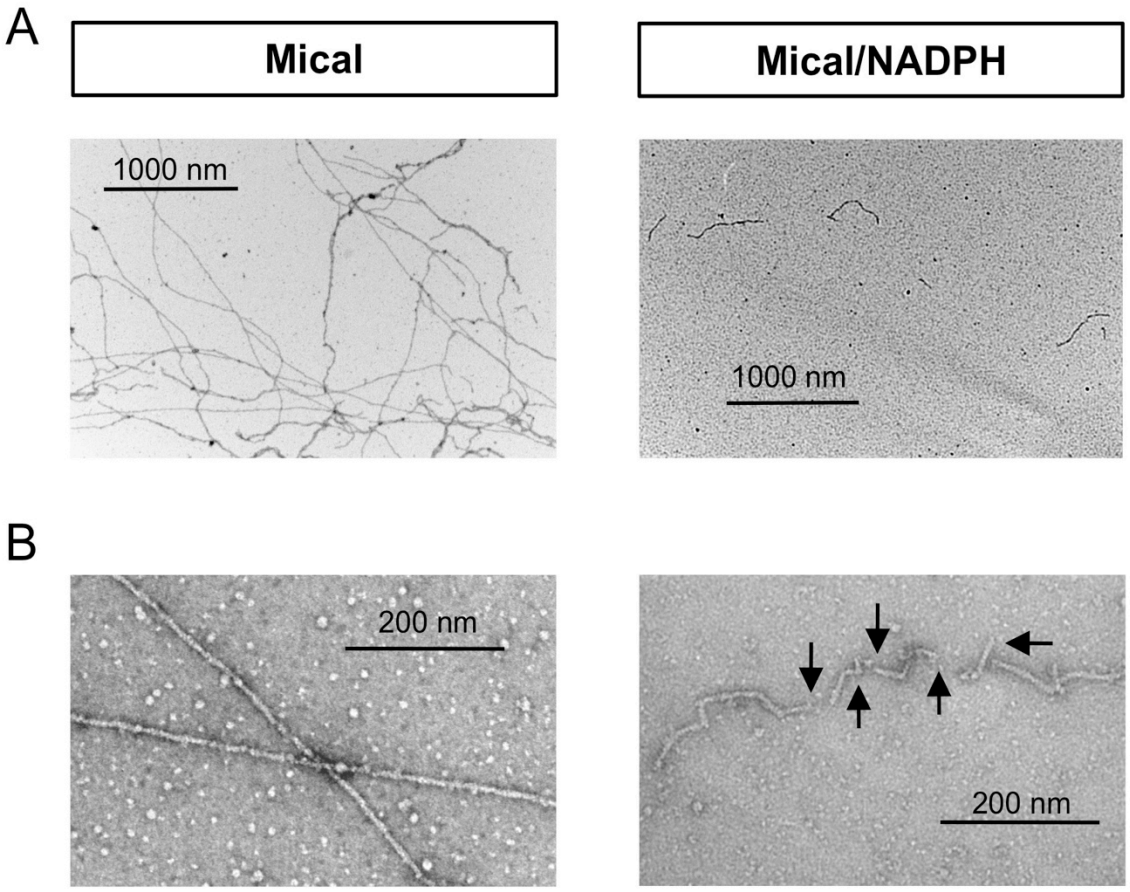

Figure S3.10. High magnification electron microscopy (EM) analyses of Mical/NADPH-treated actin filaments. Negative-staining EM indicates that actin filaments (shown at lower magnification in A) are reduced in length (see also (Hung et al., 2010)) and that Mical/NADPH cuts (arrows, B) actin filaments and generates a kinked appearance in the filament (which contrasts to normal [Mical only treated] filaments which are straight). It should also be noted that in our previous analyses using negative-staining EM (Hung et al., 2010), we had difficulty finding filaments – and it suggested to us that some of the filaments may be "disappearing" (i.e., we were only measuring those filaments that were still around – and any filaments that had been disassembled completely would not be identifiable/measurable). In the present EM study, we treated actin filaments for a shorter amount of time (and used higher magnification) to try to aid in visualizing filaments that were in the process of being altered by Mical. Using this experimental set-up, we examined actin filaments and noted their shape and cut appearance when incubated with Mical/NADPH (arrows, B). Thus, our EM analysis is consistent with our TIRF, pyrene-actin, and sedimentation assays that actin filaments become difficult to find/observe (perhaps some/many filaments are even disassembled completely) when treated with Mical/NADPH.

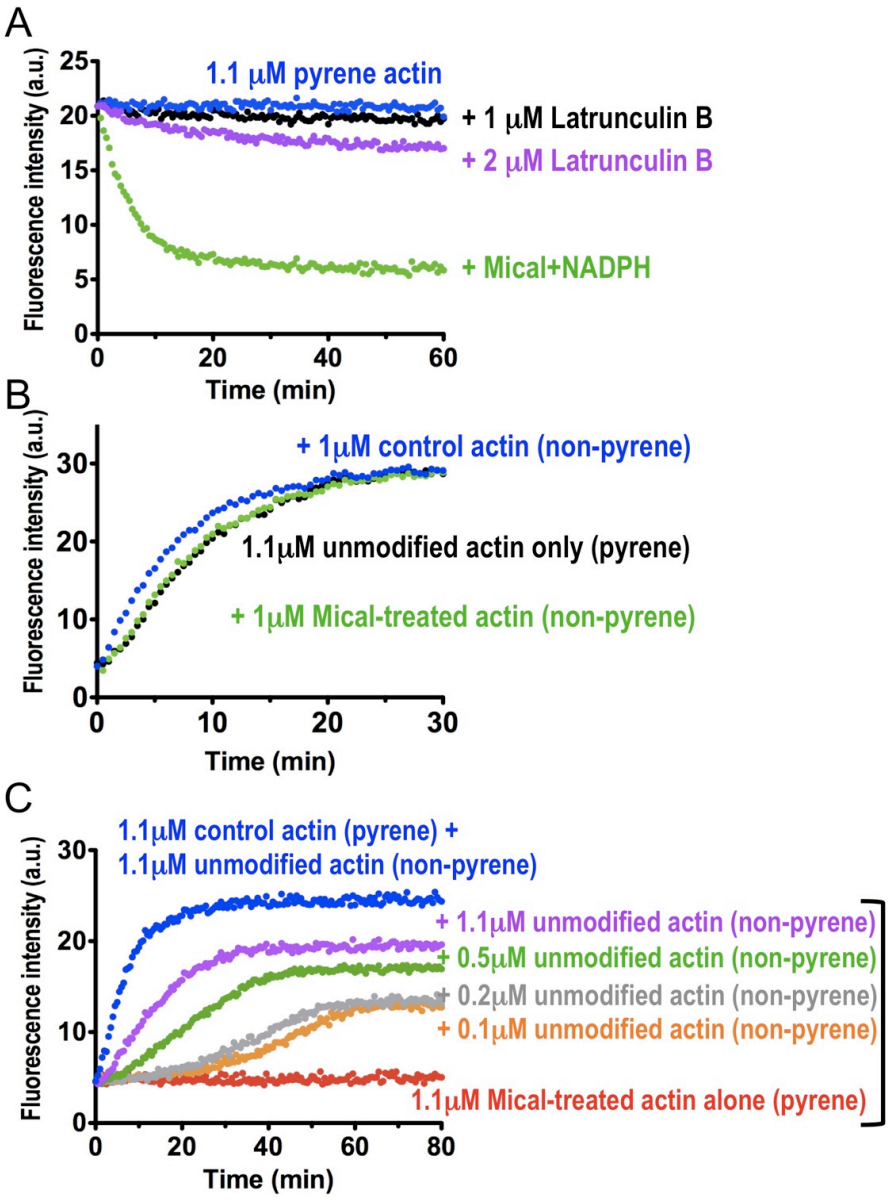

Figure S3.11. Further analyses of Mical's effects on actin. (A) The effects of Mical on F-actin are not similar to sequestering G-actin – further indicating that Mical does not only affect G-actin. The results of this actin depolymerization assay reveal that sequestering G-actin by Latrunculin B (which sequesters G-actin at a 1:1 ratio; (Spector et al., 1989; Wakatsuki et al., 2001)) doesn't induce depolymerization in a manner that is similar to Mical/NADPH. These results support our other experiments including our TIRF (**Figure 3.4B**), EM (**Figure S3.10**), and Mical enzyme activation experiments (**Figure 3.1F**) and indicate that Mical induces F-actin depolymerization at least in part by altering actin filaments – and is not consistent with a hypothesis that Mical only modifies actin monomers, preventing their polymerization and thus

shifting the equilibrium toward monomers and actin disassembly. Actin concentration is 1.1 μM, Mical concentration is 600 nM, and NADPH concentration is 100 μM. (B) The effects of Mical-modified monomers on the polymerization of unmodified actin monomers are not consistent with a hypothesis in which the effects of Mical on F-actin are due only to Mical-modified monomers incorporating into filaments and inducing their severing and disassembly. In these experiments, untreated pyrene actin (1.1 μM) was polymerized in the absence (black) or presence (green, 1 μM) of re-purified Mical-treated actin and the results revealed that Mical-treated actin does not decrease the polymerization of untreated actin. Furthermore, Mical-treated actin (green) does not incorporate into filaments in a manner that is similar to control/untreated actin (blue, 1 μM). (C) The results of these experiments complement those in B and indicate that Mical-modified actin is able to incorporate into filaments composed of unmodified actin monomers, although the rate and extent of this polymerization is abnormal. Specifically, Mical-treated actin shows no appreciable polymerization with itself at 1.1 μM (red), but polymerization occurs to some extent with increasing concentrations of untreated actin (orange, gray, green, and purple). However, the mixture of Mical-treated and untreated actin does not polymerize like untreated (control) actin at the same concentration (compare purple and blue). In this way, Mical-modified actin may be similar to the properties noted for some synthesized forms of actin (e.g., tetra-methylrhodamine maleimide/iodoacetamide (TMR)-labeled actin; (Amann and Pollard, 2001; Kudryashov et al., 2004; Otterbein et al., 2001)), which does not polymerize with itself, but can polymerize with unlabeled actin and generate short, unstable filaments (Kudryashov et al., 2004). Although, it should be noted that it is not yet clear if only the barbed (unmodified)-end of Mical-modified actin monomers incorporate within unmodified actin filaments or whether both the barbed and pointed (modified)-ends of Mical-modified actin monomers incorporate within unmodified actin filaments. Likewise, it should also be noted that it is not clear if all (100%) of the actin monomers are modified/remain modified following Mical/NADPH treatment and purification of Mical/NADPH-treated actin. Furthermore, as mentioned above, it is interesting that Mical-treated actin monomers do not show appreciable polymerization with each other (**e.g., Figure 3.1C**) but do polymerize with untreated actin (**Figure S3.11C**), although the rate and extent of this polymerization is abnormal. In light of these findings, it is interesting that Mical does not appear to decrease the rate and extent of polymerization when added to the assay in **Figure S3.11B**. However, it is also possible that the assay in **Figure S3.11B** is not sensitive enough to detect the kinetic impact of Mical-treated actin on untreated actin (e.g., this is possible because there is little difference between the polymerization kinetics of 1.1 μM pyrene actin [black] and the same actin with control [non-pyrene] actin [blue] in **Figure S3.11B**). Along these lines (as indicated by the results of **Figure S3.11C**) Mical-treated actin slowly (and incompletely) incorporates into filaments made of untreated actin (and so untreated actin would appear to be much more likely to polymerize with untreated actin than with Mical-modified actin such that the actin dynamics of labeled unmodified actin in **Figure S3.11B** are not decreased by Mical-treated actin). Thus, additional questions left for future work include more closely examining the effects of Mical-treated actin on untreated actin using other methods such as directly visualizing actin polymerization using differentially labeled actin monomers.

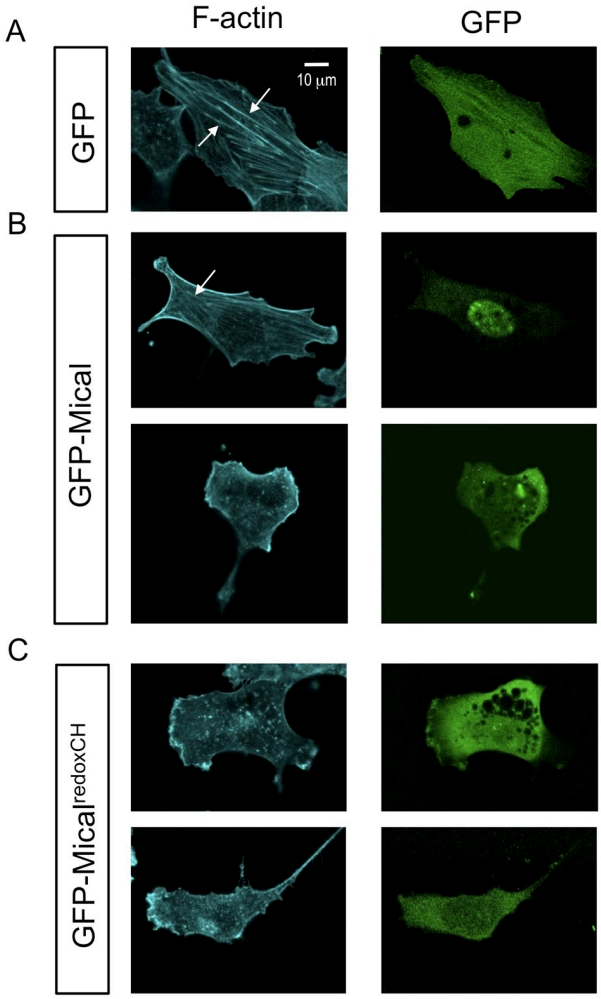

Figure S3.12. Mical alters actin organization in mammalian cells. (A) Mammalian cells (3T3 cells) expressing GFP alone have F-actin stress fibers (e.g., arrows). (B-C) In contrast, F-actin stress fiber formation and cell morphology is altered by expressing a GFP-tagged version of Mical (GFP-Mical, B) or a "constituitively-active" version (Hung et al., 2010) of Mical (GFP-Mical^{redoxCH}, C). (B) When only low amounts of GFP-Mical are found in the cytoplasm (upper panels), F-actin stress fibers are only slightly disrupted. However, when high amounts of GFP-Mical localized to the cytoplasm, cells appear smaller and lack stress fibers (lower panels). (C) Likewise, cells expressing GFP-Mical^{redoxCH} are smaller in size and do not exhibit F-actin stress fibers. These are representative examples for each condition and are based on visualizing multiple cells in each of the different conditions. These results also complement those using other mammalian cells (COS-7 cells (Schmidt et al., 2008) and neuronal growth cones (Morinaka et al., 2011)) that show that mammalian MICALs, in a Redox-dependent manner, collapse mammalian cells and their processes in culture, which are effects that are dependent on disruption of F-actin stability (as discussed in (Hung and Terman, 2011)).

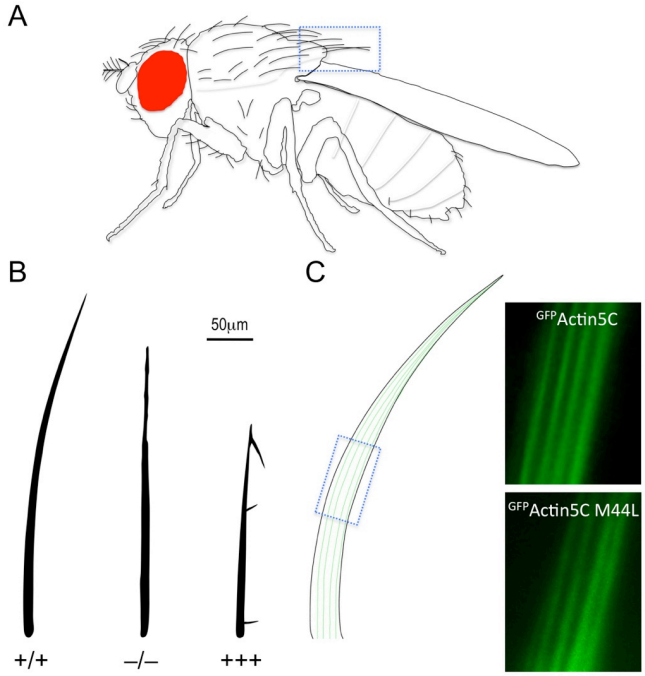

Figure S3.13. The Drosophila bristle process as a single cell in vivo model for characterizing Mical-mediated F-actin remodeling. (A) The body of Drosophila is covered with bristles, which are the long cellular processes of bristle cells (e.g., in boxed area). (B) Each bristle is an extension of a single cell, and its elongation and shape are the result of the assembly and disassembly of F-actin situated around the periphery of the bristle process (Reviewed in (Hung et al., 2010; Sutherland and Witke, 1999; Tilney and DeRosier, 2005)). Examples of individual posterior scutellar cell bristles (which are the bristles qualitatively and quantitatively examined in the experiments described in **Figures 3.4C-F**) are shown for different genotypes. Wild-type (+/+) bristles are long and slightly curved. In contrast, Mical regulates the length and abundance of F-actin in the developing bristle and generates bristles with abnormal length and shape. Specifically, loss of Mical (–/–) leads to straighter bristles, abnormalities in the tip of the bristles, and occasional angled bends (Hung et al., 2010). These morphological defects are the result of an increased abundance of F-actin in bristles (Hung et al., 2010). Increasing the levels of Mical specifically in bristles (+++) results in bristle branching, which is the result of Mical inducing a remodeling of F-actin at specific sites along the bristle that decrease the abundance of F-actin and generate new filopodia (branches) (Hung et al., 2010). Genotypes: +/+ (*UAS:^{GFP}Actin5C/+; B11-GAL4/+*); –/– (*UAS:^{GFP}Actin5C/+; B11-GAL4, Mical$^{Df(3R)swp2}$/Mical^{K583}*); +++ (*UAS:^{GFP}Actin5C/+; B11-GAL4, UAS:Mical/+)* (C) The developing bristle process is filled with longitudinally-arranged bundles of F-actin (green, where the boxed area serves as a reference for the images on the right). GFP-labeled wild-type Actin 5C (green) incorporates into the bundled actin filaments present in Drosophila bristles (Hung et al., 2010). Likewise, we find that GFP-labeled Actin 5C M44L (green) incorporates into the actin filaments present in Drosophila bristles.

BIBLIOGRAPHY

Abercrombie, M. (1970). Contact inhibition in tissue culture. In Vitro *6*, 128-142.

Abercrombie, M. (1980). The crawling movement of metazoan cells. Proc R Soc Lond B Biol Sci *207*, 129-147.

Abercrombie, M., and Heaysman, J.E. (1953). Observations on the social behaviour of cells in tissue culture. I. Speed of movement of chick heart fibroblasts in relation to their mutual contacts. Exp Cell Res *5*, 111-131.

Aguayo, A.J., Bray, G.M., Perkins, C.S., and Duncan, I.D. (1979). Axon-sheath cell interactions in peripheral and central nervous system transplants. Society for neuroscience symposia: aspects of developmental neurobiology *4*, 361-383.

Aizawa, H., Wakatsuki, S., Ishii, A., Moriyama, K., Sasaki, Y., Ohashi, K., Sekine-Aizawa, Y., Sehara-Fujisawa, A., Mizuno, K., Goshima, Y*., et al.* (2001). Phosphorylation of cofilin by LIM-kinase is necessary for semaphorin 3A- induced growth cone collapse. Nat Neurosci *4*, 367-373.

Aktories, K., Barmann, M., Ohishi, I., Tsuyama, S., Jakobs, K.H., and Habermann, E. (1986). Botulinum C2 toxin ADP-ribosylates actin. Nature *322*, 390-392.

Al-Bassam, J., Roger, B., Halpain, S., and Milligan, R.A. (2007). Analysis of the weak interactions of ADP-Unc104 and ADP-kinesin with microtubules and their inhibition by MAP2c. Cell Motil Cytoskeleton *64*, 377-389.

Amann, K.J., and Pollard, T.D. (2001). Direct real-time observation of actin filament branching mediated by Arp2/3 complex using total internal reflection fluorescence microscopy. Proc Natl Acad Sci U S A *98*, 15009-15013.

Andrianantoandro, E., and Pollard, T.D. (2006). Mechanism of actin filament turnover by severing and nucleation at different concentrations of ADF/cofilin. Mol Cell *24*, 13-23.

Ashida, S., Furihata, M., Katagiri, T., Tamura, K., Anazawa, Y., Yoshioka, H., Miki, T., Fujioka, T., Shuin, T., Nakamura, Y*., et al.* (2006). Expression of novel molecules, MICAL2-PV (MICAL2 prostate cancer variants), increases with high Gleason score and prostate cancer progression. Clin Cancer Res *12*, 2767-2773.

Ayoob, J.C., Terman, J.R., and Kolodkin, A.L. (2006). Drosophila Plexin B is a Sema-2a receptor required for axon guidance. Development *133*, 2125-2135.

Ayoob, J.C., Yu, H.H., Terman, J.R., and Kolodkin, A.L. (2004). The Drosophila receptor guanylyl cyclase Gyc76C is required for semaphorin-1a-plexin A-mediated axonal repulsion. J Neurosci *24*, 6639-6649.

Bainbridge, S.P., and Bownes, M. (1981). Staging the metamorphosis of Drosophila melanogaster. J Embryol Exp Morphol *66*, 57-80.

Bamburg, J.R. (1999). Proteins of the ADF/cofilin family: essential regulators of actin dynamics. Annu Rev Cell Dev Biol *15*, 185-230.

Barberis, D., Artigiani, S., Casazza, A., Corso, S., Giordano, S., Love, C.A., Jones, E.Y., Comoglio, P.M., and Tamagnone, L. (2004). Plexin signaling hampers integrin-based adhesion, leading to Rho-kinase independent cell rounding, and inhibiting lamellipodia extension and cell motility. Faseb J *18*, 592-594.

Bartlett, R.K., Bieber Urbauer, R.J., Anbanandam, A., Smallwood, H.S., Urbauer, J.L., and Squier, T.C. (2003). Oxidation of Met144 and Met145 in calmodulin blocks calmodulin dependent activation of the plasma membrane Ca-ATPase. Biochemistry *42*, 3231-3238.

Bashaw, G.J., and Klein, R. (2010). Signaling from axon guidance receptors. Cold Spring Harb Perspect Biol *2*, a001941.

Bauch, H., and Schaffer, J. (2006). Optical sections by means of "structured illumination": background and application in fluorescence microscopy. Photonik International, 86-88.

Bechara, A., Falk, J., Moret, F., and Castellani, V. (2007). Modulation of semaphorin signaling by Ig superfamily cell adhesion molecules. Adv Exp Med Biol *600*, 61-72.

Bergen, H.R., 3rd, Ajtai, K., Burghardt, T.P., Nepomuceno, A.I., and Muddiman, D.C. (2003). Mass spectral determination of skeletal/cardiac actin isoform ratios in cardiac muscle. Rapid communications in mass spectrometry : RCM *17*, 1467-1471.

Bernstein, B.W., and Bamburg, J.R. (2010). ADF/cofilin: a functional node in cell biology. Trends Cell Biol *20*, 187-195.

Berry, M. (1982). Post-injury myelin-breakdown products inhibit axonal growth: an hypothesis to explain the failure of axonal regeneration in the mammalian central nervous system. Bibl Anat, 1-11.

Beuchle, D., Schwarz, H., Langegger, M., Koch, I., and Aberle, H. (2007). Drosophila MICAL regulates myofilament organization and synaptic structure. Mech Dev *124*, 390-406.

Bielenberg, D.R., Shimizu, A., and Klagsbrun, M. (2008). Semaphorin-induced cytoskeletal collapse and repulsion of endothelial cells. Methods Enzymol *443*, 299-314.

Black, S.D., and Mould, D.R. (1991). Development of hydrophobicity parameters to analyze proteins which bear post- or cotranslational modifications. Anal Biochem *193*, 72-82.

Bokoch, G.M. (2003). Biology of the p21-activated kinases. Annu Rev Biochem *72*, 743-781.

Bonhoeffer, F., and Huf, J. (1980). Recognition of cell types by axonal growth cones in vitro. Nature *288*, 162-164.

Bonne, D., Heusele, C., Simon, C., and Pantaloni, D. (1985). 4',6-Diamidino-2-phenylindole, a fluorescent probe for tubulin and microtubules. J Biol Chem *260*, 2819-2825.

Bray, D., Wood, P., and Bunge, R.P. (1980). Selective fasciculation of nerve fibers in culture. Exp Cell Res *130*, 241-250.

Broadie, K., Sink, H., Van Vactor, D., Fambrough, D., Whitington, P.M., Bate, M., and Goodman, C.S. (1993). From growth cone to synapse: the life history of the RP3 motoneuron. Development *Supplement*, 227-238.

Bron, R., Vermeren, M., Kokot, N., Andrews, W., Little, G.E., Mitchell, K.J., and Cohen, J. (2007). Boundary cap cells constrain spinal motor neuron somal migration at motor exit points by a semaphorin-plexin mechanism. Neural Dev *2*, 21.

Brown, J.A., and Bridgman, P.C. (2009). Disruption of the cytoskeleton during Semaphorin 3A induced growth cone collapse correlates with differences in actin organization and associated binding proteins. Dev Neurobiol *69*, 633-646.

Brown, J.A., Wysolmerski, R.B., and Bridgman, P.C. (2009). Dorsal root ganglion neurons react to semaphorin 3A application through a biphasic response that requires multiple myosin II isoforms. Mol Biol Cell *20*, 1167-1179.

Burrows, M.T. (1911). The growth of tissues of the chick embryo outside the animal body, with special reference to the nervous system. J Exp Zool *10*, 63-84.

Cabodi, S., del Pilar Camacho-Leal, M., Di Stefano, P., and Defilippi, P. (2010). Integrin signalling adaptors: not only figurants in the cancer story. Nat Rev Cancer *10*, 858-870.

Cajal, S. (1893). La rétine des Vertébrés. La cellule *9*, 120-255.

Cajal, S. (1899). Textura del Sistema Nervioso del Hombre y de los Vertebrados, Vol I (Madrid: mprenta y Librería de Nicolás Moya).

Cajal, S. (1919). La acción neurotrópica de los epitelios. Trab Lab Invest Biol Univ Madrid *17*, 181-228.

Cajal, S. (1928). Degeneration and regeneration of the nervous system (New York: Hafner).

Campbell, D.S., Regan, A.G., Lopez, J.S., Tannahill, D., Harris, W.A., and Holt, C.E. (2001). Semaphorin 3A elicits stage-dependent collapse, turning, and branching in Xenopus retinal growth cones. J Neurosci *21*, 8538-8547.

Cant, K., Knowles, B.A., Mooseker, M.S., and Cooley, L. (1994). Drosophila singed, a fascin homolog, is required for actin bundle formation during oogenesis and bristle extension. J Cell Biol *125*, 369-380.

Carp, H., Miller, F., Hoidal, J.R., and Janoff, A. (1982). Potential mechanism of emphysema: alpha 1-proteinase inhibitor recovered from lungs of cigarette smokers contains oxidized methionine and has decreased elastase inhibitory capacity. Proc Natl Acad Sci U S A *79*, 2041-2045.

Carter, S.B. (1965). Principles of cell motility: the direction of cell movement and cancer invasion. Nature *208*, 1183-1187.

Chapman, S.K., and Reid, G.A., eds. (1999). Flavoprotein Protocols (Totowa, NJ: Humana Press).

Chhabra, E.S., and Higgs, H.N. (2007). The many faces of actin: matching assembly factors with cellular structures. Nat Cell Biol *9*, 1110-1121.

Ciorba, M.A., Heinemann, S.H., Weissbach, H., Brot, N., and Hoshi, T. (1997). Modulation of potassium channel function by methionine oxidation and reduction. Proc Natl Acad Sci U S A *94*, 9932-9937.

Comeau, M.R., Johnson, R., DuBose, R.F., Peterson, M., Gearing, P., VandenBos, T., Park, L., Farrah, T., Buller, R.M., Cohen, J.I.*, et al.* (1998). A poxvirus-encoded semaphorin induces cytokine production from monocytes and binds to a novel cellular semaphorin receptor, VESPR. Immunity *8*, 473-482.

Cooper, J.A. (1992a). Actin filament assembly and organization in vitro. In The Cytoskeleton: A Practical Approach, K.L. Carraway, and C.A.C. Carraway, eds. (New York: Oxford University Press), pp. 47-71.

Cooper, J.A. (1992b). The Cytoskeleton: A Practical Approach (Oxford University Press, New York).

Dalle-Donne, I., Rossi, R., Giustarini, D., Gagliano, N., Di Simplicio, P., Colombo, R., and Milzani, A. (2002). Methionine oxidation as a major cause of the functional impairment of oxidized actin. Free Radic Biol Med *32*, 927-937.

DalleDonne, I., Milzani, A., and Colombo, R. (1995). H2O2-treated actin: assembly and polymer interactions with cross-linking proteins. Biophys J *69*, 2710-2719.

Dalpe, G., Zhang, L.W., Zheng, H., and Culotti, J.G. (2004). Conversion of cell movement responses to Semaphorin-1 and Plexin-1 from attraction to repulsion by lowered levels of specific RAC GTPases in C. elegans. Development *131*, 2073-2088.

David, S., and Aguayo, A.J. (1981). Axonal elongation into peripheral nervous system "bridges" after central nervous system injury in adult rats. Science *214*, 931-933.

de la Cova, C., Abril, M., Bellosta, P., Gallant, P., and Johnston, L.A. (2004). Drosophila myc regulates organ size by inducing cell competition. Cell *117*, 107-116.

Dent, E.W., Barnes, A.M., Tang, F., and Kalil, K. (2004). Netrin-1 and semaphorin 3A promote or inhibit cortical axon branching, respectively, by reorganization of the cytoskeleton. J Neurosci *24*, 3002-3012.

Dickson, B.J. (2002). Molecular mechanisms of axon guidance. Science *298*, 1959-1964.

Dominguez, R., and Holmes, K.C. (2011). Actin structure and function. Annu Rev Biophys *40*, 169-186.

Dransfield, D.T., Bradford, A.J., Smith, J., Martin, M., Roy, C., Mangeat, P.H., and Goldenring, J.R. (1997). Ezrin is a cyclic AMP-dependent protein kinase anchoring protein. Embo J *16*, 35-43.

Driessens, M.H., Hu, H., Nobes, C.D., Self, A., Jordens, I., Goodman, C.S., and Hall, A. (2001). Plexin-B semaphorin receptors interact directly with active Rac and regulate the actin cytoskeleton by activating Rho. Curr Biol *11*, 339-344.

Duescher, R.J., Lawton, M.P., Philpot, R.M., and Elfarra, A.A. (1994). Flavin-containing monooxygenase (FMO)-dependent metabolism of methionine and evidence for FMO3 being the major FMO involved in methionine sulfoxidation in rabbit liver and kidney microsomes. J Biol Chem *269*, 17525-17530.

Dunn, G.A. (1971). Mutual contact inhibition of extension of chick sensory nerve fibres in vitro. J Comp Neurol *143*, 491-507.

Ebendal, T. (1976). The relative roles of contact inhibition and contact guidance in orientation of axons extending on aligned collagen fibrils in vitro. Exp Cell Res *98*, 159-169.

Ebendal, T. (1982). Orientational behavior of extending neurites. In Cell Behavior A tribute to Michael Abercrombie, R. Bellairs, A. Curtis, and G. Dunn, eds. (Cambridge: Cambridge University Press), pp. 281-297.

Egelman, E.H. (2001). Actin allostery again? Nat Struct Biol *8*, 735-736.

Eickholt, B.J., Mackenzie, S.L., Grahm, A., Walsh, F.S., and Doherty, P. (1999). Evidence for collapsin-1 functioning in the control of neural crest migration in both trunk and hindbrain regions. Development *126*, 2181-2189.

Eisenbach, M. (2004). Chemotaxis (London: Imperial College Press).

Elfarra, A.A., and Krause, R.J. (2005). Potential roles of flavin-containing monooxygenases in sulfoxidation reactions of l-methionine, N-acetyl-l-methionine and peptides containing l-methionine. Biochim Biophys Acta *1703*, 183-189.

Eppink, M.H., Schreuder, H.A., and Van Berkel, W.J. (1997). Identification of a novel conserved sequence motif in flavoprotein hydroxylases with a putative dual function in FAD/NAD(P)H binding. Protein Sci *6*, 2454-2458.

Erickson, J.R., Joiner, M.L., Guan, X., Kutschke, W., Yang, J., Oddis, C.V., Bartlett, R.K., Lowe, J.S., O'Donnell, S.E., Aykin-Burns, N.*, et al.* (2008). A dynamic pathway for calcium-independent activation of CaMKII by methionine oxidation. Cell *133*, 462-474.

Eschrich, K., van Berkel, W.J., Westphal, A.H., de Kok, A., Mattevi, A., Obmolova, G., Kalk, K.H., and Hol, W.G. (1990). Engineering of microheterogeneity-resistant p-hydroxybenzoate hydroxylase from Pseudomonas fluorescens. FEBS Lett *277*, 197-199.

Fan, J., Mansfield, S.G., Redman, T., Phillip, R., Gordon-Weeks, P.R., and Raper, J.A. (1993). The organization of F-actin and microtubules in growth cones exposed to a brain-derived collapsing factor. J Cell Biol *121*, 867-878.

Fan, J., and Raper, J.A. (1995). Localized collapsing cues can steer growth cones without inducing their full collapse. Neuron *14*, 263-274.

Fenstermaker, V., Chen, Y., Ghosh, A., and Yuste, R. (2004). Regulation of dendritic length and branching by semaphorin 3A. J Neurobiol *58*, 403-412.

Ferris, G.F. (1950). External Morphology of the Adult. In Biology of Drosophila, M. Demerec, ed. (New York: John Wiley & Sons, Inc.), pp. 368-419.

Fields, R.D., and Nelson, P.G. (1994). Growth cone collapse in response to electrical activity, cell contact and diffusible factors. Physiol Chem Phys Med NMR *26*, 27-53.

Fischer, J., Weide, T., and Barnekow, A. (2005). The MICAL proteins and rab1: a possible link to the cytoskeleton? Biochem Biophys Res Commun *328*, 415-423.

Fournier, A.E., Nakamura, F., Kawamoto, S., Goshima, Y., Kalb, R.G., and Strittmatter, S.M. (2000). Semaphorin3A enhances endocytosis at sites of receptor-F-actin colocalization during growth cone collapse. J Cell Biol *149*, 411-422.

Franco, M., and Tamagnone, L. (2008). Tyrosine phosphorylation in semaphorin signalling: shifting into overdrive. EMBO Rep *9*, 865-871.

Fritsche, J., Reber, B.F., Schindelholz, B., and Bandtlow, C.E. (1999). Differential Cytoskeletal Changes during Growth Cone Collapse in Response to hSema III and Thrombin. Mol Cell Neurosci *14*, 398-418.

Fujii, T., Iwane, A.H., Yanagida, T., and Namba, K. (2010). Direct visualization of secondary structures of F-actin by electron cryomicroscopy. Nature *467*, 724-728.

Fujioka, M., Lear, B.C., Landgraf, M., Yusibova, G.L., Zhou, J., Riley, K.M., Patel, N.H., and Jaynes, J.B. (2003). Even-skipped, acting as a repressor, regulates axonal projections in Drosophila. Development *130*, 5385-5400.

Fukuda, M., Kanno, E., Ishibashi, K., and Itoh, T. (2008). Large scale screening for novel rab effectors reveals unexpected broad Rab binding specificity. Mol Cell Proteomics *7*, 1031-1042.

Galkin, V.E., Orlova, A., Schroder, G.F., and Egelman, E.H. (2010). Structural polymorphism in F-actin. Nat Struct Mol Biol *17*, 1318-1323.

Gallo, G. (2006). RhoA-kinase coordinates F-actin organization and myosin II activity during semaphorin-3A-induced axon retraction. J Cell Sci *119*, 3413-3423.

Gallo, G. (2008). Semaphorin 3A inhibits ERM protein phosphorylation in growth cone filopodia through inactivation of PI3K. Dev Neurobiol *68*, 926-933.

Gallo, G., and Letourneau, P.C. (2004). Regulation of growth cone actin filaments by guidance cues. J Neurobiol *58*, 92-102.

Gatlin, J.C., Estrada-Bernal, A., Sanford, S.D., and Pfenninger, K.H. (2006). Myristoylated, alanine-rich C-kinase substrate phosphorylation regulates growth cone adhesion and pathfinding. Mol Biol Cell *17*, 5115-5130.

Geng, W., He, B., Wang, M., and Adler, P.N. (2000). The tricornered gene, which is required for the integrity of epidermal cell extensions, encodes the Drosophila nuclear DBF2-related kinase. Genetics *156*, 1817-1828.

Giger, R.J., Hollis, E.R., 2nd, and Tuszynski, M.H. (2010). Guidance molecules in axon regeneration. Cold Spring Harb Perspect Biol *2*, a001867.

Gimona, M., Djinovic-Carugo, K., Kranewitter, W.J., and Winder, S.J. (2002). Functional plasticity of CH domains. FEBS Lett *513*, 98-106.

Godement, P., Wang, L.C., and Mason, C.A. (1994). Retinal axon divergence in the optic chiasm: dynamics of growth cone behavior at the midline. J Neurosci *14*, 7024-7039.

Grigoriev, I., Yu, K.L., Martinez-Sanchez, E., Serra-Marques, A., Smal, I., Meijering, E., Demmers, J., Peranen, J., Pasterkamp, R.J., van der Sluijs, P.*, et al.* (2011). Rab6, Rab8, and MICAL3 Cooperate in Controlling Docking and Fusion of Exocytotic Carriers. Curr Biol *21*, 967-974.

Guan, J.-Q., Almo, S.C., Reisler, E., and Chance, M.R. (2003). Structural reorganization of proteins revealed by radiolysis and mass spectrometry: G-actin solution structure is divalent cation dependent. Biochemistry *42*, 11992-12000.

Guan, J.Q., Takamoto, K., Almo, S.C., Reisler, E., and Chance, M.R. (2005). Structure and dynamics of the actin filament. Biochemistry *44*, 3166-3175.

Guild, G.M., Connelly, P.S., Ruggiero, L., Vranich, K.A., and Tilney, L.G. (2003). Long continuous actin bundles in Drosophila bristles are constructed by overlapping short filaments. J Cell Biol *162*, 1069-1077.

Guild, G.M., Connelly, P.S., Vranich, K.A., Shaw, M.K., and Tilney, L.G. (2002). Actin filament turnover removes bundles from Drosophila bristle cells. J Cell Sci *115*, 641-653.

Gupta, N., Adhikari, D.K., Stobdan, T., Roychoudhury, P.K., and Deb, J.K. (2007). Purification of dibenzothiophene monooxygenase from a recombinant Escherichia coli. Biotechnol Lett *29*, 1465-1468.

Gupta, N., and Terman, J.R. (2008). Characterization of MICAL flavoprotein oxidoreductases: Expression and solubility of different truncated forms of MICAL. Flavins and Flavoproteins, 345-350.

Gustke, N., Trinczek, B., Biernat, J., Mandelkow, E.M., and Mandelkow, E. (1994). Domains of tau protein and interactions with microtubules. Biochemistry *33*, 9511-9522.

Guttmann-Raviv, N., Shraga-Heled, N., Varshavsky, A., Guimaraes-Sternberg, C., Kessler, O., and Neufeld, G. (2007). Semaphorin-3A and semaphorin-3F work together to repel

endothelial cells and to inhibit their survival by induction of apoptosis. J Biol Chem *282*, 26294-26305.

Hall, A. (1998). Rho GTPases and the actin cytoskeleton. Science *279*, 509-514.

Hall, A., and Lalli, G. (2010). Rho and Ras GTPases in axon growth, guidance, and branching. Cold Spring Harb Perspect Biol *2*, a001818.

Harris, A.K. (1974). Contact inhibition of cell locomotion. In Cell Communication, R.P. Cox, ed. (New York: John Wiley), pp. 147-185.

Hartenstein, V., and Posakony, J.W. (1989). Development of adult sensilla on the wing and notum of Drosophila melanogaster. Development *107*, 389-405.

He, H., Yang, T., Terman, J.R., and Zhang, X. (2009). Crystal structure of the plexin A3 intracellular region reveals an autoinhibited conformation through active site sequestration. Proc Natl Acad Sci U S A *106*, 15610-15615.

Heaysman, J.E. (1978). Contact inhibition of locomotion: a reappraisal. Int Rev Cytol *55*, 49-66.

Hochman, E., Castiel, A., Jacob-Hirsch, J., Amariglio, N., and Izraeli, S. (2006). Molecular pathways regulating pro-migratory effects of Hedgehog signaling. J Biol Chem *281*, 33860-33870.

Hofmann, C., Shepelev, M., and Chernoff, J. (2004). The genetics of Pak. J Cell Sci *117*, 4343-4354.

Holt, C.E., and Bullock, S.L. (2009). Subcellular mRNA localization in animal cells and why it matters. Science *326*, 1212-1216.

Hopmann, R., and Miller, K.G. (2003). A balance of capping protein and profilin functions is required to regulate actin polymerization in Drosophila bristle. Mol Biol Cell *14*, 118-128.

Hoshi, T., and Heinemann, S. (2001). Regulation of cell function by methionine oxidation and reduction. J Physiol *531*, 1-11.

Hou, S.T., Jiang, S.X., and Smith, R.A. (2008). Permissive and repulsive cues and signalling pathways of axonal outgrowth and regeneration. Int Rev Cell Mol Biol *267*, 125-181.

Hu, H., Marton, T.F., and Goodman, C.S. (2001). Plexin B mediates axon guidance in Drosophila by simultaneously inhibiting active Rac and enhancing RhoA signaling. Neuron *32*, 39-51.

Huang, Z., Yazdani, U., Thompson-Peer, K.L., Kolodkin, A.L., and Terman, J.R. (2007). Crk-associated substrate (Cas) signaling protein functions with integrins to specify axon guidance during development. Development *134*, 2337-2347.

Huber, A.B., Kolodkin, A.L., Ginty, D.D., and Cloutier, J.F. (2003). Signaling at the growth cone: ligand-receptor complexes and the control of axon growth and guidance. Annu Rev Neurosci *26*, 509-563.

Hughes, A. (1953). The growth of embryonic neurites; a study of cultures of chick neural tissues. J Anat *87*, 150-162.

Hung, R.-J., and Terman, J.R. (2011). Extracellular inhibitors, repellents, and Semaphorin/Plexin/MICAL-mediated actin filament disassembly. Cytoskeleton *68*, 415-433.

Hung, R.J., Yazdani, U., Yoon, J., Wu, H., Yang, T., Gupta, N., Huang, Z., van Berkel, W.J., and Terman, J.R. (2010). Mical links semaphorins to F-actin disassembly. Nature *463*, 823-827.

Ishikawa, R., Sakamoto, T., Ando, T., Higashi-Fujime, S., and Kohama, K. (2003). Polarized actin bundles formed by human fascin-1: their sliding and disassembly on myosin II and myosin V in vitro. J Neurochem *87*, 676-685.

Jin, Z., and Strittmatter, S.M. (1997). Rac1 mediates collapsin-1-induced growth cone collapse. J Neurosci *17*, 6256-6263.

Joel, P.B., Fagnant, P.M., and Trybus, K.M. (2004). Expression of a nonpolymerizable actin mutant in Sf9 cells. Biochemistry *43*, 11554-11559.

Jurney, W.M., Gallo, G., Letourneau, P.C., and McLoon, S.C. (2002). Rac1-mediated endocytosis during ephrin-A2- and semaphorin 3A-induced growth cone collapse. J Neurosci *22*, 6019-6028.

Kadrmas, J.L., and Beckerle, M.C. (2004). The LIM domain: from the cytoskeleton to the nucleus. Nat Rev Mol Cell Biol *5*, 920-931.

Kapfhammer, J.P., Grunewald, B.E., and Raper, J.A. (1986). The selective inhibition of growth cone extension by specific neurites in culture. J Neurosci *6*, 2527-2534.

Kapfhammer, J.P., and Raper, J.A. (1987a). Collapse of growth cone structure on contact with specific neurites in culture. J Neurosci *7*, 201-212.

Kapfhammer, J.P., and Raper, J.A. (1987b). Interactions between growth cones and neurites growing from different neural tissues in culture. J Neurosci *7*, 1595-1600.

Karakozova, M., Kozak, M., Wong, C.C.L., Bailey, A.O., Yates, J.R., Mogilner, A., Zebroski, H., and Kashina, A. (2006). Arginylation of beta-actin regulates actin cytoskeleton and cell motility. Science *313*, 192-196.

Kashiwagi, H., Shiraga, M., Kato, H., Kamae, T., Yamamoto, N., Tadokoro, S., Kurata, Y., Tomiyama, Y., and Kanakura, Y. (2005). Negative regulation of platelet function by a secreted cell repulsive protein, semaphorin 3A. Blood *106*, 913-921.

Kaufman, S., and Mason, K. (1982). Specificity of amino acids as activators and substrates for phenylalanine hydroxylase. J Biol Chem *257*, 14667-14678.

Kelso, R.J., Buszczak, M., Quinones, A.T., Castiblanco, C., Mazzalupo, S., and Cooley, L. (2004). Flytrap, a database documenting a GFP protein-trap insertion screen in Drosophila melanogaster. Nucleic Acids Res *32*, D418-420.

Keynes, R., and Cook, G. (1990). Cell-cell repulsion: clues from the growth cone? Cell *62*, 609-610.

Keynes, R.J., and Cook, G.M.W. (1995). Repulsive and inhibitory signals. Curr Opin Neurobiol *5*, 75-78.

Keynes, R.J., and Stern, C.D. (1984). Segmentation in the vertebrate nervous system. Nature *310*, 220-223.

Khor, H.K., Fisher, M.T., and Schoneich, C. (2004). Potential role of methionine sulfoxide in the inactivation of the chaperone GroEL by hypochlorous acid (HOCl) and peroxynitrite (ONOO-). J Biol Chem *279*, 19486-19493.

Kirilly, D., Gu, Y., Huang, Y., Wu, Z., Bashirullah, A., Low, B.C., Kolodkin, A.L., Wang, H., and Yu, F. (2009). A genetic pathway composed of Sox14 and Mical governs severing of dendrites during pruning. Nat Neurosci *12*, 1497-1505.

Kolodkin, A.L., Matthes, D., and Goodman, C.S. (1993). The semaphorin genes encode a family of transmembrane and secreted growth cone guidance molecules. Cell *75*, 1389-1399.

Kolodkin, A.L., Matthes, D., O'Connor, T., Patel, N.H., Admon, A., Bentley, D., and Goodman, C.S. (1992). Fasciclin IV: Sequence, expression, and function during growth cone guidance in the grasshopper embryo. Neuron *9*, 831-835.

Komiyama, T., Sweeney, L.B., Schuldiner, O., Garcia, K.C., and Luo, L. (2007). Graded expression of semaphorin-1a cell-autonomously directs dendritic targeting of olfactory projection neurons. Cell *128*, 399-410.

Kudryashov, D.S., Phillips, M., and Reisler, E. (2004). Formation and destabilization of actin filaments with tetramethylrhodamine-modified actin. Biophys J *87*, 1136-1145.

Kuhn, J.R., and Pollard, T.D. (2005). Real-time measurements of actin filament polymerization by total internal reflection fluorescence microscopy. Biophys J *88*, 1387-1402.

Kuhn, T.B., Brown, M.D., Wilcox, C.L., Raper, J.A., and Bamburg, J.R. (1999). Myelin and collapsin-1 induce motor neuron growth cone collapse through different pathways: Inhibition of collapse by opposing mutants of Rac1. J Neurosci *19*, 1965-1975.

Laing, N.G., Dye, D.E., Wallgren-Pettersson, C., Richard, G., Monnier, N., Lillis, S., Winder, T.L., Lochmuller, H., Graziano, C., Mitrani-Rosenbaum, S.*, et al.* (2009). Mutations and polymorphisms of the skeletal muscle alpha-actin gene (ACTA1). Hum Mutat *30*, 1267-1277.

Langer, C.C., Ejsmont, R.K., Schonbauer, C., Schnorrer, F., and Tomancak, P. (2010). In vivo RNAi rescue in Drosophila melanogaster with genomic transgenes from Drosophila pseudoobscura. PLoS One *5*, e8928.

Lassing, I., Schmitzberger, F., Bjornstedt, M., Holmgren, A., Nordlund, P., Schutt, C.E., and Lindberg, U. (2007). Molecular and structural basis for redox regulation of beta-actin. Journal of molecular biology *370*, 331-348.

Lawrence, P.A. (1975). The structure and properties of a compartment border: the intersegmental boundary in Oncopeltus. Ciba Found Symp *0*, 3-23.

Lee, T., and Luo, L. (1999). Mosaic analysis with a repressible cell marker for studies of gene function in neuronal morphogenesis. Neuron *22*, 451-461.

Lepelletier, Y., Moura, I.C., Hadj-Slimane, R., Renand, A., Fiorentino, S., Baude, C., Shirvan, A., Barzilai, A., and Hermine, O. (2006). Immunosuppressive role of semaphorin-3A on T cell proliferation is mediated by inhibition of actin cytoskeleton reorganization. Eur J Immunol *36*, 1782-1793.

Letourneau, P.C. (1975). Possible roles for cell-to-substratum adhesion in neuronal morphogenesis. Dev Biol *44*, 77-91.

Letourneau, P.C. (1987). What happens when growth cones meet neurites: attraction or repulsion? Trends Neurosci *10*, 390-393.

Li, X., and Lee, A.Y. (2010). Semaphorin 5A and plexin-B3 inhibit human glioma cell motility through RhoGDIalpha-mediated inactivation of Rac1 GTPase. J Biol Chem *285*, 32436-32445.

Lipscomb, L.A., Gassner, N.C., Snow, S.D., Eldridge, A.M., Baase, W.A., Drew, D.L., and Matthews, B.W. (1998). Context-dependent protein stabilization by methionine-to-leucine substitution shown in T4 lysozyme. Protein Sci *7*, 765-773.

Liu, Y., and Halloran, M.C. (2005). Central and peripheral axon branches from one neuron are guided differentially by Semaphorin3D and transient axonal glycoprotein-1. J Neurosci *25*, 10556-10563.

Loeb, J. (1906). Chemotropism and related phenomena. In The Dynamics of Living Matter (New York: The Columbia University Press), pp. 152-155.

Lugaro, E. (1906). Sul neurotropismo e sui trapianti dei nervi. Riv di Patol Nerv Ment *11*, 320-327.

Luna, E.J. (1998). F-actin blot overlays. Methods Enzymol *298*, 32-42.

Luo, J., Xu, Y., Zhu, Q., Zhao, F., Zhang, Y., Peng, X., Wang, W., and Wang, X. (2011). Expression pattern of Mical-1 in the temporal neocortex of patients with intractable temporal epilepsy and Pilocarpine-induced rat model. Synapse.

Luo, Y., Raible, D., and Raper, J.A. (1993). Collapsin: a protein in brain that induces the collapse and paralysis of neuronal growth cones. Cell *75*, 217-227.

Luo, Y., Shepherd, I., Li, J., Renzi, M.J., Chang, S., and Raper, J. (1995). A family of molecules related to collapsin in the embryonic chick nervous system. Neuron *14*, 1131-1140.

Magi, B., and Liberatori, S. (2005). Immunoblotting techniques. Methods Mol Biol *295*, 227-254.

Mann, F., Chauvet, S., and Rougon, G. (2007). Semaphorins in development and adult brain: Implication for neurological diseases. Prog Neurobiol *82*, 57-79.

Martz, E., and Steinberg, M.S. (1973). Contact inhibition of what? An analytical review. J Cell Physiol *81*, 25-37.

Massey, V. (1995). Introduction: flavoprotein structure and mechanism. Faseb J *9*, 473-475.

Mayor, R., and Carmona-Fontaine, C. (2010). Keeping in touch with contact inhibition of locomotion. Trends Cell Biol *20*, 319-328.

Melani, M., and Weinstein, B.M. (2010). Common factors regulating patterning of the nervous and vascular systems. Annu Rev Cell Dev Biol *26*, 639-665.

Miao, H.-Q., Soker, S., Feiner, L., Alonso, J.L., Raper, J.A., and Klagsbrun, M. (1999). Neuropilin-1 mediates collapsin-1/semaphorin III inhibition of endothelial cell motility: Functional competition of collapsin-1 and vascular endothelial growth factor-165. J Cell Biol *146*, 233-241.

Mikule, K., Gatlin, J.C., de la Houssaye, B.A., and Pfenninger, K.H. (2002). Growth cone collapse induced by semaphorin 3A requires 12/15- lipoxygenase. J Neurosci *22*, 4932-4941.

Milzani, A., Rossi, R., Di Simplicio, P., Giustarini, D., Colombo, R., and DalleDonne, I. (2000). The oxidation produced by hydrogen peroxide on Ca-ATP-G-actin. Protein Sci *9*, 1774-1782.

Mintz, C.D., Carcea, I., McNickle, D.G., Dickson, T.C., Ge, Y., Salton, S.R., and Benson, D.L. (2008). ERM proteins regulate growth cone responses to Sema3A. J Comp Neurol *510*, 351-366.

Miura, K., and Imaki, J. (2008). Molecular cloning of Ebitein1: a novel extracellular signal-regulated kinase 2-binding protein in testis. Biochem Biophys Res Commun *368*, 336-342.

Morinaka, A., Yamada, M., Itofusa, R., Funato, Y., Yoshimura, Y., Nakamura, F., Yoshimura, T., Kaibuchi, K., Goshima, Y., Hoshino, M*., et al.* (2011). Thioredoxin Mediates Oxidation-Dependent Phosphorylation of CRMP2 and Growth Cone Collapse. Sci Signal *4*, ra26.

Muller, U., and Littlewood-Evans, A. (2001). Mechanisms that regulate mechanosensory hair cell differentiation. Trends Cell Biol *11*, 334-342.

Murakami, K., Yasunaga, T., Noguchi, T.Q., Gomibuchi, Y., Ngo, K.X., Uyeda, T.Q., and Wakabayashi, T. (2010). Structural basis for actin assembly, activation of ATP hydrolysis, and delayed phosphate release. Cell *143*, 275-287.

Murray, M.J., Merritt, D.J., Brand, A.H., and Whitington, P.M. (1998). In vivo dynamics of axon pathfinding in the Drosophilia CNS: a time-lapse study of an identified motorneuron. J Neurobiol *37*, 607-621.

Nadella, M., Bianchet, M.A., Gabelli, S.B., Barrila, J., and Amzel, L.M. (2005). Structure and activity of the axon guidance protein MICAL. Proc Natl Acad Sci U S A *102*, 16830-16835.

Nakai, J. (1964). The movement of neurons in tissue culture. In Primitive motile systems in cell biology, R.D. Allen, and N. Kamija, eds. (New York: Academic Press), pp. 377-385.

Nakajima, S. (1965). Selectivity in fasciculation of of nerve fibers in vitro. J Comp Neurol *125*, 193-195.

Negishi, M., Oinuma, I., and Katoh, H. (2005). R-Ras as a key player for signaling pathway of Plexins. Mol Neurobiol *32*, 217-222.

Neufeld, G., and Kessler, O. (2008). The semaphorins: versatile regulators of tumour progression and tumour angiogenesis. Nat Rev Cancer *8*, 632-645.

Nukazuka, A., Fujisawa, H., Inada, T., Oda, Y., and Takagi, S. (2008). Semaphorin controls epidermal morphogenesis by stimulating mRNA translation via eIF2alpha in Caenorhabditis elegans. Genes Dev *22*, 1025-1036.

Nuttall, R.P., and Zinsmeister, P.P. (1983). Differential response to contact during embryonic nerve-nonnerve cell interactions. Cell Motil *3*, 307-320.

Oda, T., Iwasa, M., Aihara, T., Maeda, Y., and Narita, A. (2009). The nature of the globular- to fibrous-actin transition. Nature *457*, 441-445.

Oda, T., and Maeda, Y. (2010). Multiple Conformations of F-actin. Structure *18*, 761-767.

Oinuma, I., Ishikawa, Y., Katoh, H., and Negishi, M. (2004). The Semaphorin 4D receptor Plexin-B1 is a GTPase activating protein for R-Ras. Science *305*, 862-865.

Okada, K., Obinata, T., and Abe, H. (1999). XAIP1: a Xenopus homologue of yeast actin interacting protein 1 (AIP1), which induces disassembly of actin filaments cooperatively with ADF/cofilin family proteins. J Cell Sci *112 (Pt 10)*, 1553-1565.

Ono, S. (2007). Mechanism of depolymerization and severing of actin filaments and its significance in cytoskeletal dynamics. Int Rev Cytol *258*, 1-82.

Oser, M., and Condeelis, J. (2009). The cofilin activity cycle in lamellipodia and invadopodia. J Cell Biochem *108*, 1252-1262.

Otterbein, L.R., Graceffa, P., and Dominguez, R. (2001). The crystal structure of uncomplexed actin in the ADP state. Science *293*, 708-711.

Pak, C.W., Flynn, K.C., and Bamburg, J.R. (2008). Actin-binding proteins take the reins in growth cones. Nat Rev Neurosci *9*, 136-147.

Pasterkamp, R.J., Dai, H.N., Terman, J.R., Wahlin, K.J., Kim, B., Bregman, B.S., Popovich, P.G., and Kolodkin, A.L. (2006). MICAL flavoprotein monooxygenases: Expression during neural development and following spinal cord injuries in the rat. Mol Cell Neurosci *31*, 52-69.

Peterson, E.R., and Crain, S.M. (1982). Preferential growth of neurites from isolated fetal mouse dorsal root ganglia in relation to specific regions of co-cultured spinal cord explants. Devl Brain Res *2*, 363-382.

Pini, A. (1993). Chemorepulsion of axons in the developing mammalian central nervous system. Science *261*, 95-98.

Pollard, T.D., and Borisy, G.G. (2003). Cellular motility driven by assembly and disassembly of actin filaments. Cell *112*, 453-465.

Pollard, T.D., and Cooper, J.A. (2009). Actin, a central player in cell shape and movement. Science *326*, 1208-1212.

Poodry, C.A. (1975). A Temporal Pattern in the Development of Sensory Bristles in Drosophila. Wilhelm Roux's Archives *178*, 203-213.

Porter, S.L., Wadhams, G.H., and Armitage, J.P. (2011). Signal processing in complex chemotaxis pathways. Nat Rev Microbiol *9*, 153-165.

Potiron, V., Nasarre, P., Roche, J., Healy, C., and Boumsell, L. (2007). Semaphorin signaling in the immune system. Adv Exp Med Biol *600*, 132-144.

Puschel, A.W. (2007). GTPases in semaphorin signaling. Adv Exp Med Biol *600*, 12-23.

Raper, J.A., Bastiani, M., and Goodman, C.S. (1983). Pathfinding by neuronal growth cones in grasshopper embryos. II. Selective fasciculation onto specific axonal pathways. J Neurosci *3*, 31-41.

Raper, J.A., and Grunewald, E.B. (1990). Temporal retinal growth cones collapse on contact with naasal retinal axons. Exp Neurol *109*, 70-74.

Raper, J.A., and Kapfhammer, J.P. (1990). The enrichment of a neuronal growth cone collapsing activity from embryonic chick brain. Neuron *4*, 21-29.

Reier, P.J., Stensaas, L.J., and Guth, L. (1983). The astrocytic scar as an impediment to regeneration in the central nervous system. In Spinal Cord Reconstruction, C.C. Kao, R.P. Bunge, and P.J. Reier, eds. (New York: Raven Press), pp. 163-195.

Roche, F.K., Marsick, B.M., and Letourneau, P.C. (2009). Protein synthesis in distal axons is not required for growth cone responses to guidance cues. J Neurosci *29*, 638-652.

Rosen, W.G. (1962). Cellular chemotropism and chemotaxis. Q Rev Biol *37*, 242-259.

Roth, L., Koncina, E., Satkauskas, S., Cremel, G., Aunis, D., and Bagnard, D. (2009). The many faces of semaphorins: from development to pathology. Cell Mol Life Sci *66*, 649-666.

Rudolph, T.K., and Freeman, B.A. (2009). Transduction of redox signaling by electrophile-protein reactions. Sci Signal *2*, re7.

Sakai, J.A., and Halloran, M.C. (2006). Semaphorin 3d guides laterality of retinal ganglion cell projections in zebrafish. Development *133*, 1035-1044.

Sanchez-Soriano, N., and Prokop, A. (2005). The influence of pioneer neurons on a growing motor nerve in Drosophila requires the neural cell adhesion molecule homolog FasciclinII. J Neurosci *25*, 78-87.

Schlatter, M.C., Buhusi, M., Wright, A.G., and Maness, P.F. (2008). CHL1 promotes Sema3A-induced growth cone collapse and neurite elaboration through a motif required for recruitment of ERM proteins to the plasma membrane. J Neurochem *104*, 731-744.

Schmidt, E.F., Shim, S.O., and Strittmatter, S.M. (2008). Release of MICAL autoinhibition by semaphorin-plexin signaling promotes interaction with collapsin response mediator protein. J Neurosci *28*, 2287-2297.

Schmidt, E.F., and Strittmatter, S.M. (2007). The CRMP family of proteins and their role in Sema3A signaling. Adv Exp Med Biol *600*, 1-11.

Schmoller, K.M., Semmrich, C., and Bausch, A.R. (2011). Slow down of actin depolymerization by cross-linking molecules. J Struct Biol *173*, 350-357.

Schwab, M.E., Kapfhammer, C.E., and Bandtlow, C.E. (1993). Inhibitors of neurite growth. Annu Rev Neurosci *16*, 565-595.

Schwab, M.E., and Thoenen, H. (1985). Dissociated neurons regenerate into sciatic but not optic nerve explants in culture irrespective of neurotrophic factors. J Neurosci *5*, 2415-2423.

Scott, G.A., McClelland, L.A., Fricke, A.F., and Fender, A. (2009). Plexin C1, a receptor for semaphorin 7a, inactivates cofilin and is a potential tumor suppressor for melanoma progression. J Invest Dermatol *129*, 954-963.

Serini, G., Valdembri, D., Zanivan, S., Morterra, G., Burkhardt, C., Caccavari, F., Zammataro, L., Primo, L., Tamagnone, L., Logan, M.*, et al.* (2003). Class 3 semaphorins control vascular morphogenesis by inhibiting integrin function. Nature *424*, 391-397.

Sheterline, P.J., Clayton; John C., Sparrow (1998). Actin, fourth edn (oxford).

Shimizu, A., Mammoto, A., Italiano, J.E., Jr., Pravda, E., Dudley, A.C., Ingber, D.E., and Klagsbrun, M. (2008). ABL2/ARG tyrosine kinase mediates SEMA3F-induced RhoA inactivation and cytoskeleton collapse in human glioma cells. J Biol Chem *283*, 27230-27238.

Siebold, C., Berrow, N., Walter, T.S., Harlos, K., Owens, R.J., Stuart, D.I., Terman, J.R., Kolodkin, A.L., Pasterkamp, R.J., and Jones, E.Y. (2005). High-resolution structure of the catalytic region of MICAL (molecule interacting with CasL), a multidomain flavoenzyme-signaling molecule. Proc Natl Acad Sci U S A *102*, 16836-16841.

Smalheiser, N.R., Peterson, E.R., and Crain, S.M. (1981). Neurites from mouse retina and dorsal root ganglion explants show specific behavior within co-cultured tectum or spinal cord. Brain Res *208*, 499-505.

Spector, I., Shochet, N.R., Blasberger, D., and Kashman, Y. (1989). Latrunculins--novel marine macrolides that disrupt microfilament organization and affect cell growth: I. Comparison with cytochalasin D. Cell Motil Cytoskeleton *13*, 127-144.

Speidel, C.C. (1933). Studies of living nerves. II. Activities of ameboid growth cones, sheath cells, and myelin segments, as revealed by prolonged observation of individual nerve fibers in frog tadpoles. Am J Anat *52*, 1-79.

Sperry, R.W. (1963). Chemoaffinity in the orderly growth of nerve fiber patterns and connections. Proc Natl Acad Sci USA *50*, 703-710.

Stamler, J.S., Lamas, S., and Fang, F.C. (2001). Nitrosylation. the prototypic redox-based signaling mechanism. Cell *106*, 675-683.

Sun, H., Dai, H., Zhang, J., Jin, X., Xiong, S., Xu, J., Wu, J., and Shi, Y. (2006). Solution structure of calponin homology domain of Human MICAL-1. J Biomol NMR *36*, 295-300.

Sutherland, J.D., and Witke, W. (1999). Molecular genetic approaches to understanding the actin cytoskeleton. Current opinion in cell biology *11*, 142-151.

Suzuki, K., Kumanogoh, A., and Kikutani, H. (2008). Semaphorins and their receptors in immune cell interactions. Nat Immunol *9*, 17-23.

Suzuki, T., Nakamoto, T., Ogawa, S., Seo, S., Matsumura, T., Tachibana, K., Morimoto, C., and Hirai, H. (2002). MICAL, a novel CasL interacting molecule, associates with vimentin. J Biol Chem *277*, 14933-14941.

Sweeney, L.B., Couto, A., Chou, Y.H., Berdnik, D., Dickson, B.J., Luo, L., and Komiyama, T. (2007). Temporal target restriction of olfactory receptor neurons by Semaphorin-1a/PlexinA-mediated axon-axon interactions. Neuron *53*, 185-200.

Takahashi, T., Fournier, A., Nakamura, F., Wang, L.-H., Murakami, Y., Kalb, R.G., Fujisawa, H., and Strittmatter, S.M. (1999). Plexin-neuropilin-1 complexes form functional semaphorin-3A receptors. Cell *99*, 59-69.

Takahashi, T., and Strittmatter, S.M. (2001). PlexinA1 Autoinhibition by the Plexin Sema Domain. Neuron *29*, 429-439.

Takamatsu, H., Takegahara, N., Nakagawa, Y., Tomura, M., Taniguchi, M., Friedel, R.H., Rayburn, H., Tessier-Lavigne, M., Yoshida, Y., Okuno, T.*, et al.* (2010). Semaphorins guide the entry of dendritic cells into the lymphatics by activating myosin II. Nat Immunol *11*, 594-600.

Takamoto, K., Kamal, J.K., and Chance, M.R. (2007). Biochemical implications of a three-dimensional model of monomeric actin bound to magnesium-chelated ATP. Structure *15*, 39-51.

Tamagnone, L., Artigiani, S., Chen, H., He, Z., Ming, G.-L., Song, H.-J., Chedotal, A., Winberg, M.L., Goodman, C.S., Poo, M.-M.*, et al.* (1999). Plexins are a large family of receptors for transmembrane, secreted, and GPI-anchored semaphorins in vertebrates. Cell *99*, 71-80.

Terman, J.R., and Kashina, A. (2012). Post-translational modification and regulation of actin. Current opinion in cell biology.

Terman, J.R., Mao, T., Pasterkamp, R.J., Yu, H.H., and Kolodkin, A.L. (2002). MICALs, a family of conserved flavoprotein oxidoreductases, function in plexin-mediated axonal repulsion. Cell *109*, 887-900.

Tessier-Lavigne, M., and Goodman, C.S. (1996). The molecular biology of axon guidance. Science *274*, 1123-1133.

Tilney, L.G., Connelly, P., Smith, S., and Guild, G.M. (1996). F-actin bundles in Drosophila bristles are assembled from modules composed of short filaments. J Cell Biol *135*, 1291-1308.

Tilney, L.G., Connelly, P.S., Ruggiero, L., Vranich, K.A., and Guild, G.M. (2003). Actin filament turnover regulated by cross-linking accounts for the size, shape, location, and number of actin bundles in Drosophila bristles. Mol Biol Cell *14*, 3953-3966.

Tilney, L.G., Connelly, P.S., Ruggiero, L., Vranich, K.A., Guild, G.M., and Derosier, D. (2004). The role actin filaments play in providing the characteristic curved form of Drosophila bristles. Mol Biol Cell *15*, 5481-5491.

Tilney, L.G., Connelly, P.S., Vranich, K.A., Shaw, M.K., and Guild, G.M. (1998). Why are two different cross-linkers necessary for actin bundle formation in vivo and what does each cross-link contribute? J Cell Biol *143*, 121-133.

Tilney, L.G., Connelly, P.S., Vranich, K.A., Shaw, M.K., and Guild, G.M. (2000a). Actin filaments and microtubules play different roles during bristle elongation in Drosophila. J Cell Sci *113 (Pt 7)*, 1255-1265.

Tilney, L.G., Connelly, P.S., Vranich, K.A., Shaw, M.K., and Guild, G.M. (2000b). Regulation of actin filament cross-linking and bundle shape in Drosophila bristles. J Cell Biol *148*, 87-100.

Tilney, L.G., and DeRosier, D.J. (2005). How to make a curved Drosophila bristle using straight actin bundles. Proceedings of the National Academy of Sciences of the United States of America *102*, 18785-18792.

Tilney, L.G., Tilney, M.S., and Guild, G.M. (1995). F actin bundles in Drosophila bristles. I. Two filament cross-links are involved in bundling. J Cell Biol *130*, 629-638.

Torres-Vazquez, J., Gitler, A.D., Fraser, S.D., Berk, J.D., Van, N.P., Fishman, M.C., Childs, S., Epstein, J.A., and Weinstein, B.M. (2004). Semaphorin-plexin signaling guides patterning of the developing vasculature. Dev Cell *7*, 117-123.

Tosney, K.W., and Landmesser, L.T. (1985). Growth cone morphology and trajectory in the lumbosacral region of the chick embryo. J Neurosci *5*, 2345-2358.

Toyofuku, T., Yoshida, J., Sugimoto, T., Zhang, H., Kumanogoh, A., Hori, M., and Kikutani, H. (2005). FARP2 triggers signals for Sema3A-mediated axonal repulsion. Nat Neurosci *8*, 1712-1719.

Tran, T.S., Kolodkin, A.L., and Bharadwaj, R. (2007). Semaphorin regulation of cellular morphology. Annu Rev Cell Dev Biol *23*, 263-292.

Tran-Van, H., Avota, E., Bortlein, C., Mueller, N., and Schneider-Schaulies, S. (2011). Measles virus modulates dendritic cell/T-cell communication at the level of plexinA1/neuropilin-1 recruitment and activity. Eur J Immunol *41*, 151-163.

Turner, C.M., and Adler, P.N. (1998). Distinct roles for the actin and microtubule cytoskeletons in the morphogenesis of epidermal hairs during wing development in Drosophila. Mech Dev *70*, 181-192.

Turner, L.J., and Hall, A. (2006). Plexin-induced collapse assay in COS cells. Methods Enzymol *406*, 665-676.

Turner, L.J., Nicholls, S., and Hall, A. (2004). The activity of the plexin-A1 receptor is regulated by Rac. J Biol Chem *279*, 33199-33205.

Usui, H., Taniguchi, M., Yokomizo, T., and Shimizu, T. (2003). Plexin-A1 and plexin-B1 specifically interact at their cytoplasmic domains. Biochem Biophys Res Commun *300*, 927-931.

van Berkel, W., Westphal, A., Eschrich, K., Eppink, M., and de Kok, A. (1992). Substitution of Arg214 at the substrate-binding site of p-hydroxybenzoate hydroxylase from Pseudomonas fluorescens. Eur J Biochem *210*, 411-419.

van Berkel, W.J., Benen, J.A., Eppink, M.H., and Fraaije, M.W. (1999). Flavoprotein kinetics. Methods Mol Biol *131*, 61-85.

Van Vactor, D., Sink, H., Fambrough, D., Tsoo, R., and Goodman, C.S. (1993). Genes that control neuromuscular specificity in Drosophila. Cell *73*, 1137-1153.

Varshavsky, A., Kessler, O., Abramovitch, S., Kigel, B., Zaffryar, S., Akiri, G., and Neufeld, G. (2008). Semaphorin-3B is an angiogenesis inhibitor that is inactivated by furin-like pro-protein convertases. Cancer Res *68*, 6922-6931.

Vastrik, I., Eickholt, B.J., Walsh, F.S., Ridley, A., and Doherty, P. (1999). Sema3A-induced growth-cone collapse is mediated by Rac1 amino acids 17- 32. Curr Biol *9*, 991-998.

Verna, J.-M. (1985). In vitro analysis of interactions between sensory neurons and skin: evidence for selective innervation of dermis and epidermis. J Embryol Exp Morphol *86*, 53-70.

Vikis, H.G., Li, W., and Guan, K.L. (2002). The Plexin-B1/Rac interaction inhibits PAK activation and enhances Sema4D ligand binding. Genes Dev *16*, 836-845.

Volkman, L., Storm, K., Aivazachvili, V., and Oppenheimer, D. (1996). Overexpression of actin in AcMNPV-infected cells interferes with polyhedrin synthesis and polyhedra formation. Virology *225*, 369-376.

Wakatsuki, T., Schwab, B., Thompson, N.C., and Elson, E.L. (2001). Effects of cytochalasin D and latrunculin B on mechanical properties of cells. J Cell Sci *114*, 1025-1036.

Walter, J., Henke-Fahle, S., and Bonhoeffer, F. (1987a). Avoidance of posterior tectal membranes by temporal retinal axons. Development *101*, 909-913.

Walter, J., Kern-Veits, R., Huf, J., Stolze, B., and Bonhoeffer, F. (1987b). Recognition of position-specific properties of tectal cell membranes by retinal axons in vitro. Development *101*, 685-696.

Walzer, T., Galibert, L., Comeau, M.R., and De Smedt, T. (2005). Plexin C1 engagement on mouse dendritic cells by viral semaphorin A39R induces actin cytoskeleton rearrangement and inhibits integrin-mediated adhesion and chemokine-induced migration. J Immunol *174*, 51-59.

Weide, T., Teuber, J., Bayer, M., and Barnekow, A. (2003). MICAL-1 isoforms, novel rab1 interacting proteins. Biochem Biophys Res Commun *306*, 79-86.

Weiss, P. (1947). The problem of specificity in growth and development. Yale J Biol Med *19*, 235-278.

Weiss, P. (1958). Cell contact. Int Rev Cytol *7*, 391-423.

Wessells, N.K., Letourneau, P.C., Nuttall, R.P., Luduena-Anderson, M., and Geiduschek, J.M. (1980). Responses to cell contacts between growth cones, neurites and ganglionic non-neuronal cells. J Neurocytol *9*, 647-664.

Wessells, N.K., Spooner, B.S., Ash, J.F., Bradley, M.O., Luduena, M.A., Taylor, E.L., Wrenn, J.T., and Yamaa, K. (1971). Microfilaments in cellular and developmental processes. Science *171*, 135-143.

Wierenga, R.K., Terpstra, P., and Hol, W.G. (1986). Prediction of the occurrence of the ADP-binding beta alpha beta-fold in proteins, using an amino acid sequence fingerprint. J Mol Biol *187*, 101-107.

Winberg, M.L., Noordermeer, J.N., Tamagnone, L., Comoglio, P.M., Spriggs, M.K., Tessier-Lavigne, M., and Goodman, C.S. (1998). Plexin A is a neuronal semaphorin receptor that controls axon guidance. Cell *95*, 903-916.

Windle, W.F. (1955). Regeneration in the central nervous system (Springfield: Charles C. Thomas).

Wolf, E.P. (1921). Experimental Studies on Inflammation : I. The Influence of Chemicals Upon the Chemotaxis of Leucocytes in Vitro. J Exp Med *34*, 375-396.

Woo, S., and Gomez, T.M. (2006). Rac1 and RhoA promote neurite outgrowth through formation and stabilization of growth cone point contacts. J Neurosci *26*, 1418-1428.

Wu, J.S., and Luo, L. (2006). A protocol for mosaic analysis with a repressible cell marker (MARCM) in Drosophila. Nat Protoc *1*, 2583-2589.

Xu, X.M., Fisher, D.A., Zhou, L., White, F.A., Ng, S., Snider, W.D., and Luo, Y. (2000). The transmembrane protein semaphorin 6A repels embryonic sympathetic axons. J Neurosci *20*, 2638-2648.

Xue, Y., Kuok, C., Xiao, A., Zhu, Z., Lin, S., and Zhang, B. (2010). Identification and expression analysis of mical family genes in zebrafish. J Genet Genomics *37*, 685-693.

Yamada, K.M., Spooner, B.S., and Wessells, N.K. (1970). Axon Growth: Roles of microfilaments and microtubules. Proc Natl Acad Sci U S A *66*, 1206-1212.

Yamada, K.M., Spooner, B.S., and Wessells, N.K. (1971). Ultrastructure and function of growth cones and axons of cultured nerve cells. J Cell Biol *49*, 614-635.

Yang, T., and Terman, J.R. (2013). Regulating small G protein signaling to coordinate axon adhesion and repulsion. Small GTPases *4*, 34-41.

Yazdani, U., Huang, Z., and Terman, J.R. (2008). The Glucose Transporter (GLUT4) Enhancer Factor Is Required for Normal Wing Positioning in Drosophila. Genetics *178*, 919-929.

Yazdani, U., and Terman, J.R. (2006). The Semaphorins. Genome Biol *7*, 211-225.

Yin, H.L., and Stossel, T.P. (1979). Control of cytoplasmic actin gel-sol transformation by gelsolin, a calcium-dependent regulatory protein. Nature *281*, 583-586.

Yoon, J., and Terman, J.R. (submitted). Disassembling F-actin networks in vivo through manipulations of Mical and actin bundling proteins.

Yoon, M.G. (1979). Reciprocal transplantations between the optic tectum and the cerebellum in adult goldfish. J Physiol *288*, 211-225.

Young, J.D., Lawrence, A.J., MacLean, A.G., Leung, B.P., McInnes, I.B., Canas, B., Pappin, D.J., and Stevenson, R.D. (1999). Thymosin beta 4 sulfoxide is an anti-inflammatory agent generated by monocytes in the presence of glucocorticoids. Nat Med *5*, 1424-1427.

Yu, H.H., Araj, H.H., Ralls, S.A., and Kolodkin, A.L. (1998). The transmembrane Semaphorin Sema I is required in Drosophila for embryonic motor and CNS axon guidance. Neuron *20*, 207-220.

Yukawa, K., Tanaka, T., Bai, T., Ueyama, T., Owada-Makabe, K., Tsubota, Y., Maeda, M., Suzuki, K., Kikutani, H., and Kumanogoh, A. (2005). Semaphorin 4A induces growth cone collapse of hippocampal neurons in a Rho/Rho-kinase-dependent manner. Int J Mol Med *16*, 115-118.

Zhou, Y., Gunput, R.A., Adolfs, Y., and Pasterkamp, R.J. (2011a). MICALs in control of the cytoskeleton, exocytosis, and cell death. Cell Mol Life Sci.

Zhou, Y., Gunput, R.A., Adolfs, Y., and Pasterkamp, R.J. (2011b). MICALs in control of the cytoskeleton, exocytosis, and cell death. Cell Mol Life Sci *68*, 4033-4044.

Zhou, Y., Gunput, R.A., and Pasterkamp, R.J. (2008). Semaphorin signaling: progress made and promises ahead. Trends Biochem Sci *33*, 161-170.

Zhuang, B., Su, Y.S., and Sockanathan, S. (2009). FARP1 promotes the dendritic growth of spinal motor neuron subtypes through transmembrane Semaphorin6A and PlexinA4 signaling. Neuron *61*, 359-372.

Zinsmeister, P.P., and Nuttall, R.P. (1986). Age and cell type influences on nerve--non-nerve contact interactions. Devl Brain Res *25*, 143-146.